University of Strathclyde

Department of Electronic and Electrical Engineering

Diversity Gain Enhancement for Extended Orthogonal Space-Time Block Coding in Wireless Communications

By

Mohamed Nuri Ahmed Hussin

A thesis presented in fulfilment of the requirements for the degree
of
Doctor of Philosophy

2013

Declaration

This thesis is the result of the author's original research. It has been composed by the author and has not been previously submitted for examination which has lead to the award of a degree.

Acknowledgements

Thanks to God for his blessings. It is my pleasure to thank my supervisor Dr Stephan Weiss for the opportunity to be his research student. His guidance and support throughout the research has been indispensable. His nice nature, valuable insights, clarity of thought, and comments have no doubt significantly improved this thesis. It has been an honour to work with Stephan through my research, and it has been an exceptional experience for me. I would like to express my most sincere gratitude for his taking the time to give me lots of useful feedback and comments on my papers.

I would also like to thank my companions in CeSIP with whom I enjoyed discussing problems and sharing ideas. I am especially thankful to all my colleagues in room R3.49 who no doubt made research life more interesting.

I wish to extend my thanks to my parents, brothers and sisters for their support. Finally, I am very grateful to my wife for her kindness and for steadily and patiently encouraging my life abroad. Thanks also for the lovely kids for every day a great time.

Abstract

Transmit diversity is a powerful technique for enhancing the channel capacity and reliability of multiple-input and multiple-output (MIMO) wireless systems. This thesis considers extended orthogonal space-time block coding (EO-STBC) with beamsteering angles, which have previously been shown to potentially achieve full diversity and array gain with four transmit and one receive antenna. The optimum setting of beamsteering angles applied in the transmitter, which has to be calculated based on channel state information (CSI) at the receiver side, must be quantised and feed back to the transmitter via a reverse feedback link.

When operating in a fading scenario, channel coefficients vary smoothly with time. This smooth evolution of channel coefficients motivates the investigation of differential feedback, which can reduce the number of feedback bits, while potentially maintaining near optimum performance. The hypothesis that the smooth evolution of channel coefficients translates into smooth evolution of feedback angles is justified by simulations. The maximum attainable gain under optimum unquantised beamsteering angles is derived, which allows to experimentally assess the effect that quantisation in the feedback channel has on the system performance. In characterising the degradation experienced through time-variation and limited quantised feedback, we demonstrate that the new differential feedback approach offers a practical bandwidth-efficient scheme. Simulation results with Doppler spread conditions confirm that the proposed scheme achieves significant bandwidth savings over previously proposed systems. With a single feedback bit per beamsteering angle the proposed differentially encoded EO-STBC approach can achieve near optimum performance and exceed the performance of non-differential feedback schemes that employ a higher word length.

We further propose combining differential encoding with channel estimation

that is practically useful because the EO-STBC receiver requires knowledge of the channel coefficients for both detecting the transmitted symbols as well as for computing the optimum angles to be fed back to the transmitter. Channel estimation accompanied by a decision-directed (DD) tracking scheme by means of a Kalman filter has been adopted. The Kalman filter exploits the smooth evolution of the channel coefficients as a motivation for tracking as well as for differential feedback. Further we propose applying an auto-regressive (AR) predictor with order greater than one in the Kalman model. This can be shown to offer advantages in terms of temporal smoothness when addressing channels whose coefficient trajectories evolve smoothly. Simulation results show that the overall EO-STBC system achieves longer tracking periods with suitable bit error (BER) values, and that the performance of the proposed system offers a distinct advantage for lower Doppler spreads with the inclusion of second order AR model instead of the standard first order AR model.

The earlier work on EO-STBC systems is for frequency-flat channels. However, in frequency-selective channel a multi-carrier approach can help to split into independent subcarriers. Therefore, the EO-STBC scheme is then applied for a dedicated chirp-based multicarrier based on a fractional Fourier transformer (FrFT) system over doubly dispersive channels, where FrFT-domain is developed to further increase robustness against channel time-variations. Applied in near-stationary channel conditions, the performance of orthogonal frequency division multiplexing (OFDM) receivers that mitigate crosstalk between individual subcarriers are evaluated for open and closed loop schemes. A higher degree of non-stationarity in mobile scenarios will destroy the orthogonality of subcarriers and result in intercarrier interference (ICI) and intersymbol interference (ISI). In this case, minimum mean square error (MMSE) of a reduced system matrix is considered for open loop EO-STBC. The equaliser complexity can be decreased even furtherby using least squares minimum residual (LSMR) iterative algorithm, equalisation are underlined by simulations, demonstrating the overall practical use if the contributions wihtin this thesis towards EO-STBC diversity schemes over both time- and frequency-dispersive channels.

Publications

- W. Al-Hanafy, M. N. Hussin, and S.Weiss, "Incremental rate maximisation power loading with BER improvements," in 18th European Signal Processing Conference, 2010.
- M. N. Hussin and S. Weiss, "Extended orthogonal space-time block coded transmission with quantised differential feedback," in 7th IEEE International Symposium on Wireless Communication Systems, September 2010.
- M. N. Hussin and S. Weiss, "Channel estimation and tracking for closed loop EO-STBC with differentially encoding feedback," in 11th IEEE International Symposium on signal processing and information technology, December 2011.
- M. N. Hussin, A. Solomon, S. Weiss, and J. Soraghan, "Fractional Fourier transformer based on extended orthogonal space-time coding for multicarrier system over doubly-dispersive channel ," in 9th IEEE International Symposium on Wireless Communication Systems, 2012.
- M. N. Hussin, M. Alrmah, and S. Weiss, " Distributed Closed-Loop EO-STBC for a time-varying Relay Channel Based on Kalman Tracking ," in 9th IMA International Conference on Mathematics in Signal Processing, 2012.
- M. Alrmah, M. N. Hussin, S. Weiss, and S. Lambotharan, "Comparison of Broadband Direction of Arrival Estimation Algorithms ," in 9th IMA International Conference on Mathematics in Signal Processing, 2012.

Dedication

Dedicated to my family

Contents

List of Figures

List of Tables

Acronyms

AAF	Amplify-and- Forward
AR-M	M order Auto-Regressive Prediction Model
ASTBC	Adaptive Space Time Code
AWGN	Additive White Gaussian Noise
BER	Bit Error Ratio
BPSK	Binary Phase Shift Keying
CP	Cyclic Prefix
CSI	Channel State Information
DAF	Decode-and- Forward
DFE	Decision Feedback Equaliser
DD	Decision-Directed
DSP	Digital Signal Processing
EO-STBC	Extended Orthogonal Space time block coding
FFT	Fast Fourier Transform
FrFT	Fractional Fourier Transform
FGWN	Filtering Gaussian White Noise
i.i.d	independent and identically distributed
ICI	Inter-Carrier Interference
ISI	Inter-Symbol Interference
JML	Joint Maximum likelihood
LS	Least Squares
LSMR	Least Squares Minimum Residual
LTE	Long Term Evolution
MIMO	Multi Input Multi Output
MMSE	Minimum mean square error

OFDM	Orthogonal Frequency Division Multiplexing
O-STBC	Orthogonal Space Time Block Coding
PDP	Power Delay Profile
QO-STBC	Quasi Orthogonal Space Time Block Coding
RF	Radio Frequency
SIMO	Single-Input Multiple-Output
SISO	Single-Input Single-Output
SML	Simple Maximum Likelihood
STBC	Space time block codes
STC	Space Time Coding
STTC	Space Time Trellis Coding
STTD	Space Time Transmit Diversity
TDL	Tap Delay Line
UMTS	Universal Mobile Telecommunications System
WiFi	Wireless Fidelity
WiMax	Worldwide Interoperability for Microwave Access
WLAN	Wireless Local Area Network
WMF	Whitened Matched Filter
WSS	Wide Sense Stationary
ZFE	Zero forcing equaliser

List of Symbols

h	Scalar Quantity
$\mathbf{h}$	Vector Quantity
$\mathbf{H}$	Matrix Quantity
$\|x\|$	Absolute value of x
$\|\|\cdot\|\|_{\mathrm{F}}$	Frobenius norm
N_T	Number of Transmit Antennas
N_R	Number of Receive Antennas
$(\cdot)^{\mathrm{T}}$	Transpose Operation
$(\cdot)^{\mathrm{H}}$	Hermitian (Conjugate Transpose) Operation
$(\cdot)^*$	Conjugate Operation
$\mathcal{E}\{\cdot\}$	Expectation Operation
$\angle\{\cdot\}$	Angle/ Radian
$\Re\{\cdot\}$	Real Part of Complex Number
$\Im\{\cdot\}$	Imaginary Part of Complex Number
$\mathbb{C}$	Set of Complex Number
$\mathcal{F}$	Code Book
$\mathbf{F}$	Precoder
B	Feedback Bits
μ	Step Size
α	Diversity Gain
β	Array Gain
ϑ	Feedback Angle
$\mathbf{F}_a$	Discrete FrFT Matrix
a	FrFT order
$\mathbf{F}_1$	FFT Matrix

N_a	Number of Active Sub-carrier
$\mathbf{C}[n]$	Equivalent multicarrier channel matrix
$\mathbf{G}[n]$	System channel matrix
$\mathbf{\Phi}[n]$	Beamsteering rotations
$\mathbf{\Theta}[n]$	Beamsteering rotations
$\mathbf{W}_{n,\mathrm{MMSE}}$	MMSE Channel Equaliser
$\mathbf{W}_{n,\mathrm{ZF}}$	ZF Channel Equaliser
$\mathbf{B}_n$	Banded Channel Equaliser
$\bar{\mathbf{B}}_n$	Permuted Banded Channel Equaliser
$\mathbf{P}_{M,N}$	Permutation Matrix
Ω_D	Doppler Angular Spread
f_D	Doppler Spread
$\Delta\Omega$	Normalised Angular Sub-Carrier Spacing
f_s	Sampling Frequency
Q	Bandwidth Parameter
$\mathcal{O}$	Complexity Factor
$\arg(a_1, \cdots, a_n)$	Argument of $a_1, \cdots, a_n$
$\mathrm{diag}(a_1, \cdots, a_n)$	$n \times n$ diagonal matrix with on-diagonal elements $a_1, \cdots, a_n$
$\max(a_1, \cdots, a_n)$	Maximum of $a_1, \cdots, a_n$
$\mathrm{tr}(\mathbf{X})$	Trace of a matrix $\mathbf{X}$

Chapter 1

Introduction

This chapter introduces some basic definitions, presents the motivation, provides the contributions of this work, and outlines the organisation of this thesis.

1.1 MIMO Systems

Wireless communication systems consisting of a transmitter, a radio channel, and a receiver, are classified by their input and output ports [4]. The simplest formation is a single antenna at both sides of the radio channel, denoted as single input single output (SISO) system. Systems with multiple antennas on the receive side only are called single input multiple output (SIMO) systems and systems with multiple antennas at the transmitter side and a single antenna at the receiver side are called multiple input single output (MISO) systems. The multiple input multiple output (MIMO) system is the most universal mode of a wireless communication system, and includes SISO, MISO, SIMO systems as particular cases. Thus, the acronym MIMO will be used in general for multiple antenna systems. The equivalent baseband signal model for narrowband stationary MIMO system shown in Fig. 1.1 is given by

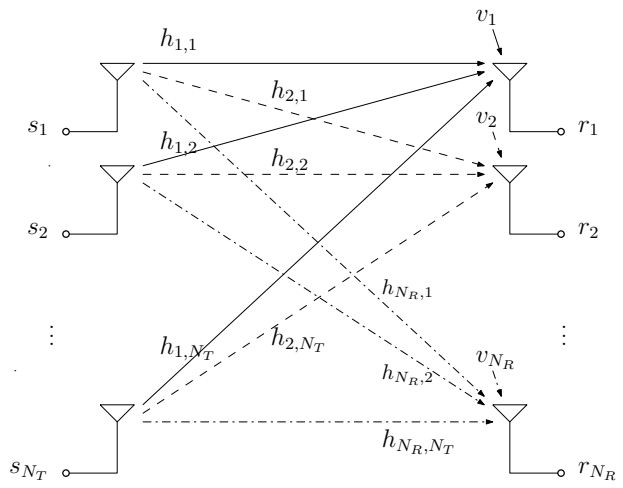

Figure 1.1: MIMO system with N_T transmit and N_R receive antennas

$$\mathbf{R} = \mathbf{HS} + \mathbf{V}, \tag{1.1}$$

assuming channel $\mathbf{H}$ is to be constant for the entire T channel uses; therefore, $\mathbf{S}$ is the $N_T \times T$ transmitted matrix and is often normalized to satisfy a transmit-power constraint

$$\mathcal{E}\left\{\mathrm{tr}\left(\mathbf{SS}^{\mathrm{H}}\right)\right\} = 1, \tag{1.2}$$

where $\mathcal{E}\{\cdot\}$ denotes statistical expectation, $(\cdot)^{\mathrm{H}}$ denotes Hermitian operation, and $\mathrm{tr}(\cdot)$ stands for the trace of a matrix. $\mathbf{R}$ is the $N_R \times T$ received matrix, and $\mathbf{V} \in \mathbb{C}^{N_R \times T}$ is the additive zero mean circular white Gaussian noise (AWGN) with zero mean and unit variance.

The channel matrix is $\mathbf{H} \in \mathbb{C}^{N_R \times N_T}$ with entry $h_{i,j}$ represents the complex channel fade coefficient between the i-th transmit antenna and j-th receive antenna given as

$$\mathbf{H} = \begin{bmatrix} h_{1,1} & h_{1,2} & \cdots & h_{1,N_T} \\ h_{2,1} & h_{2,2} & \cdots & h_{2,N_T} \\ \vdots & \vdots & \cdots & \vdots \\ h_{N_T,1} & h_{N_T,2} & \cdots & h_{N_T,N_R} \end{bmatrix} \tag{1.3}$$

Recently, new products based on MIMO technology have been adopted for a number of practical applications in IEEE standards such as wireless personal area networks (WPANs), wireless local area network (WLAN), Wireless Metropolitan area networks (WMAN), wireless wide area networks (WAN), and other standards such as third generation partnership project (3GPP), long term evolution (LTE), and LTE-advanced (LTE-A).

With various configurations of MIMO, the spatial dimension can be exploited to improve wireless system performances such as capacity, range, and reliability [5] [6] [7]. Due to increasing demand for high data rate services, the wireless infrastructure is required to deliver an increasingly transmission rate at a suitable quality of service (QoS). Moreover, mobile devices are required to deal with excessively high data rate demands, to combat fading through diversity, and to conserve transmitted power and bandwidth which are scarce resources.

Multipath propagation causes interference, which generally leads to degraded performance. However, MIMO employs multiple, spatially separated antennas to take advantage of multipath occurring in wireless channel [8]. MIMO can offer spatial multiplexing (SM) and spatial diversity (SD) with feasible bandwidth and adequate power consumption [9] [10]. SM techniques provide high data rate with multiple data streams transmitted in a MIMO channel at the same time. In addition, space time transmit diversity (STTD) can provide MIMO diversity gains [11]. Furthermore, MIMO can trade off between throughput and QoS without any increase either in the bandwidth or in the transmitted power.

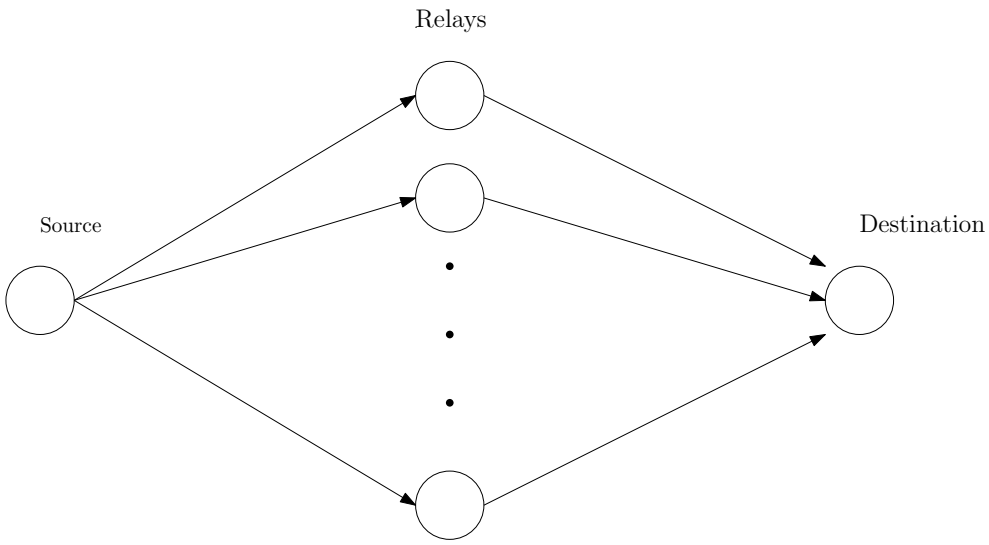

Figure 1.2: A basic wireless relay structure.

Nowadays, wireless systems aim to deliver simultaneously speed, coverage, and reliability improvements. The receiving end uses signal processing to collect signals received over different transmit paths by different antennas to produce one combined signal that resembles the originally transmitted signal. Such coherent combining needs to estimate channel state information (CSI) between MIMO antennas at the receiving end [12]. Moreover, pre-processing at the transmitter with MIMO precoding is a technique that can be used to maximise capacity and reliability of the system [13]. Practically, the receiver can send quantised CSI to the transmitter through a limited feedback link [14], such as in precoded space-time block coding where the transmitter can use this information to further improve the system performance [15] [16].

1.1.1 Virtual MIMO

In practice, wireless transceiver systems may be unable to support multiple antennas due to limitations such as size, cost, and hardware. However user devices can collaboratively operate as a virtual MIMO system [17] [18]. Virtual MIMO

can be achieved by using antennas of different users acting as relays for each other, exploiting independent paths between the transmit and receive antennas to provide MIMO advantages. Fig. 1.2, shows a basic wireless relay structure.

The wireless communication applications and design are mainly related to the power use and communication range [19] [20]. Accordingly, distributed antennas on multiple radio devices can be utilised to group multiple devices into virtual antenna arrays [21] [22]. Such technique enables cooperative diversity, which can achieve diversity gain with even one antenna per relay node. In cooperative MIMO, which is a special case of cooperative diversity, it has been found that wireless relay networks can extend the coverage through using other terminals or relays and reduce the need to use high power at the transmitter or source terminal by split the available time slot into two or more phases [23]. Such technique can achieve MIMO gains in both transmitter and receiver even with one antenna per relay node such that sending group and receiving group in an ad-hoc networks or sensor networks.

The transmissions can be performed in broadcasting and relaying phases over time orthogonal channels through conventional half-duplex relaying, which is easy for implementation. Generally, relaying strategies can be either decode-and-forward (DAF) or amplify-and-forward (AAF). In DAF relaying systems, the relay fully decodes the broadcast signal and retransmits the decoded symbol to the destination [24]. In contrast, AAF relaying systems simply amplify the broadcast signal and forward it to the destination, which may therefore include any noise from the source to relay link. Performance bounds for two-way half-duplex AAF relaying techniques have been studied in [25]. Distributed STBC (D-STBC) can achieve significant diversity gain when applied either at end terminals, each equipped with more than one antenna, or at multiple relay nodes so that a transmit diversity order is achieved [26].

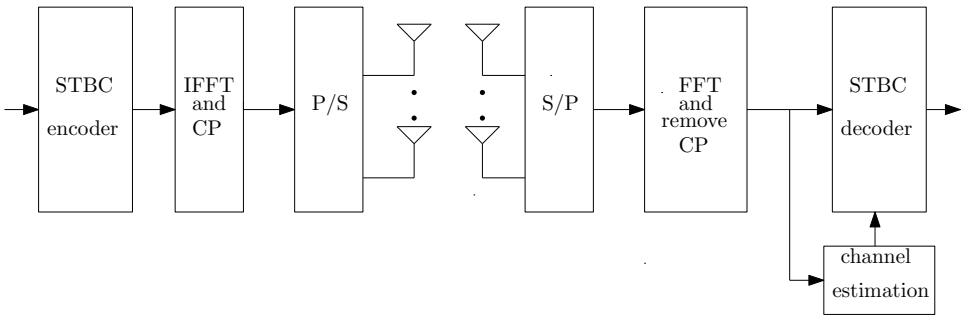

Figure 1.3: A basic MIMO OFDM structure.

1.1.2 MIMO OFDM

The benefits of narrowband MIMO techniques can be utilised for wideband or alternatively broadband communication systems when coupled with multicarrier transmission. Given the frequency selectivity of the broadband channel, the basic idea of multi-carrier transmission is to turn the wide-band frequency selective wireless channel into a set of frequency-flat narrowband channels. As a consequence, the complexity of any equalisation technique for stationary frequency-selective channel reduces considerably to a single tap channel equaliser [27] [28] [29].

The combination of MIMO techniques with OFDM is very powerful, a basic MIMO OFDM structure based on space-time block coding (STBC) is shown in Fig. 1.3. OFDM forms the basis of wireless local area network (WLAN) standards IEEE 802.11a, IEEE 802.11g, mobile-WiMAX, IEEE 802.16e, and the downlink of the 3GPP long term evolution (LTE). The main principle of OFDM is to time-multiplex data over a channel. The time-multiplexed system is characterised by system matrix, which through the inclusion of a cyclic prefix (CP) the matrix becomes circulant. The resulting circulant matrix is then decoupled through IFFT/FFT operation in the transmitter and receiver respectively. This works as long as the cyclic prefix is more or equal to the order of the channel and is able

to suppress both ISI and ICI in the case where OFDM is perfectly synchronised. In the case of synchronisation errors or transmission over a doubly-dispersive, the system is no longer orthogonal and the resulting ISI and ICI need to be taken into account.

1.1.3 Transmit-Diversity

Antenna diversity effectively mitigates the adverse impact of multipath fading in MIMO channels. The transmission performance over a Rayleigh fading wireless channel is significantly degraded in a deep fade even at high transmitted power. Antenna diversity techniques, which make use of an array of spatially separated antennas, can protect against deep fades [30]. Spatial diversity gain due to redundancy, is characterised by the number of independently fading branches between different transmit-receive antenna pairs, known also as diversity order, and is equal to the product of the number of transmit and receive antennas.

Transmit diversity is applicable to channels with multiple transmit antennas. This technique has been widely adopted in practice and has become an active research area [15]. The drawback of receive diversity is that most of computational burden is on the receiver side, which may incur high power consumption [31]. One of the attractive ways to exploit the multiple transmit antennas is to use STBC [32] [33]. STBC requires CSI knowledge and their combining at the receiver gives full diversity gain. Moreover, if transmitter knows the CSI, adaptive STBC (ASTBC) can further maximis the SNR at the receive antenna by weighting each transmit antenna's signal with the conjugate of the respective channel coefficient and gives maximal ratio combining (MRC) performance [34].

The common combining scheme for STBC is a matched filter (MF). This maximises SNR of desired signal in additive white Gaussian noise such that the resultant power of the signal at the receiver is maximised. Therefore, received

signals are combined coherently in presence of known CSI to the receiver. Which requires CSI to enhance system performance by given that independent received signals with different amplitudes and phases as determined by the propagation conditions [35]. Transmit diversity using STBC can be advantageous to offer a diversity gain with a simple implementation for MIMO system.

1.1.4 Space-Time Block Coding (STBC)

STBC is a MIMO transmit strategy which exploits transmit diversity. For STBC, data symbols are encoded in both the time domain and the spatial domain. Originally proposed by [32] orthogonal STBC (O-STBC) for two transmit antennas and one receive antenna, can achieve full diversity gain and code rate one. The scheme known as Alamouti STBC is easy to implement and use, and as a result has been included in e.g. the wideband-code division multiple access (W-CDMA) standard [36]. Generalisations of Alamouti's STBC in [37] are the case of three antennas or more with code rate less than one. Such block codes and their maximum likelihood (ML) decoding metrics have been presented in [37] [33].

Space time trellis coding (STTC) can achieve both coding and diversity gain, but this advantage is achieved with higher encoding and decoding complexity where transmitter and receiver perform in more complicated way. In contrast, O-STBC is designed such that the transmitter has no knowledge of the CSI and the receiver has a low complexity decoding. Further, the extended orthogonal STBC (EO-STBC) for more than two transmit antennas can provide diversity plus an additional array gain by exploiting CSI at the transmitter side with lower complexity than STTC.

O-STBC performance can be further improved by incorporating CSI knowledge that can be exploited at the transmitter side, such as precoded Alamouti and EO-STBC with optimum beamsteering angles [38].

1.1.5 Mobile Wireless Channel

The performance of mobile communication systems depends to a large extent on the nature of the wireless channel [39], which impairs the signal by a number of effects, including channel noise, time-selective fading, and frequency-selective fading.

Channel noise is undesired random disturbance of received signal, which can be considered here as linear addition of white noise with a constant spectral density so called additive white Gaussian noise (AWGN). This can be represented by a random constant complex-valued coefficient, where its real and imaginary parts are the independent and identically-distributed (i.i.d.) Gaussian random variables with a zero mean and variance of σ^2.

The variation of the signal amplitude over time known as temporal fading can be broadly classified into two different types; long-term fading and short-term fading. Long-term fading is caused by path loss due to distance as well as shadowing by large objects, which results in reflection, diffraction, and scattering [40]. Short-term fading refers to rapid variation of signal levels caused by fluctuations of constructive and destructive interference of multiple propagations paths over short distances. The used channels over mobile transmission model are time-varying. Depending on the mobile speed, the maximum Doppler spread is inversely related to the channel coherence time and quantify the time selectivity of the channel.

The system with high data rates in mobile communications is typically affected by multi-path with delay spread relative to the symbol duration, which is inversely related and quantify the frequency selectivity of the broadband channel. The received signal over individual path is represented by the relative power of each path with respect to the power of the earliest path, which can be modelled by the power delay profile (PDP).

In doubly-dispersive channel, the time-dispersion can be modelled as a tap delay line (TDL) with power delay profile (PDP) such as in [41]. Moreover, Doppler spectrum determines the frequency-dispersion that can be modelled using filtering Gaussian white noise (FWGN) or Jake's models. Jake's model has been originally developed for the hardware simulation, where a large number of sinusoids have to be added to approximate the Doppler spectrum for a Rayleigh fading channel. Each complex sinusoid weighted to generate the desired Doppler spectrum while the FWGN is implemented by appropriately designed filters to capturing the important first and second order channel statistics. For spatially uncorrelated channel, the output of independent FWGN generators is multiplied by each tap power of PDP to produce coefficients of the channel impulse response.

1.2 Motivation of Research

This research is directed at applying closed loop EO-STBC over time-varying channels for a point to point [42] [38] [43] and for relaying system [44] [45]. In particular, aim to enhance the diversity gain in the presence of quantised feedback. Therefore, the investigations, enhancements, and modifications that are required to achieve low computational complexity will be addressed.

One of the design difficulties of EO-STBC systems with quantised feedback is to achieve near optimum performance using only one or two bits per feedback parameter. This topic has received attention in quasi-static fading channel conditions, where [46] achieves enhanced performance compared to open-loop scheme performance with two feedback bits. Here, the first objective is to investigate the effect that quantisation in the feedback channel has on the system performance. Secondly, considering slowly time-varying channel conditions and motivated by the smooth evolution of channel coefficients over time, we aim to attain maximum gain by developing a novel differential feedback. Moreover, due to limited

feedback bandwidth we are looking to reduce feedback bits to only one bit for each feedback parameter compared to [46]. This design with near optimum performance and very low feedback overhead is an attractive option to the practical wireless applications.

Channel state information (CSI) should be available at the receiver in order to calculate a suitable set of steering angles estimation. Therefore, the investigation of channel and tracking schemes need to be considered. Based on the smooth evolve of channel coefficients over time, we have followed channel estimation and tracking scheme based on the Kalman filter, which performs joint channel tracking and EO-STBC data detection. The Kalman filter tracking efforts are aided by periodically injected pilot symbols for training to prevent divergence. This scheme is referred to as decision-directed (DD) updating [47] [48] [49]. The smooth channel variation motivates the use of a higher order auto-regressive model (AR-M) within the Kalman filter for a priori prediction step within DD estimation method. Simulation results indicate that using of second order AR can further improve the performance for a longer tracking period over standard first order AR model used in [49].

In frequency-selective channel conditions, narrowband EO-STBC can be applied within a multicarrier system. Cross-talk between subcarriers due to synchronisation errors or time variation of the channel has motivated cross-talk detectors for EO-STBC receiver. We aim to applied these detectors over near-stationary channel conditions for enhancing the diversity gain of an closed-loop EO-STBC multicarrier system.

Additionally, for non-stationary channel conditions, we aim to generalise standard OFDM multicarrier using DFT/FFT operation to one based on the fractional Fourier transform (FrFT).

1.3 Research Contribution

The contributions of this thesis are concerned with a simple EO-STBC scheme with two angles feedback for four transmit antennas and one receive antenna. We force our contributions for real environment of wireless mobile network when transmitting is performed over time-varying channel, with realistic Doppler spreads. Therefore, they are listed as follows:

1. A new feedback scheme applying differential feedback is implemented in Doppler-fading environments and then compared to the previous uniform quantisation feedback. In order to evaluate the proposed scheme, diversity and array gain with various feedback bits for the uniform quantisation feedback are conducted through simulation. Moreover, a mathematical formula for the maximum attainable gain is derived. This maximum attainable gain is used as benchmark to show the limitations of uniformly quantised feedback. The design parameters that affect the differential feedback in the optimum case, the difficulties in implementation and the required processing are described in details. Near optimum performance and a significant further reduction in feedback overhead compared to [46] can be achieved by our proposed scheme.

2. A Kalman filter tracking technique with an auto-regressive AR-2 model is proposed for combining differential feedback with channel estimation in the presence of beam-steering. The main difficulties in reliably tracking the channel coefficients arises from the fact the channel coefficients are seen with beamsteering angles applied, and only through the EO-STBC decoding process. The later, with its processing across two successive symbol periods introduces a greater degree of time variation than what experienced in a single symbol period. This leads to adaptations of the Kalman technique

specific to our EO-STBC problem.

3. The cross-talk detectors for near-stationary channel conditions proposed in [3] are adopted here for a multicarrier system FrFT-OFDM based on closed-loop EO-STBC transmission. In conventional O-STBC decoding, the channel is assumed stationary over two time slot. However, in the framework of a near-stationary channel, ICI terms can be ignored by using only the elements on the main diagonal of the channel matrix, and thus considered as additive noise. Motivated by a related approach for Alamouti OSTBC in [3] using a receiver based on cross-talk detectors, we adopt this idea for open-loop and closed-loop EO-STBC schemes in order to maximise both diversity and array gain.

4. An equalisation scheme for non-stationary doubly-dispersive channel conditions is proposed which aims to mitigate ISI and ICI in fast time-varying environment. We use a minimum mean square error (MMSE) equaliser. This equaliser increases the receiver complexity, but removes the need for feedback of angles to the transmitter. Moreover, near-banded structure of the resulting equivalent channel matrix of the FrFT-multicarrier system admits MMSE equalisation with low complexity using a recently proposed least squares minimum residual (LSMR) implementation with a considerably lower number of iterations compared to alternative state-of-the-art techniques.

1.4 Thesis Organisation

An introduction and brief summary of MIMO systems, space-time coding, and mobile wireless channel has been presented in Chapter 1. The remainder of the thesis is divided into the following additional chapters.

Chapter 2 provides an overview of precoded Alamouti as well as EO-STBC schemes [38]. Closed-loop techniques associated with EO-STBC are presented, and the signal model throughout the forward system structure and reverse feedback link is reviewed. In this context, one and two-phase feedback methods are evaluated with basic uniform quantised feedback for various number of feedback bits [46]. BER performances of Alamouti, precoded Alamouti, QO-STBC, and EO-STBC systems are compared.

Chapter 3 proposes a new feedback scheme based on differential encoding that aims to achieve near optimum performance while reducing feedback bits. The maximum diversity gain of EO-STBC for a four transmit antenna system is derived. We investigate how the smoothness of channel coefficients translates into the smoothness of feedback angle trajectories, and how in turn smoothness of the feedback angle trajectory in EO-STBC affects the implementing of proposed differential feedback scheme. Therefore, the impact of Doppler spread and variation of angles is evaluated. Before investigating the performance of EO-STBC with the proposed scheme, step size optimisation of coders under Doppler spread constraints is conducted through simulations. The results show that the proposed scheme is a powerful tool when compared to non differential feedback scheme.

Chapter 4 addresses linking between differential feedback and channel estimation, and presents approaches to channel estimation and tracking via a Kalman filter employing a DD estimation method, which can offer symbol by symbol joint decoding and tracking. To take the time-varying nature of the channel into account, a Kalman model for the specific characteristics of a pre-steered EO-STBC encoded channel is presented. The benefits of the proposed scheme are highlighted in simulations, and discussed.

Chapter 5 proposes the enhancement of the EO-STBC when transmitting over a doubly-dispersive channel where the frequency selective nature of the channel

favours the combination with a multicarrier approach such as OFDM. In near-stationary channel condition scenario, cross-talk receivers in [3] have been used for an EO-STBC scheme. However, for non-stationary channel conditions, OFDM loses its orthogonality, resulting in severe ICI. This is addressed firstly by the generalisation of OFDM to FrFT-based multicarrier approaches, which can provide better resilience in the non-stationary case. Secondly, an MMSE equalisation scheme is adopted whos lower complexity in the FrFT due to an approximation of the channel matrix as banded matrix is complemented by a recently proposed iterative LSMR algorithm which is suited to solve sparse equalisation problems. Simulation results are presented, highlighting the potential performance improvements under the consideration of computational complexity.

Chapter 6 includes a summary and conclusions, along with a suggestion of potential areas for future work.

Chapter 2

Space-Time Block Coding Exploiting CSI at the Transmitter Side

This chapter provides an overview of Alamouti orthogonal space-time coding (O-STBC) schemes that exploit channel state information (CSI) at the transmitter in order to further improve their performances as compared to non-CSI approaches in terms of bit error ratio (BER). In particular, we review an extended orthogonal STBC (EO-STBC) system whos diversity gain can be enhanced by appropriate beamsteering. Depending on the availability of CSI at the transmitter, the phase angles used for beamsteering are either calculated locally at the transmitter or need to be fed back in a closed-loop architecture from the receiver. Such EO-STBC systems with phase rotation will be used for the remainder of this thesis with the aim to achieve near optimum performance with a minimum feedback overhead.

The organisation of this chapter is as follows. Sec. 2.2 introduces Alamouti's STBC code. Then, the basics of a precoded Alamouti scheme are presented in

Sec. 2.3. After that, in Sec. 2.4 EO-STBC with single phase and two phase rotation algorithms are reviewed based on optimum feedback. Sec. 2.5 compares the various approaches in simulations in terms of BER performances using BPSK for simplicity and without loss generality, and Sec. 2.6 summarises the chapter.

2.1 Introduction

Space-time block coding (STBC) is a MIMO transmit strategy which exploits transmit diversity. Amongst various STBC schemes [32] [37] [33], Alamouti or orthogonal STBC (O-STBC) for two transmit antennas has low decoding complexity, and with a complex constellation, it can achieve full diversity gain at a code rate equal to one. When extending O-STBC to 3 or more transmit antennas, it is no longer possible to simultaneously achieve both full diversity gain and full code rate, resulting in codes rate lower than one [37]. However, [38] have presented a simple design for group-coherent codes based on an extension method to utilise STBC codes for more than two transmit antennas referred as extended orthogonal STBC (EO-STBC). In EO-STBC, the rate loss is replaced by a marginal loss in the form of feedback, which extends the Alamouti scheme to more than two antennas while preserving full diversity benefits, full data rate, and low decoding complexity.

Linear precoding with different matrix sizes can be combined with STBC to efficiently improve the diversity order of the MIMO system [16]. Such linear precoding matrices based on the full CSI are quite time-consuming and not straightforward for the general MIMO case [50]. However, an approach based on the codebook that is shared by the transmitter and receiver, can solve the Grassmannian packing problem that allows to condense a set of unitary matrices that can be used for precoding to only few parameter [51] [52] [53]. Many studies have been carried out to find low rate feedback methods, one particular design method

is to use unitary linear precoding matrices such as the Fourier, Vandermonde or complex Hadamard matrices [54]. Further, [55] has proposed a suboptimal practical design method derived from a DFT matrix modified by a codebook approach and is popularly used in e.g. the long term evolution (LTE) standard using a coarse code book approach [56]. However, a simple phase rotation scheme based on feedback has been widely used in different STBC approaches such as [42] in order to obtain full diversity gain. Phase feedback has been suggested as a way to combine space-time block codes over groups of antennas to ensure the full diversity advantage from an arbitrary number of transmit antennas at full rate [38]. Thus, phase rotation can provide a significant improvement in BER performance of space-time coded systems.

Quasi-orthogonal STBC (QO-STBC) has been introduced as a new family of STBCs. These codes achieve full rate at the expense of a slightly reduced diversity gain [33]. The cause of the diversity loss is due to some coupling term between the estimated symbols, since these codes typically introduce interference require decoders with high complexity. However, constellation rotation was proposed for QO-STBC in order to mitigate interference between symbols to attain full code rate and full diversity [57] at the cost of an increase in system complexity. Moreover, construction of QO-STBC approach with minimum decoding complexity has been proposed in [58]. Depending on the phase feedback, QO-STBC using four transmit antennas achieves full diversity gain and full code rate [42].

It is beneficial to achieve better system performance with a lower feedback rate and fewer computations. Most closed-loop diversity techniques require the feedback information to be complex-valued matrices or vectors of the quantised channel state information (CSI) [55]. With the availability of quantised feedback with finite rate, closed loop transmit diversity schemes for five or six transmit antennas have been proposed in [59]. Adaptive STBC (ASTBC) uses a number of

feedback bits B to adjust the power of each transmit antenna. This technique in general requires $B = N_T \log_2(L)$ bits of feedback where N_T is the number of transmit antennas, and L denotes the number of quantisation levels [14]. Therefore some bandwidth in the reverse link will be consumed by the feedback information. To maximise bandwidth efficiency, the feedback rate from the receiver to the transmitter, should be kept as small as possible. Moreover, the computational complexity increases with the number of transmit antennas.

In previous work on ASTBC systems over quasi-stationary channels, where the same symbols are transmitted from all the transmit antennas, phase constraining feedback is proposed in [60]. In the reverse link, a finite rate feedback can be used to return an appropriate phase for each antenna. In order to reduce feedback bits, a quadrant phase constraining feedback method can be computed at the receiver based on the phases $\vartheta_i,\ i = 1 \cdots N_T$ of the estimated CSI. The angles' differences, restricted to $|\Delta\vartheta_{ij}| \leq \frac{\pi}{2}\ \ i \neq j$, can be fed back with only $2N_T - 2$ bits of feedback information. Systems with N_T transmit antenna achieve enhanced system performance with less feedback information compared to ASTBC in [14].

EO-STBC for an arbitrary number of transmit antennas inherits low decoding complexity and also can achieve rate one coding, and full diversity gain plus array gain. EO-STBC replaces the bandwidth rate loss of O-STBC by a marginal loss in the form of feedback, while still preserving full performance [38]. Closed loop EO-STBC has been proposed in [46] for 4 transmit antennas and one receive antenna using a phase beamsteering that provides an improvement in BER performance with less feedback information over above the ASTBC systems. Moreover, the bandwidth loss due to feedback is negligible compared to O-STBC are equipped with four transmit antennas and use code rate 1/2 .

EO-STBC is therefore is a promising technique with one or two phases feedback using 4 transmit antennas, which can achieve better system performance

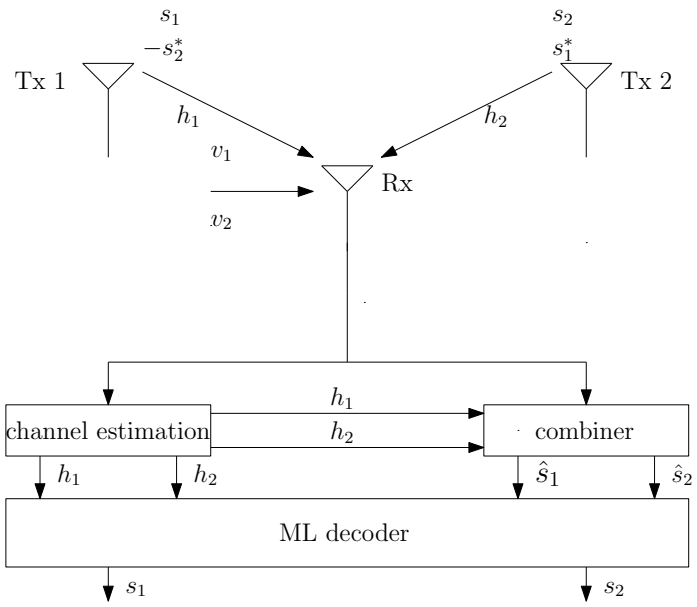

Figure 2.1: A block diagram of the Alamouti space-time scheme.

with lower a feedback rate and lower computational complexity than other four-antenna STBC schemes. In this thesis, we will focus on advancing EO-STBC techniques, firstly in terms of further reducing feedback aiming to minimise performance loss, and secondly by introducing EO-STBC schemes suitable for time-varying and ultimately doubly-dispersive channels. As a foundation for this work, the remainder of this chapter will focus on the review of various STBC approaches that are relevant in the context of our proposed schemes.

2.2 Alamouti Scheme

In this section, we briefly review the well-known Alamouti O-STBC scheme [32] for two transmit antennas and one receive antenna as shoen in Fig. 2.1, which is designed for an open loop scheme over quasi-stationary blocks. During the first time period, symbols s_1 and s_2 are sent from transmit antenna 1 and 2 respectively. Then,$-s_2^*$ and s_1^* are sent from transmit antenna 1 and 2 respectively

during the second time period, which can be described by a code matrix, where the columns of the matrix represent the transmit antennas, and the rows are the time (symbol) periods as

$$\mathbf{S} = \begin{bmatrix} s_1 & s_2 \\ -s_2^* & s_1^* \end{bmatrix}. \tag{2.1}$$

Matrix in (2.1) satisfies the following constraint,

$$\mathbf{S}\mathbf{S}^{\mathrm{H}} = \left(|s_1|^2 + |s_2|^2\right) \mathbf{I}_2, \tag{2.2}$$

where I_2 is a 2×2 identity matrix. This property enables the receiver to detect s_1 and s_2 separately by a simple operation [32]. When the single receive antenna case is considered with a quasi-stationary channel over one STBC-block, assuming $h_i, \;\; i = 1, 2$, the receiver collects samples over two successive time slots as

$$\begin{aligned} r_1 &= h_1 s_1 + h_2 s_2 + v_1 \\ r_2 &= -h_1 s_2^* + h_2 s_1^* + v_2 \end{aligned} \tag{2.3}$$

which can be stacked into a 2×1 vector as

$$\begin{bmatrix} r_1 \\ r_2 \end{bmatrix} = \mathbf{S} \begin{bmatrix} h_1 \\ h_2 \end{bmatrix} + \begin{bmatrix} v_1 \\ v_2 \end{bmatrix}, \tag{2.4}$$

where $\mathbf{S}$ is the code matrix in (2.1), and $[\; v_1 \quad v_2 \;]^{\mathrm{T}}$ is the equivalent noise vector over two successive time slots. The noise samples are independent, zero-mean circularly symmetric and Gaussian additive white. Alternately, by conjugating the second row, this system of equations can be represented equivalently as

$$\begin{bmatrix} r_1 \\ r_2^* \end{bmatrix} = \mathbf{H} \begin{bmatrix} s_1 \\ s_2 \end{bmatrix} + \begin{bmatrix} v_1 \\ v_2^* \end{bmatrix}. \tag{2.5}$$

The equivalent channel matrix has an orthogonal structure [32], which is due to the fact the transmitted symbol block has an orthogonal structure, and can be written as

$$\mathbf{H} = \begin{bmatrix} h_1 & h_2 \\ h_2^* & -h_1^* \end{bmatrix}. \tag{2.6}$$

Assuming perfect channel knowledge at the receiver, symbols can be decoded via a matched filter by applying multiplication of $\mathbf{r}$ by $\mathbf{H}^{\mathrm{H}}$

$$\hat{\mathbf{s}} = \mathbf{H}^{\mathrm{H}}\mathbf{r} = \begin{bmatrix} |h_1|^2 + |h_2|^2 & 0 \\ 0 & |h_1|^2 + |h_2|^2 \end{bmatrix} \begin{bmatrix} s_1 \\ s_2 \end{bmatrix} + \tilde{\mathbf{v}}, \tag{2.7}$$

which is equivalent to maximum ratio combining. From (2.7), it can be seen that the noise samples get combined incoherently as $\tilde{\mathbf{v}}_n = \mathbf{H}^{\mathrm{H}}\mathbf{v}_n$, while symbols can be detected coherently. Moreover, the decoupled diagonal structure of (2.7) means that the two symbols can be detected independently, and transmitted symbols are weighted by an on-diagonal element $\alpha = |h_1[n]|^2 + |h_2[n]|^2$, which represent the diversity gain. The use of Alamouti can be generalised to cases with more than one receive antenna [37]. Therefore, Alamouti O-STBC has the benefits of both a simple decoding structure and a full diversity gain with code rate one.

2.3 Precoded Alamouti

One of the numerous extensions to STBC is the use of precoding matrices at the transmitter side called precoded Alamouti, which is of interest here for comparing with EO-STBC with beamsteering angles. A precoder can be combined with Alamouti codewords to improve the space-time diversity order of the multiple antenna system, whereby the codeword matrix is multiplied by the precoding matrix before being passed to the transmit antennas.

Consider the MISO system with N_T antennas, that is, $\mathbf{h} \in \mathbb{C}^{1\times N_T}$. Let $\mathbf{S}$ denote a matrix of STBC codewords with a length of M and $M \leq N_T$. In the precoded Alamouti system, let the codeword $\mathbf{S}\in \mathbb{C}^{M\times M}$ is multiplied by a precoding matrix $\mathbf{F} \in \mathbb{C}^{N_T\times M}$. This precoding matrix is chosen from a codebook $\mathcal{F} = \left\{ \begin{array}{cccc} \mathbf{F}_1 & \mathbf{F}_2 & \cdots & \mathbf{F}_L \end{array} \right\}$. Note that the received signal for a given channel can be expressed as

$$\mathbf{r} = \mathbf{h}\mathbf{F}_l\mathbf{S} + \mathbf{v}, \tag{2.8}$$

where $\mathbf{v} \in \mathbb{C}^{1\times M}$ is zero mean uncorrelated complex Gaussian noise with variance σ_v^2. The objective is to select an appropriate precoding matrix $\mathbf{F}_{\text{opt}}$ that improves the overall system performance. Using the orthogonal property of the Alamouti code, a selection criterion can be implemented by computing a matrix multiplication and Frobenius norm for each of the L codebook matrices. This leads to choose the precoder according to

$$\mathbf{F}_{\text{opt}} = \arg \max_{\mathbf{F}_l\in\mathcal{F}} \left\{ \|\mathbf{H}\mathbf{F}_l\|_F^2 \right\}. \tag{2.9}$$

2.3.1 Precoding with DFT Matrices

In practical design cases, a suboptimal method for an arbitrary N_T transmit antennas can be used for a codeword length M code-book and size L with a number of feedback bits $B = \log_2(L)$. The code book $\mathcal{F}$ uses unitary linear precoding matrices constructed with discrete Fourier transform (DFT) matrices [55]. The code book $\mathcal{F}$ can be given by considering codebooks of the form

$$\mathcal{F} = \left\{ \begin{array}{cccc} \mathbf{F}_{\text{DFT}} & \mathbf{F}_{\text{DFT}} & \cdots & \mathbf{\Theta}^{L-1}\mathbf{F}_{\text{DFT}} \end{array} \right\}, \tag{2.10}$$

whereby the first codeword $\mathbf{F}_{\mathrm{DFT}}$ is obtained by selecting M columns from the DFT matrix, and further $\mathbf{\Theta}$ is a unitary diagonal matrix. This matrix $\mathbf{\Theta}$ is given by

$$\mathbf{\Theta} = \mathrm{diag}\left\{ \; e^{j2\pi u_1/L} \quad e^{j2\pi u_2/L}, \quad \cdots \quad e^{j2\pi u_{N_T}/L} \; \right\}, \tag{2.11}$$

where variables $\{u_i\}$, $i = 1 \cdots N_T$ referred as rotation vector. Given the first codeword $\mathbf{W}_{\mathrm{DFT}}$, the remaining $(L-1)$ codewords are obtained by multiplying $\mathbf{F}_{\mathrm{DFT}}$ by $\mathbf{\Theta}_i$, $i = 1, 2, \cdots, L-1$. The values of the rotation vector are to be determined such that the minimum chordal distance is maximised, which is the distance between two points located on a curve. This is given as

$$\mathbf{u} = \arg \max_{\{u_1 \; u_2 \cdots u_{N_T}\}} \min_{l=1,2,\cdots L-1} \mathrm{d}\left(\mathbf{F}_{\mathrm{DFT}}, \mathbf{\Theta}^l \mathbf{F}_{\mathrm{DFT}}\right). \tag{2.12}$$

Thus, there are different L^{N_T} possibilities for $\mathbf{\Theta}$ that must be checked. Clearly, this method requires the feedback bits $\mathbf{B} = N_T \log_2(L)$. Alternatively, reduction in the feedback overhead can be made through the EO-STBC transmission scheme designed based on the phase angle feedback.

2.4 ExtendedOrthogonal-Space-Time Block Codes

Among various possible methods that use CSI for the diversity system, we will focus on an extension method that can be used for systems with an arbitrary number of transmit antennas proposed in [38]. It is worth pointing out that EO-STBC can balance between the system performance and the computational complexity related to the feedback processing as will be shown later. One particular EO-STBC design extends Alamouti O-STBC to 4 transmit antennas. In this

case, the Alamouti codeword in (2.1) is repeated twice such that the combined diversity gain and array gain can be achieved. The EO-STBC code word matrix can be written as

$$\mathbf{S}_2 = \zeta \begin{bmatrix} s_1 & s_1 & s_2 & s_2 \\ -s_2^* & -s_2^* & s_1^* & s_1^* \end{bmatrix}, \tag{2.13}$$

where $\zeta = \frac{1}{2}$ is a constant normalisation factor. Note that if we assume that the channel coefficients over two consecutive symbol periods are time-invariant then the EO-STBC codeword $\mathbf{S}_2$ in (2.13) is orthogonal. In this case, symbols can be detected independently using (2.7). The 4 antennas channel paths h_i, $i = 1 \cdots 4$, are assumed to be independent zero-mean complex Gaussian random variables with variance σ_h^2 and considered constant over two time slots.

The received signal collected over two time slots is the sum of the propagation signals from all 4 transmit antennas weighted by the channel coefficients and additive white Gaussian noise (AWGN) with variance σ_v^2. The received signal over two time slots is

$$\begin{aligned} r_1 &= \tfrac{1}{2}\left[h_1 s_1 + h_2 s_1 + h_3 s_2 + h_4 s_2\right] + v_1\,, \\ r_2 &= \tfrac{1}{2}\left[-h_1 s_2^* - h_2 s_2^* + h_3 s_1^* + h_4 s_1^*\right] + v_2\,. \end{aligned} \tag{2.14}$$

Similar to (2.4) and (2.5), we can rewrite (2.14) into matrix notation as

$$\begin{bmatrix} r_1 \\ r_2^* \end{bmatrix} = \mathbf{H} \begin{bmatrix} s_1 \\ s_2 \end{bmatrix} + \begin{bmatrix} v_1 \\ v_2^* \end{bmatrix}, \tag{2.15}$$

where $\mathbf{v} = [\ v_1 \quad v_2^*\ ]^{\mathrm{T}}$ is the equivalent noise vector, and $\mathbf{H}$ is the equivalent

channel matrix which can be implemented as

$$\mathbf{H} = \begin{bmatrix} h_1 + h_2 & h_3 + h_4 \\ h_3^* + h_4^* & -h_1^* - h_2^* \end{bmatrix}. \tag{2.16}$$

Here $\mathbf{H}$ contains channel coefficients corresponding to h_n, $n = 1 \cdots 4$. Decoding can be performed through simple matched filtering as in (2.7). In STBC systems, the channels are normally considered block stationary. Writing the diagonal elements of $\mathbf{H}^{\mathrm{H}}\mathbf{H}$ in terms of diversity α and array gain β, we obtain

$$\mathbf{H}^{\mathrm{H}}\mathbf{H} = \frac{1}{4}(\alpha + \beta)\,\mathbf{I}_2 \tag{2.17}$$

$$\alpha = \sum_{m=1}^{4} |h_m|^2 + \sum_{m=3}^{4} |h_m|^2 \tag{2.18}$$

$$\beta = 2\Re\{h_1 h_2^* + h_3 h_4^*\}, \tag{2.19}$$

where $|\cdot|^2$ denotes the modulus squared of a complex number and $\Re\{\cdot\}$ the real part. It is clear that interference between channels introduced by β can be forced to be positive with optimum angles feedback based on phase rotation at the transmitter in which case a significant array gain can be achieved [46].

2.4.1 Closed-Loop Scheme

2.4.1.1 Single-Phase Rotation

Based on feedback from the receiver, a single rotation angle ϑ is applied to rotate signals from the first and third antennas. The actual effect of the angle ϑ can be absorbed into the channel coefficients because the phase rotation on the channel coefficients is equivalent to rotating the phases of the corresponding transmitted symbols. Hence, the equivalent channel matrix $\mathbf{H}$ with a single absorbed rotation

angle ϑ becomes

$$\mathbf{H} = \begin{bmatrix} e^{j\vartheta}h_1 + h_2 & e^{j\vartheta}h_3 + h_4 \\ e^{-j\vartheta}h_3^* + h_4^* & -e^{-j\vartheta}h_1^* - h_2^* \end{bmatrix}. \tag{2.20}$$

With $\mathbf{H}^{\mathrm{H}}\mathbf{H}$ being diagonal independent of the rotation angle ϑ, the array gain β in (2.19) can be driven to a positive value if we select ϑ such that all the summed elements of β are positive,

$$\beta = 2\Re\{(h_1h_2^* + h_3h_4^*)\, e^{j\vartheta}\}. \tag{2.21}$$

It can be seen that β is to be positive with a real part when the feedback angle ϑ is determined as

$$\vartheta[n] = -\angle\{h_1h_2^* + h_3h_4^*\}, \tag{2.22}$$

where $\vartheta \in [0, 2\pi)$ is to be fed back from the receiver to the transmitter. This guarantees a positive feedback array gain, which however would generally be lower than maximum attainable gain. This method has been proposed to reduce the feedback whereby the transmitter needs to provided only one phase angle.

2.4.1.2 Two-Phase Rotation

It is possible to further increase the β compared to Sec. 2.4.1.1 by rotating the signals transmitted from the first and third antennas independently by ensuring that the angles ϑ_1 and ϑ_2. This will provide advantages in terms of diversity and array gain, but requires to feedback the two angles.

Below we demonstrate how is technique can be applied to 4 transmitter antennas. The equivalent channel matrix $\mathbf{H}$ with absorbed ϑ_1 and ϑ_2 can be expressed as

$$\mathbf{H} = \begin{bmatrix} e^{j\vartheta_1}h_1 + h_2 & e^{j\vartheta_2}h_3 + h_4 \\ e^{-j\vartheta_2}h_3^* + h_4^* & -e^{-j\vartheta_1}h_1^* - h_2^* \end{bmatrix}. \tag{2.23}$$

Consequently, factor β can be written as,

$$\beta = 2\Re\{h_1 h_2^* e^{j\vartheta_1}\} + 2\Re\{h_3 h_4^* e^{j\vartheta_2}\}, \tag{2.24}$$

where the phase rotations for antenna one and three essentially result in a new set of channel coefficients. It can be seen that β is maximum when the feedback angles ϑ_1 and ϑ_2 are determined as

$$\vartheta_1 = -\angle\{h_1 h_2^*\} \tag{2.25}$$

$$\vartheta_2 = -\angle\{h_3 h_4^*\}. \tag{2.26}$$

According to [1], the optimum steering parameters can be selected and appropriately fed back to the transmitter, e.g. via a quantised feedback link. Next we are going to find the combined diversity and array gain attainable with B information bits per feedback angle.

2.4.1.3 Uniform Quantisation

Due to the bandwidth limitations, generally, feeding back the exact actual value of the phase angles requires too much a feedback overhead. Therefore, quantised feedback needs to be practically applied. A quantiser, as defined here, acts as a function that maps a real valued phase angle onto a set of discrete finite values, where with B feedback bits we can realise only 2^B level.

In this approach, phase angles are computed at the receiver side, and rather than feeding back the full CSI, only B feedback bits containing the quantised phase values are returned. The expression to obtain uniform quantisation across

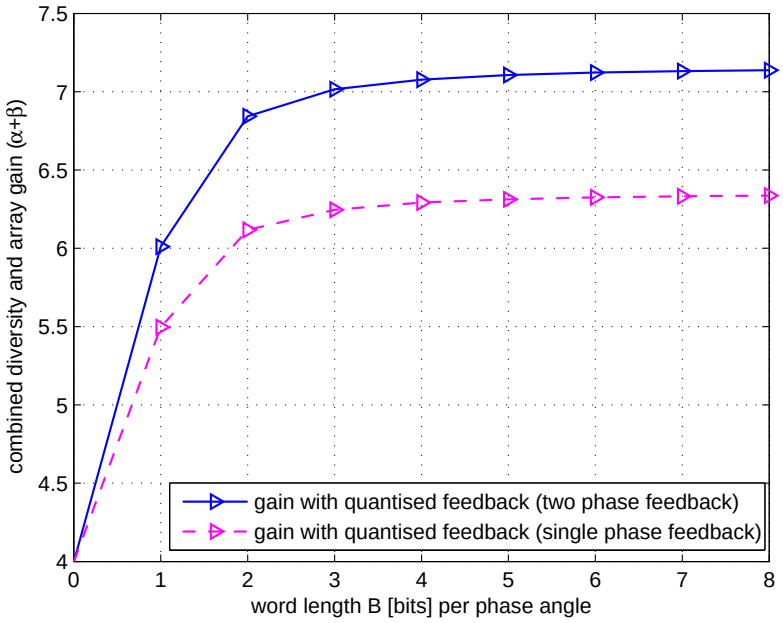

Figure 2.2: Comparing of combined diversity and array gain for a 4×1 EO-STBC system for quantised feedback of the optimum single angles ϑ and and two angles$\{\vartheta_1, \vartheta_2\}$ with variable word length B.

the entire range $\vartheta_i \in [-\pi; \pi)$ can be viewed as

$$\left\{\bar{\vartheta}_i\right\}_{i=1}^{2^B} = \left\{\frac{(2b-1)\pi}{2^B}\right\} \quad \forall i \in \{1,\ 2\},\ b = 0, 1, \ldots (2^B - 1). \tag{2.27}$$

With the above analysis, the feedback angle ϑ_i is determined at the receiver based on the estimated channel. The receiver selects the closest index, and B information bits are returned, to be used as beamsteering angles at the transmitter side.

2.4.1.4 Comparing Phase Rotation Beamsteering

This section presents simulation results for quantised feedback of one or two phase feedback using B bits. Simulation are performed over of an ensemble of 10^5, 4×1 MISO channels with uncorrelated complex Gaussian coefficients, variance $\sigma_h^2 = 1$.

Fig. 2.2 shows the effect of increasing the word length B from 0 bit (open loop scheme) to 8 bits on combined diversity and array gain. For $B = 0$, the ensemble averaged results show that the open loop scheme only provides diversity gain. For higher B, the maximum attainable gain is around 7, which can be reached by the two phase feedback, while single phase feedback method consistently only reaches a lower diversity. The gain of around 7 is the maximum value attainable by two phase feedback, which consists of a maximum diversity gain equal to 4, and an array gain with maximum value of around 3.

There are two choice of feedback single or two angles, when using single phase aim for reducing feedback bits B, and two phases can achieve maximum attainable gain. We concentrate our attention on a new differential feedback can reduce feedback bits B, for the sake of approaching the maximum attainable gain, two phase feedback will be considered in Chapter 3.

2.5 Comparison of BER Performances

In this section, we present simulation results for comparing BER performances with BPSK for systems introduced in this chapter. Channels are considered to be spatially uncorrelated whose coefficients are independent and identically distributed (i.i.d.) complex Gaussian random variables with zero mean and unit variance. Moreover, perfect channel estimation is assumede at the receiver.

2.5.1 BER Performance of Receive and Transmit Diversity Schemes

Firstly, we compare and contrast transmit and receive diversity. Fig. 2.3 shows the BER performances of various receive and transmit diversity schemes for BPSK systems. It can be seen that Alamouti O-STBC achieves the same diversity order

as 1×2 SIMO with MRC technique. Moreover, we can see that the 2×2 O-STBC technique achieves the same diversity order as 1×4 SIMO with MRC technique. However, it should be noted that MRC technique outperforms O-STBC technique due to a total transmit power split into each antenna by one half in the O-STBC transmission scheme. Compared to SISO channel performance, receive and transmit diversity schemes with MIMO channel can be effectively used for improving the BER performance.

2.5.2 BER Performance of Precoded Alamouti

Fig. 2.4 shows the BER performance of precoded Alamouti O-STBC using the design method in (2.10) with $N_T = 4$, $M = 2$, and $L = 64$ as given in [54]. Fig. 2.4 compares the performance of Alamouti O-STBC in [32] to precoded Alamouti O-STBC in a Rayleigh fading channel. It has been shown that the precoded Alamouti O-STBC scheme outperforms the traditional Alamouti O-STBC scheme without increasing transmit power or increasing spectral bandwidth. However, it may require complete or partial CSI at the transmitter side, which is not easily achievable in practice mainly due to the limited bandwidth of the feedback link. It is desirable to maximise diversity gain while reducing the number of feedback bits. Therefore, EO-STBC with optimum feedback has nearly the same performance as will be shown below, but with less feedback overhead.

2.5.3 BER Performance of EO-STBC

The feedback approach presented in Sec. 2.4.1.2 can be also applied with full-rate QO-STBC in order to orthogonalise its channel matrix [42]. Therefore, in Fig. 2.5 we show the BER performance of QO-STBC with optimum two feedback angles in addition to EO-STBC. This comparison considers open-loop and closed-loop EO-STBC schemes. The results show that the EO-STBC closed loop scheme

significantly outperforms the EO-STBC open-loop scheme. In addition, the EO-STBC closed loop scheme outperforms the closed-loop QO-STBC, whereby both systems require the same amount of feedback.

2.6 Conclusion

In this chapter, we have introduced Alamouti's O-STBC system. In particular, we have considered systems based on the phase angle feedback such as precoded O-STBC and EO-STBC with optimum feedback. We have provided basic definitions for EO-STBC system, which offers a good trade-off between performance, complexity, and feedback overhead, and will form the major system to be investigated and further developed in different scenarios.

We observe that with the aid of feedback the studied systems provide a significant performance enhancement in terms of BER over standard open loop O-STBC approaches at the expense of feedback overhead. Single phase and two phase feedback have been investigated and compared in terms of combined diversity and array gain, and results demonstrate that the two phase method can provide maximum gain with less feedback overhead compared to other types of transmit diversity system such as precoded O-STBC system.

The next chapter will present a new feedback scheme based on differential feedback that will be able to achieve near optimum performance with a reduced number of feedback bits compared to methods reported in this chapter.

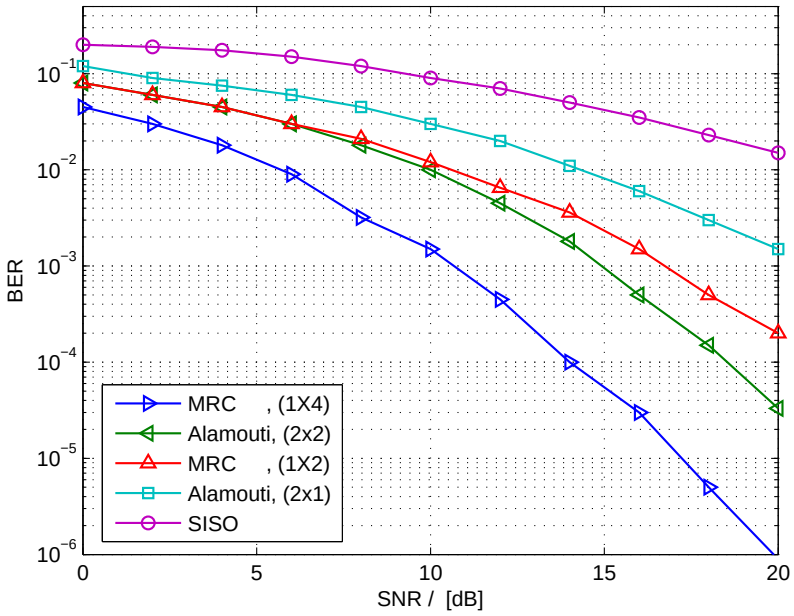

Figure 2.3: BER performance of of various receive and transmit diversity schemes.

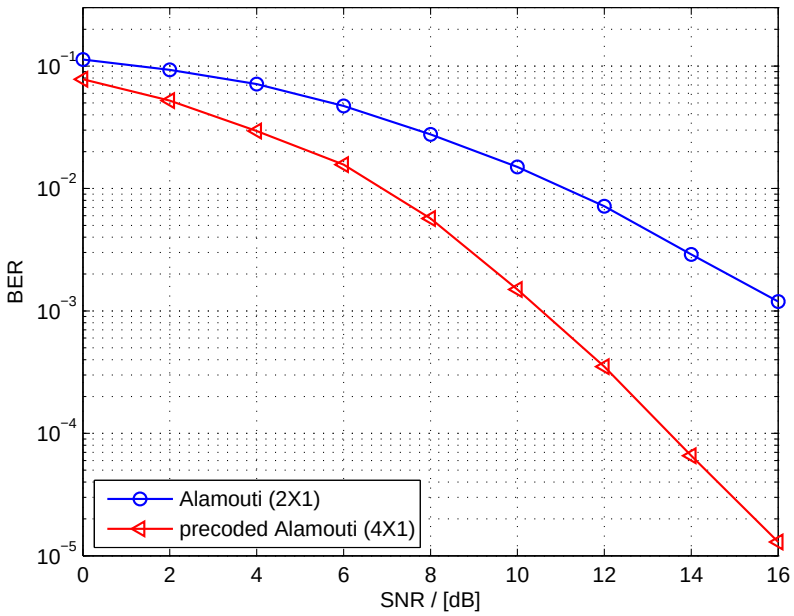

Figure 2.4: BER performance of OSTBC with and without precoding in Rayleigh fading channel.

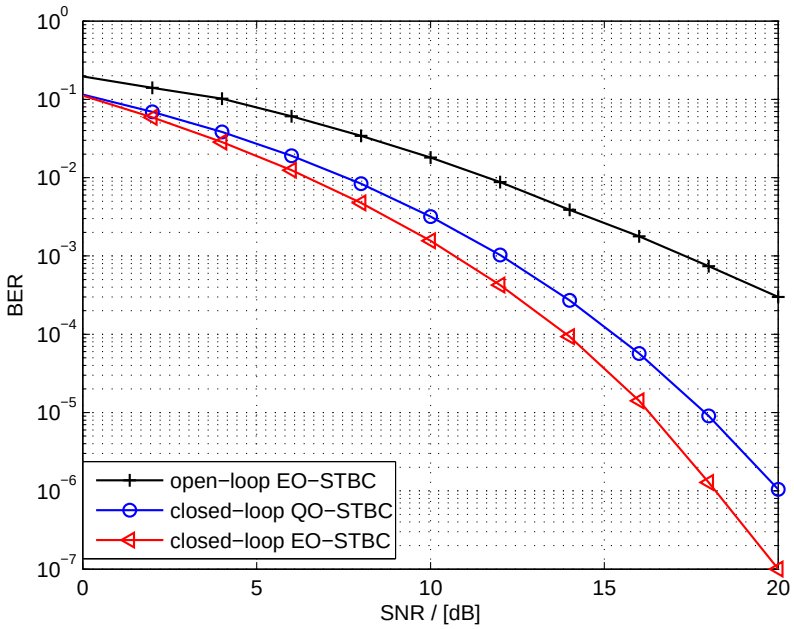

Figure 2.5: Comparison of average BER performance enhancement by two-phase rotation.

Chapter 3

Differential Feedback Scheme for EO-STBC System

This chapter shows how to compute the maximum attainable gain for a two-phase rotated extended-orthogonal STBC (EO-STBC) system. Moreover, the effect that uniform quantisation in the feedback channel has on the system performance is evaluated and compared through simulations. In particular, this chapter introduces a new differential feedback scheme, which quantises the relative difference between neighbours. This scheme is developed to attain maximum diversity gain, motivated by the smooth evolution of time-varying channel coefficients. Assuming such a smooth evolution of channel coefficient trajectories, our objective is to obtain near optimum performance by differential feedback based on a finite rate feedback. Depending on Doppler spread conditions, it is shown that with only one bit feedback the proposed scheme can achieve a near optimum performance even in situations of high Doppler spread.

After the introduction in Sec. 3.1, EO-STBC transmission over a time-varying channel is outlined in Sec. 3.2, and the maximum gain is analysed. In Sec. 3.3, differential feedback is presented. The proposed scheme is introduced by checking

how the smoothness of coefficient trajectories translates into smoothness of the angle in the EO-STBC scheme. Then the possibility of performing differential encoding assuming perfect channel estimation is outlined. The performance of the proposed system is benchmarked against standard quantised feedback in Sec. 3.4, before conclusions are drawn in Sec. 3.5.

3.1 Introduction

In transmit diversity such as for antenna selection, code selection or beam-steering, feedback has been applied via a reverse link in frequency division duplex (FDD) mode when the feedback delay is less than the channel coherence time. Practically, the feedback link has a limited bandwidth so that only a few feedback bits B are to be returned to the transmitter. Hence, for such applications finite rate feedback is to be used to reduce the amount of feedback [61], which can be achieved by a quantised feedback scheme. Differential multilevel quantisation have been discussed in [62] to reduce the number of feedback bits required. Differential pulse code modulation (DPCM) can be used to encode the feedback for time varying channel information [63]. Depending on maximum Doppler spread, we discuss the design of the differential quantiser for beamsteering angles such that the the diversity gain of the extended O-STBC scheme is maximised.

As given previously in Chaper 2, EO-STBC transmission, enhanced by phase rotation beam-steering, can offer full diversity gain plus additional array gain [38]. In situations with large coherence time [64], instantaneous values of the two phase angles for beam-steering, can be finely quantised and sent back to the transmitter over the feedback channel. In [46], it has been shown that the optimum angle being quantised to $B = 2$ bits precision in the feedback channel leads to no significant degradation over an unquantised, optimal closed loop operation, aiming to halve the feedback bandwidth compared to [1] without loss in performance. The

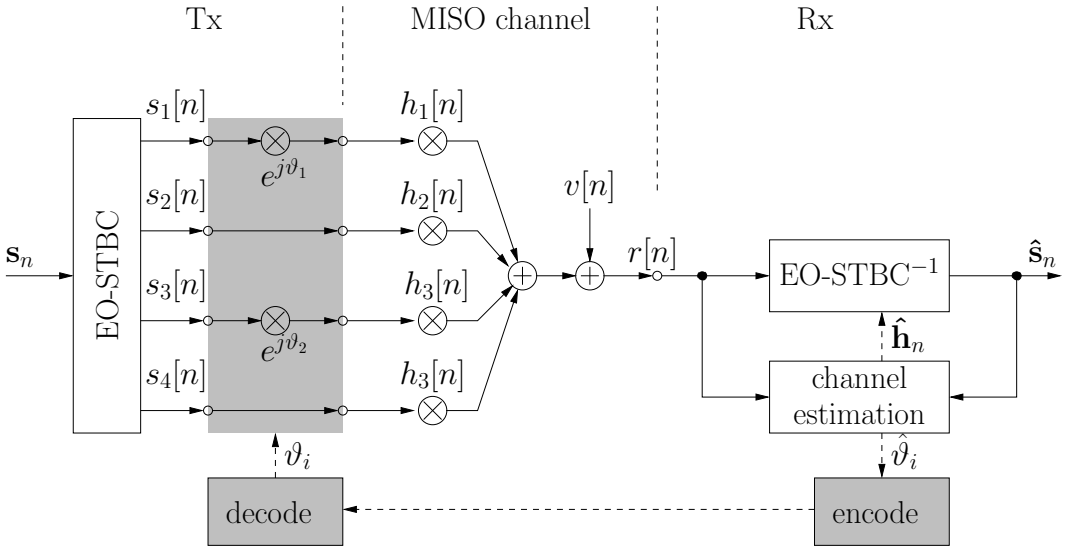

Figure 3.1: EO-STBC system with perfect channel estimation in the receiver to aid symbol detection and computing of the optimum beam-steering angles ϑ_1 and ϑ_2, which are differentially encoded and returned to the transmitter.

BER performance of the proposed EO-STBC system is evaluated through simulations. Simulation results over realistic Doppler spread confirm that the proposed scheme achieves bandwidth savings and near optimum performance over systems which uses non differential feedback.

3.2 System Model

In this section we introduce the downlink behaviour for point to point transmission. For simplicity, EO-STBC is to be used over four transmitters and one receiver, giving a model for a MISO system. The feedback link is required to return information on the steering angles ϑ_1 and ϑ_2, with which the first and third antenna signal are modified as required by EO-STBC. By judiciously selecting these angles based on knowledge of the channel at the receiver, the combined diversity and array gain of the system can be maximised. Further we consider that a limited feedback link is available from the receiver to the transmitter in

the form of a minimum of B bits per frame/channel coherence period.

Consider the point-to-point EO-STBC structure as shown in Fig. 3.1. For simplicity, let the equivalent baseband forward received signal $r[n]$ at time slot n be characterised by

$$r[n] = \mathbf{h}_n^{\mathrm{T}} \mathbf{\Lambda}_n \mathbf{s}_n + v[n], \tag{3.1}$$

where $\mathbf{s}_n$ is the transmit data vector, $\mathbf{\Lambda}_n$ is a unitary diagonal matrix included feedback angles, and $v[n]$ is zero mean uncorrelated complex Gaussian noise with variance σ_v^2. Further, the MISO channel $\mathbf{h}_n \in \mathbb{C}^4$ contains i.d.d wide-sense stationary (WSS) Rayleigh fading channel, which will be characterised further below. The transmitting antennas are assumed to be placed sufficiently far apart from each other so that symbols transmitted from each antenna follow different uncorrelated paths to the receiver. In practice, the transmitting antennas are spatially correlated by an amount that depends on the propagation environment as well as on the polarisation of the antenna elements and the spacing between them. In mobile communications environment, the channel gains are considered time-variant. We assume a slow fading process as a consequence of the slow motion of surrounding objects. The channel coefficients in $\mathbf{h}_n = [h_1[n]\ h_2[n]\ h_3[n]\ h_4[n]]^{\mathrm{T}}$ are varying smoothly over time. Their maximum variation is determined by the maximum normalised angular Doppler spread $\Omega_D = 2\pi f_D / f_s$, measured in radians, with Doppler frequency f_D and sampling rate f_s. Here $f_D = v f_c / c\,[\mathrm{Hz}]$, where v is the mobile speed in meters per second [m/s], f_c is the carrier frequency, and c is the speed of light (3×10^8[m/s]). The well known Doppler spectrum [40] is given by

$$R_i(e^{j\Omega}) = \sum_{m=-\infty}^{\infty} \mathcal{E}\left\{h_i[n] h_i^*[n-m]\right\} e^{-jm\Omega} \tag{3.2}$$

$$= \begin{cases} \frac{2}{\Omega_D \sqrt{1-\left(\frac{\Omega}{\Omega_D}\right)^2}} & , \quad |\Omega| < \Omega_D \\ 0 & \Omega_D \leq |\Omega| \leq \pi. \end{cases} \tag{3.3}$$

Encoding and decoding is processed over two successive symbol periods so that we consider a transmit vector per time slot that includes four elements one element per each transmit antenna. The selection of the transmit vector $\mathbf{s}_n$ for two successive time slots is determined by EO-STBC,

$$\mathbf{s}_n = \frac{1}{2} \begin{bmatrix} s[n] \\ s[n] \\ s[n+1] \\ s[n+1] \end{bmatrix}, n \text{ even} \quad \text{, and } \mathbf{s}_n = \frac{1}{2} \begin{bmatrix} -s^*[n] \\ -s^*[n] \\ s^*[n-1] \\ s^*[n-1] \end{bmatrix}, n \text{ odd.} \tag{3.4}$$

At the receiver, two successively received samples are collected in a vector

$$\begin{bmatrix} r[n] \\ r^*[n+1] \end{bmatrix} = \mathbf{H}_n \cdot \begin{bmatrix} s[n] \\ s[n+1] \end{bmatrix} + \mathbf{v}_n. \tag{3.5}$$

In (3.5), $\mathbf{H}_n$ is the equivalent channel transfer matrix containing linear combinations of the channels and their conjugates. The noise is assumed to be uncorrelated additive Gaussian with variance $\mathcal{E}\left\{\mathbf{v}_n \mathbf{v}_n^{\mathrm{H}}\right\} = \sigma_v^2 \mathbf{I}_2$. For deriving the maximum attainable gain, it is assumed that the channel remains stationary over one transmit block. In addition, we assume that the receiver can perfectly estimate the channels from each transmit antenna $\mathbf{h}_n = [\ h_1[n] \quad h_2[n] \quad h_3[n] \quad h_4[n]\ ]^{\mathrm{T}}$.

3.2.1 Open Loop Scheme

For the open loop scheme, when transmitting is without beam-steering, the diagonal matrix $\mathbf{\Lambda}_n$ given in (3.1) is a 4×4 identity matrix. We assume that the receiver has perfect knowledge of $\mathbf{H}_n$. This consideration guides the linear decoding process, which can be performed by multiplying the received vector in (3.5) by $\mathbf{H}_n^{\mathrm{H}}$. The equation for estimating the decision variable $\hat{\mathbf{s}}_n$ from $\mathbf{r}_n$ is therefore given by

$$\hat{\mathbf{s}}_n = \mathbf{H}_n^{\mathrm{H}}\mathbf{r}_n = \mathbf{H}_n^{\mathrm{H}}\mathbf{H}\mathbf{s}_n + \mathbf{H}_n^{\mathrm{H}}\mathbf{v}_n. \tag{3.6}$$

Since $\mathbf{H}_n^{\mathrm{H}}\mathbf{H}_n$ is diagonal, (3.7) can be verified that the code can be decoded with a simple receiver [32].

$$\mathbf{H}_n^{\mathrm{H}}\mathbf{H}_n = \begin{bmatrix} \alpha+\beta & 0 \\ 0 & \alpha+\beta \end{bmatrix}. \tag{3.7}$$

For the on-diagonal terms of (3.7), the diversity gain α,

$$\alpha = \sum_{m=1}^{4} |h_m[n]|^2 \quad , \tag{3.8}$$

is fixed given the channel gains of the MISO system, while β,

$$\begin{aligned} \beta &= (h_1[n]h_2^*[n] + h_3[n]h_4^*[n]) \\ &+ (h_1[n]h_2^*[n] + h_3[n]h_4^*[n])^* \quad , \end{aligned} \tag{3.9}$$

can make a positive or negative contribution, depending on the specific values of the channel coefficients. If β is positive, it corresponds to a type of array gain.

With $z + z^* = 2\Re\{z\}$ where $\Re\{\cdot\}$ its real part of a complex valued variable z,

the term β simplifies to

$$\beta = 2\Re\{h_1[n]h_2^*[n] + h_3[n]h_4^*[n]\}. \tag{3.10}$$

In (3.8), α is the conventional diversity gain with

$$\mathcal{E}\{\alpha\} = 4\sigma_h^2 \tag{3.11}$$

based on σ_h^2 being the variance of a circularly symmetric, complex Gaussian distributed random channel coefficient.

The additional term β in (3.9), even though $\mathcal{E}\{\beta\} = 0$, cannot be directly controlled and will potentially degrade the diversity gain if e.g. its value is negative for a specific set of channel coefficients. In order to ensure its value is maximised, the additive components in (3.10) need to be controlled in the transmitter by e.g. inclusion of appropriate steering angles, whose valued has to be determined at and fed back from the receiver.

3.2.2 Closed Loop Scheme with Optimum Two-phase Feedback

The EO-STBC system includes the selection of feedback angles $\{\vartheta_1, \vartheta_2\}$, performing beam-steering at the transmitter based on a precoding matrix

$$\mathbf{\Lambda}_n = \begin{bmatrix} e^{j\vartheta_1} & 0 & 0 & 0 \\ 0 & 1 & 0 & 0 \\ 0 & 0 & e^{j\vartheta_2} & 0 \\ 0 & 0 & 0 & 1 \end{bmatrix}, \tag{3.12}$$

which applies a phase rotation to the first and third transmit antenna signals as indicated in Sec. 2.4.1.1.

3.2.3 Maximum Attainable Gain

In this section, we derive the maximum attainable gain of the system shown in Fig. 3.1. Decoding can be performed through simple matched filtering using $\mathbf{H}_n^{\mathrm{H}}$, which has been shown to be equivalent to ML decoding [65]. Decoding with $\mathbf{H}_n^{\mathrm{H}}$ leads to the detected symbol vector

$$\begin{bmatrix} \hat{s}[n] \\ \hat{s}[n+1] \end{bmatrix} = \mathbf{H}_n \mathbf{H}_n^{\mathrm{H}} \begin{bmatrix} s[n] \\ s[n+1] \end{bmatrix} + \mathbf{H}_n \mathbf{v}_n \tag{3.13}$$

$$= (\alpha+\beta) \begin{bmatrix} s[n] \\ s[n+1] \end{bmatrix} + \tilde{\mathbf{v}}_n, \tag{3.14}$$

where the noise covariance yields $\mathcal{E}\left\{\mathbf{v}_n \mathbf{v}_n^{\mathrm{H}}\right\} = (\alpha+\beta)\sigma_v^2\mathbf{I}$. The term $(\alpha+\beta)$ reflects the combined diversity and array gain at the receiver with

$$\alpha = \sum_{i=1}^{4} |h_i[n]|^2 \tag{3.15}$$

$$\beta = 2\Re\{h_1[n]h_2^*[n]e^{j\vartheta_1}\} + 2\Re\{h_3[n]h_4^*[n]e^{j\vartheta_2}\}. \tag{3.16}$$

Equation (3.16) is derived form of (3.10), where the angles ϑ_i, $i = \{1,2\}$ have been introduced in [1] due to the observation of increasing the combined array gain and diversity gain beyond a factor of 4by ensuring that the term β is positive and maximised. Referred to as enhanced EO-STBC in [1], the optimum steering

coefficients are selected as

$$\vartheta_1 = -\angle\{h_1 h_2^*\} \tag{3.17}$$

$$\vartheta_2 = -\angle\{h_3 h_4^*\}, \tag{3.18}$$

which maximises the gain β to

$$\max_{\vartheta_1,\vartheta_2} \beta = 2|h_1| \cdot |h_2| + 2|h_3| \cdot |h_4|. \tag{3.19}$$

In the case of selecting ϑ_i optimally, the mean for $\mathcal{E}\{\beta\}$ can be rewritten as

$$\mathcal{E}\left\{\max_{\vartheta_1,\vartheta_2} \beta\right\} = 4\mathcal{E}\{|h_i| \cdot |h_j|\}, \tag{3.20}$$

where h_i and h_j are circularly symmetric independent complex Gaussian random variables with variance σ_h^2, i.e. $\Re\{h_i\} \sim \mathcal{N}(0, \frac{1}{2}\sigma_h^2)$ and $\Im\{h_j\} \sim \mathcal{N}(0, \frac{1}{2}\sigma_h^2)$, such that $|h_i|$ and $|h_j|$ are Rayleigh distributed with scale parameter $\sqrt{\frac{1}{2}}\sigma_h$. According to [66], if Y is the product of P independent Rayleigh distributed random variables, then the first moment is

$$\mathcal{E}\{Y\} = (2^P \sigma_Y^2)^{\frac{1}{2}} (\sqrt{\pi}/2)^P \quad , \tag{3.21}$$

where $\sigma_Y = \prod_{i=1}^{P} \sigma_X$ with σ_X the scale parameter of the distribution of X.

Therefore, using (3.21) with $P = 2$ and $\sigma_Y = \frac{1}{2}\sigma_h^2$, we can write

$$\mathcal{E}\left\{\alpha + \max_{\vartheta_1,\vartheta_2} \beta\right\} = (4 + \pi)\sigma_h^2 = 3.1415 \cdot \sigma_h^2 \quad , \tag{3.22}$$

such that by beam steering with two optimally selected angles ϑ_1 and ϑ_2, the combined diversity and array gain is almost doubled with respect to the standard full diversity EO-STBC scheme according to (3.11). This result has also been

reached experimentally in [1]. Thus the SNR, assuming the total transmit power to be $4\sigma_s^2$, is given by

$$\text{SNR} = (4+\pi)\sigma_h^2 \frac{\sigma_s^2}{\sigma_v^2}. \tag{3.23}$$

Note that with the optimum feedback chosen as in (3.16), it is possible to maximise SNR by just about twice the value of the open loop scheme.

3.2.4 Combined Diversity and Array Gain with Quantised Feedback

The standard approach to quantising a value is to resolved into a fixed grid. However, such a process can be coarse and therefore leads to diversity loss w.r.t. (3.22). Here we compare gain-based uniform quantised feedback with the maximum gain in (3.22). The maximum attainable gain is achievable if the transmission system offers perfect feedback of the optimum angle values ϑ_1 and ϑ_2 to the transmitter, which is the ideal case derived in (3.2.3).

Fig.3.2 shows both the gain in dependency of the word length B, as well as the asymptote for unquantised feedback according to (3.22). Comparing this feedback method with the maximum attainable gain, a significant loss is incurred for $B = 1$ while feedback with angles ϑ_1 and ϑ_2 quickly approaches the asymptote as B increases. For values $B \geq 7$, the system is seen to approach the optimal performance.

3.3 Differentially Encoded Feedback

In order to save word length B while sacrificing as little performance as possible, we propose to use differential quantised feedback. For a slowly time-varying channel, we first investigate whether the smooth variation of channel coefficients translates into a smooth variation of ϑ_1 and ϑ_2. Thereafter we discuss differential

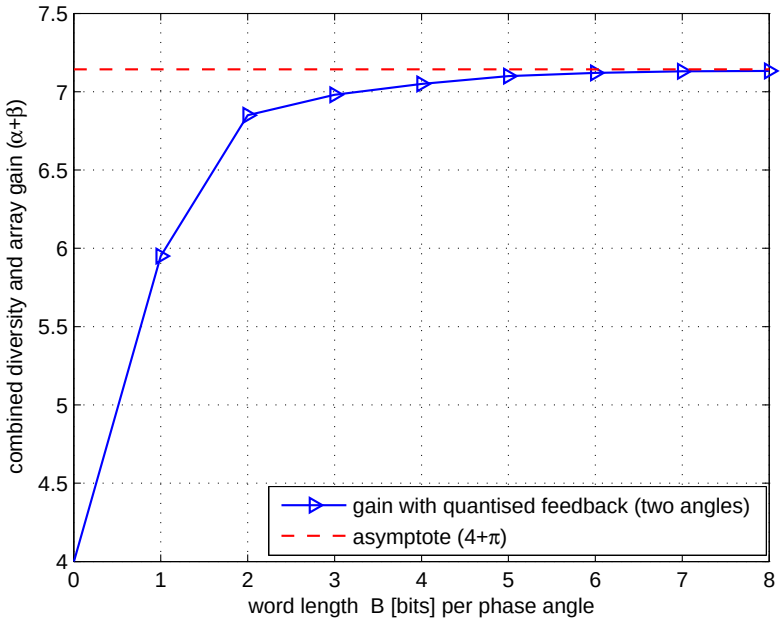

Figure 3.2: Combined diversity and array gain for a 4×1 EO-STBC system according to [1] for quantised feedback of the optimum angles ϑ_1 and ϑ_2 with variable word length B.

coding approaches for both angles.

3.3.1 Doppler Spread and Variation of Angles

In this subsection we investigate the smoothness of feedback angle in a slowly time-varying system. The maximum rate of change in a channel coefficient $h_i[n]$ is governed by the maximum Doppler shift Ω_D. In the time domain, each coefficient $h_i[n]$ follows a smooth trajectory in the complex plane. The trajectory of angles $\vartheta_1[n]$ and $\vartheta_2[n]$ are not as smooth as the coefficients for two reasons. Firstly, the angle can be prone to phase jumps by 2π, which can be suppressed by unwrapping the angle suitably. Secondly, if a coefficient trajectory passes close to the origin, then a rapid phase change by π will be experienced, which cannot be mitigated.

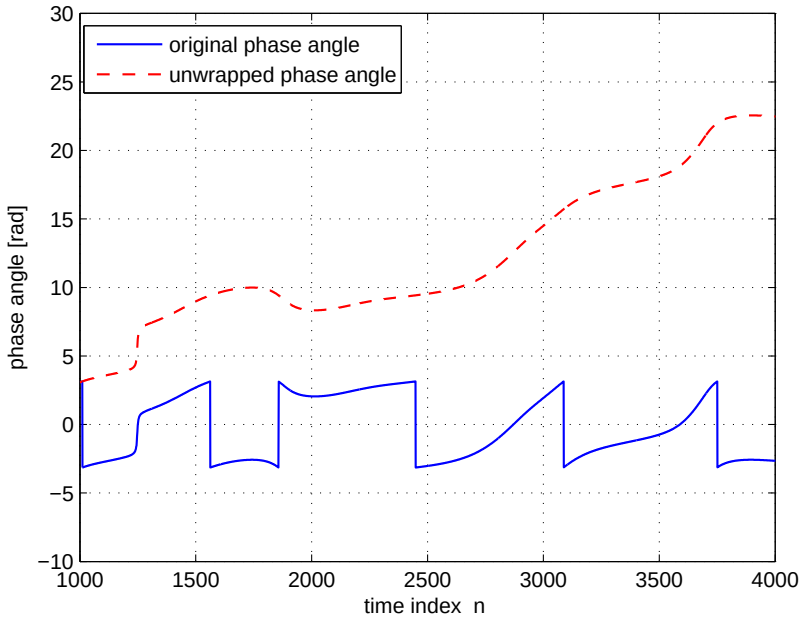

Figure 3.3: Time-varying optimum angle ϑ_1 as a result of fading of the coefficient $h_1[n]$ and $h_2[n]$ with $\Omega_D = 0.003\pi$.

3.3.1.1 Unwrapping Angles

As an example, Fig. 3.3 shows $\vartheta_1[n]$, which is initially restricted to $\vartheta_1[n] \in [-\pi; \pi)$, and as a consequence demonstrates discontinuities which lead to overloading if encoded differentially. After unwrapping the phase, such discontinuities are suppressed. However at around time instance $n = 1250$, a rapid change by π can be observed, which arises from close proximity of a coefficient trajectory, either $h_1[n]$ or $h_2[n]$ in the case of $\vartheta_1[n]$, to the origin, which therefore unwrapping cannot resolve it.

3.3.2 Differential Coding

Standard differential coding uses a linear predictor, whose coefficients need to be transmitted along with the residual prediction error. In order to avoid the overhead of feeding back coefficients, we use a simple difference between adjacent

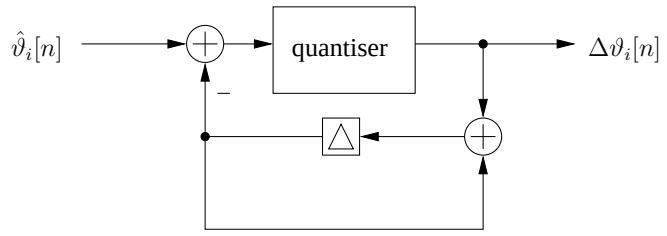

Figure 3.4: Differential pulse code modulation of the estimated phase $\vartheta_i[n]$ in the receiver. The residual $\Delta\vartheta_i[n]$ is fed back to the transmitter.

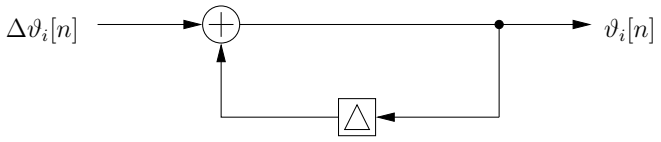

Figure 3.5: DPCM decoder to recover the angle $\vartheta_i[n]$ from the fed back residual $\Delta\vartheta_i[n]$.

samples. Since the word length after quantisation is very short, the encoding will be based on the quantised difference, using the encoder shown in Fig. 3.4. We assume that the encoder uses a fixed quantisation step size μ and a fixed word length B. The corresponding decoder operated in the transmitter is depicted in Fig. 3.5.

For a short word length B and a small step size μ, the rapid phase change by π as discussed in Sec. 3.3.1 will lead to a slope overload. However, since such a rapid change occurs only for a coefficient passing close to the origin, the contribution to β will be small, and a slope overload leading to an inaccurate angle applied in the transmitter is very likely to be of little consequence. The optimum step size value μ_{opt} that maximises the combined diversity and array gain, and will depend on B and the Doppler frequency Ω_{D} which is responsible for the smoothness of $\vartheta_i[n]$.

3.4 Simulations and Results

In simulations, we have used a BPSK signal constellation. The realisations of (4×1) MISO channel is spatially uncorrelated and each path coefficients are modelled as complex zero mean Gaussian random variables with unit variance and varying over time with maximum variation is determined by the maximum angular Doppler spread Ω_D. Below we first evaluate the best setting for the quantisation step size prior to embarking on a BER comparison with the existing scheme in [1] using non-differential feedback.

3.4.1 Step Size Optimisation

The main difficulty in designing a differential feedback system is to determine the best setting for the quantisation step size. In the absence of a closed form solution for the optimum setting of the quantisation step size μ_{opt}, we resort to an approximate optimisation based on simulations. The simulation in Fig. 3.6 shows the impact of the word length on the combined diversity and array gain for differential feedback with $B = 1$ and $B = 2$ coefficients for various Doppler frequencies Ω_{D}. It is evident that for small step sizes, the slope overload leads to an inability to sufficiently track the changes in $\vartheta_i[n]$. This has a more serious effect when the Doppler frequency Ω_{D} is large.

For larger step sizes μ, there is a consistent drop in diversity and array gain performance across all variations in Doppler frequencies. This is because the quantisation becomes too coarse to appropriately represent the optimum angles $\vartheta_i[n]$ regardless of how fast they are changing. Interestingly, for $\mu = \pi/2$, the differential feedback will resemble a non-differential feedback with $B = 1$ bits returning the values $\pm\frac{\pi}{2}$ according to (2.27). As evident from Fig. 3.2, the non-differential feedback system for $B = 1$ yields a combined diversity and array gain of approximately 6, which matches the value for $\mu = \pi$ in Fig. 3.6.

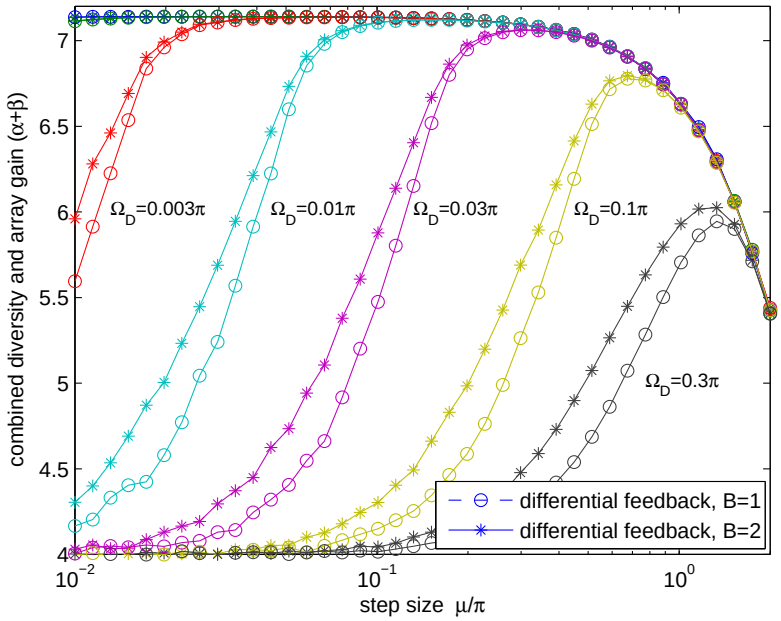

Figure 3.6: Combined diversity and array gain for differential feedback with B bits per angle ϑ_i, $B \in \{1, 2\}$, dependent on the quantisation step size μ simulated over 2^{18} symbols.

In terms of performance, it can be noted that differential feedback with $B = 2$ coefficients does not provide a large advantage over the case $B = 1$. The only noticeable difference in performance occurs for larger Doppler frequencies and step sizes μ. According to Fig. 3.2, non-differential feedback with two coefficients provides a combined diversity and array gain of about 6.8. This can only be reached in Fig. 3.6 for both $B = 1$ and $B = 2$ for a Doppler frequency of less than $\Omega_\mathrm{D} = 0.1\pi$ with an appropriately selected step size. Therefore, there is no performance advantage for differential feedback with $B = 2$ over the case $B = 1$. Thus, only the differential case $B = 1$ will be further investigated in the following. Tab. 3.1 shows the optimal values for the step size μ_opt and corresponding diversity and array gain $(\alpha + \beta)$ in dependency of the Doppler frequency Ω_D, as extracted from Fig. 3.6.

Ω_D	0.003π	0.01π	0.03π	0.1π	0.3π
μ_{opt}	0.0767	0.1514	0.2986	0.6246	1.3305
$(\alpha+\beta)$	7.1314	7.1214	7.0609	6.7778	5.9455

Table 3.1: Optimum quantisation step size μ_{opt} for single bit differential feedback of $\hat{\vartheta}_i[n]$ based on Fig. 3.6

3.4.2 BER Performance

In the following simulation, the proposed differential feedback scheme with $B = 1$ is evaluated in terms of its BER performance. As comparison, Fig. 3.7 also contains the BER curves for the open loop system with a diversity gain of 4, which is due to the fact that $\mathcal{E}\{\beta\} = 0$, and the non-differential closed loop systems with $B = 1$, $B = 2$, and $B \to \infty$ (no quantisation), yielding combined diversity and array gains of approximately 6, 6.8, and $4 + \pi = 3.1415$, respectively as shown in Fig. (3.2). The proposed scheme performs close to the optimum of unquantised feedback, and significantly outperforms the non-differentially encoded case for $B = 1$, requiring the same feedback bandwidth, and outperforming the case of non-differential feedback with $B = 2$. Therefore the proposed system performs better than a non-differential feedback system that requires twice the bandwidth in the feedback channel.

3.5 Conclusion

In this chapter we have analysed EO-STBC and proposed a new differential feedback scheme for extended EO-STBC, for which we have analytically derived the maximum attainable combined diversity and array gain, agreeing with earlier reported, heuristically obtained results. The differential encoding scheme has been shown to work well over a range of realistic Doppler spreads. On the analysis side, we have analytically derived the asymptotically achievable diversity and

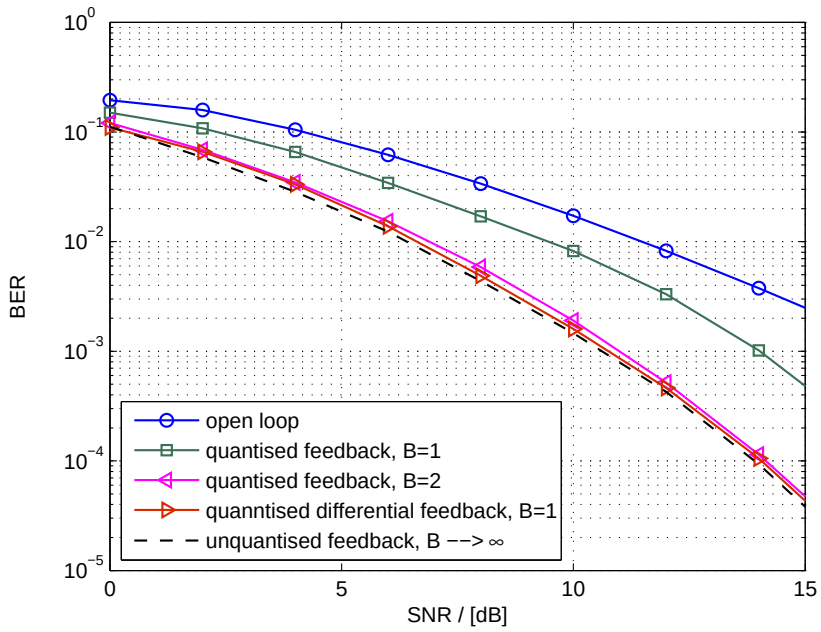

Figure 3.7: Comparison of the BER performance between the proposed scheme with single bit differential feedback to the open loop system, and a system with non-differential feedback for $\Omega_D = 0.003\pi$, utilising word lengths $B = 1$, 2, and $B \to \infty$.

array gain, which has confirmed experiments both in the literature as well as simulations presented here.

In order to efficiently feedback the required beamstearing angles from the receiver to the transmitter, the smooth evolution of the channel coefficients over time has motivated a differential encoding scheme. It has been demonstrated how the smoothness from channel coefficient's trajectories translates into smooth feedback angles, and whereby unwrapping of angles is important to avoid discontinuities. In order to implement this differential feedback scheme, differential pulse code modulation (DPCM) encoders were proposed. To develop the DPCM scheme, an optimum step size was investigated, where the Doppler spread is controlled according to the variations of the feedback angles. Based on simulations, we have found that the proposed differential feedback scheme can significantly improve closed loop EO-STBC scheme by halving the feedback bandwidth com-

pared to existing non-differential approaches with a BER performance that is close to optimum.

The near-optimal, low bandwidth feedback scheme for closed-loop EO-STBC presented in this chapter requires accurate knowledge of the optimum feedback angles in the receiver. The next chapter will investigate algorithms operating in the receiver, which can identify these angles and track any required parameters over time, based on the same idea of smooth channel coefficient trajectories that has motivated the differential feedback scheme above.

Chapter 4

Combining Differential Feedback & Channel Tracking

This chapter proposes a channel estimation and tracking scheme based on a Kalman filter in decision-directed (DD) mode, which is applied to extended orthogonal STBC (EO-STBC) with differential feedback. Inside the Kalman filter, it is shown that an employing a first order auto-regressive (AR-1) model for estimating the trajectory of a channel coefficient and can be significantly enhanced by considering higher order models that enable a smoother prediction. Moreover, this system needs to be adapted in order to interlink with the EO-STBC symbol detection in the Kalman filter's correction step. Practical simulations on the combined estimation of channel coefficients with differential feedback as implemented in Chapter 3, will be investigated.

The chapter commences with an outline in Sec. 4.1. Sec. 4.2 provides a brief overview over EO-STBC with differential feedback, recapitulating the main results of Chapter 3. After that in Sec. 4.3, channel estimation and tracking by means of a Kalman filter is introduced. Simulation results are presented in Sec. 4.5, and Sec. 4.6 provides a summary and conclusions.

4.1 Introduction

For conventional coherent detection, EO-STBC requires accurate knowledge of channel state information (CSI) at the receiver for decoding. This CSI is needed to determine the beamsteering angles that are to be fed back to the transmitter to enable exploitation of diversity and array as outlined in earlier chapters. Channel estimation is therefore crucial, and can only be avoided through the use of STBC based on differential or double differential modulation [67]. This alleviates the need for CSI, but requires the channel to remain stationary for at least a few successive symbol periods, and incurs performance degradation by 3 dB and 6 dB, respectively, compared to coherent modulation [68]. Thus, channel estimation is an integral part of the EO-STBC receiver for fading channels.

For the channel estimation based on training symbols [69], the CSI corresponding to training symbols is first estimated. Thereafter, CSI corresponding to the subsequent data symbols can be tracked and further improved by decision directed channel estimation [70]. To obtain reliable channel estimates, initial channel estimation can be performed based on training symbols, which are periodically inserted prior to EO-STBC tracked symbols. The design of optimal training sequences for time-varying channels whose impulse response can be modelled as an AR process can be found in [69].

In addition, to improve tracking efficiency, sequential filtering algorithms such as the Kalman filter [71] have been proposed for tracking time-varying fading channels [48], having the desirable property of being able to approximate channel variations. Kalman filtering consists of an iterative prediction-correction process whereby the tracking algorithm exploits the structure of Alamouti space time codes as adopted in [47] [70]. In order to track the non-stationary channel, in this chapter we evaluate the performance of Kalman filtering for tracking a slow fading, EO-STBC encoded channel in Gaussian noise.

Decision directed channel estimation (DD) has been adopted, following the approach in [70] for O-STBC. If the channel varies slowly, the estimated CSI based on previous predicted symbols are generally reliable such that the estimated channel state of a previous symbol period may be used in the detection of current data. Therefore in this chapter, we focus our attention on channel estimation based on an AR-M model for the approximation of the time-varying channel coefficients. For example, an AR-1 model has been used in [49]. Hence, we have proposed a general AR-M [72] in order to enable better prediction particularly for slow-fading scenarios where the smooth evolution of channel coefficients appears to be better suited for $M > 1$.

4.2 System Model

Based on the channel model outlined in Chapter 3, we now turn our attention to combining channel estimation with differential feedback. The system set-up in Fig. 4.1 has been constructed to address both differential feedback and channel estimation. For simplicity, we assume below that the feedback channel is error free with no latency.

For slow fading channels, each channel coefficient evolves smoothly over time. The received signal $r[n]$ is characterised by (3.1). The channel $\mathbf{h}_n \in \mathbb{C}^4$, contains spatially independent and identically distributed wide-sense stationary (WSS) Rayleigh fading channel coefficients. With EO-STBC encoding over two successive time slots, the selection of the transmit vector is given by

$$\mathbf{s}_n = \begin{cases} \frac{1}{2}[\ s[n] \quad s[n] \quad s[n+1] \quad s[n+1]\ ]^{\mathrm{T}} & , n \quad \text{even} \\ \frac{1}{2}[\ -s^*[n] \quad -s^*[n] \quad s^*[n-1] \quad s^*[n-1]\ ]^{\mathrm{T}} & , n \quad \text{odd.} \end{cases} \tag{4.1}$$

The diagonal beam-steering matrix $\mathbf{\Lambda}_n = \mathrm{diag}\left\{ e^{j\hat{\vartheta}_1[n]} \quad 1 \quad e^{j\hat{\vartheta}_2[n]} \quad 1 \right\}$ effect-

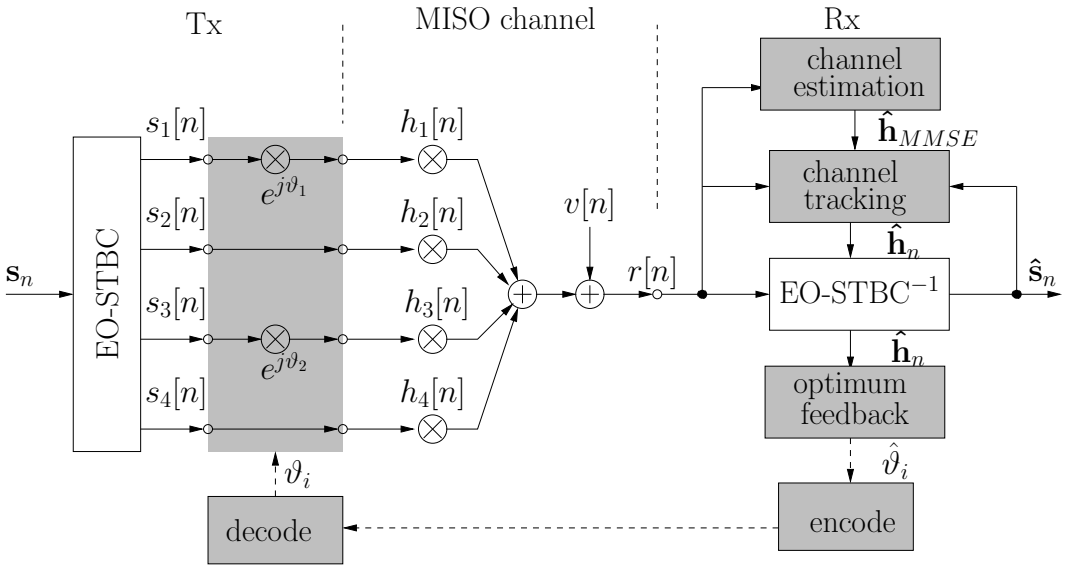

Figure 4.1: EO-STBC system with channel estimation and tracking in the receiver to aid symbol detection and estimation of the optimum beam-steering angles ϑ_1 and ϑ_2, which are differentially encoded and returned to the transmitter.

ively rotates the channel taps $h_1[n]$ and $h_3[n]$. Since $\mathbf{\Lambda}_n$ is unitary, it has no effect on the transmit power. As in a standard STBC system, the receiver gathers two subsequent samples in a vector $\mathbf{r}_n$ such that

$$\mathbf{r}_n = \begin{bmatrix} r[n] \\ r^*[n+1] \end{bmatrix} = \mathbf{H}_n \mathbf{s}_n + \mathbf{v}_n, \tag{4.2}$$

based on the equivalent transmit vector $\mathbf{s}_n = [\ s[n] \quad s[n+1]\ ]^{\mathrm{T}}$, equivalent noise vector $\mathbf{v}_n = [\ v[n] \quad v^*[n+1]\ ]^{\mathrm{T}}$, and the space-time equivalent transmission channel matrix $\mathbf{H}_n$. The latter can be formulated as

$$\mathbf{H}_n = \begin{bmatrix} h_{11}[n] & h_{12}[n] \\ h_{21}[n+1] & h_{22}[n+1] \end{bmatrix}. \tag{4.3}$$

The components of $\mathbf{H}_n$ are a mixture of channel coefficients and rotations due to beam-steering $\mathbf{\Lambda}_n$

$$
\begin{aligned}
h_{11}[n] &= e^{j\hat{\vartheta}_1[n]}h_1[n] + h_2[n] && (4.4)\\
h_{12}[n] &= e^{j\hat{\vartheta}_2[n]}h_3[n] + h_4[n] && (4.5)\\
h_{21}[n+1] &= e^{-j\hat{\vartheta}_2[n+1]}h_3^*[n+1] + h_4^*[n+1] && (4.6)\\
h_{22}[n+1] &= -e^{-j\hat{\vartheta}_1[n+1]}h_1^*[n+1] - h_2^*[n+1]. && (4.7)
\end{aligned}
$$

Detection is performed over a block duration consisting of two successive symbols periods. The decision statistic vector $\hat{\mathbf{s}}_n = [\ \hat{s}[n] \quad \hat{s}^*[n+1]\ ]^{\mathrm{T}}$ can be obtained via linear combination with the estimated equivalent space-time channel matrix $\hat{\mathbf{H}}_n$

$$\hat{\mathbf{s}}_n = \hat{\mathbf{H}}_n^{\mathrm{H}}\mathbf{H}_n\mathbf{s}_n + \tilde{\mathbf{v}}_n, \tag{4.8}$$

where $\tilde{\mathbf{v}}_n = \hat{\mathbf{H}}_n^{\mathrm{H}}\mathbf{v}_n$ is the noise after decoding. Let the matrix $\mathbf{G}_n = \hat{\mathbf{H}}_n^{\mathrm{H}}\mathbf{H}_n$, which can be decomposed into $\mathbf{G}_n = \mathbf{H}_n^{\mathrm{H}}\mathbf{H}_n + (\Delta\mathbf{H}_n)^{\mathrm{H}}\mathbf{H}_n$. The matrix $\Delta\mathbf{H}_n$ represents the error due to both estimation and time variation, which creates inter-symbol interference (ISI) in the detection process and increases the noise floor. The derivation of this error term is straightforward but tedious, and presented in Appendix A. In the absence of estimation errors, i.e. $\hat{\mathbf{H}}_n = \mathbf{H}_n$, any errors are only due to time-variations and $\mathbf{G}_n$ becomes

$$\mathbf{G}_n = \begin{bmatrix} g_{11}[n] & g_{12}[n] \\ g_{21}[n] & g_{22}[n] \end{bmatrix} \quad , \tag{4.9}$$

with elements

$$
\begin{aligned}
g_{11}[n] &= \sum_{m=1}^{2} |h_m[n]|^2 + \sum_{m=3}^{4} |h_m[n+1]|^2 \\
&\quad +2\Re\{e^{j\vartheta_1[n]} h_1[n] h_2^*[n] \\
&\quad + \; e^{j\vartheta_2[n+1]} h_3[n+1] h_4^*[n+1]\} \qquad (4.10) \\
g_{12}[n] &= e^{j(\vartheta_2[n]-\vartheta_1[n])} h_1^*[n] h_3[n] \\
&\quad -e^{j(\vartheta_2[n+1]-\vartheta_1[n+1])} h_1^*[n+1] h_3[n+1] \\
&\quad +e^{-j\vartheta_1[n]} h_1^*[n] h_4[n] \\
&\quad -e^{-j\vartheta_1[n+1]} h_1^*[n+1] h_4[n+1] \\
&\quad +e^{j\vartheta_2[n]} h_2^*[n] h_3[n] \\
&\quad -e^{j\vartheta_2[n+1]} h_2^*[n+1] h_3[n+1] \\
&\quad +h_2^*[n] h_4[n] - h_2^*[n+1] h_4[n+1] \qquad (4.11) \\
g_{21}[n] &= g_{12}^*[n] \\
g_{22}[n] &= \sum_{m=1}^{2} |h_m[n+1]|^2 + \sum_{m=3}^{4} |h_m[n]|^2 \\
&\quad +2\Re\{e^{j\vartheta_1[n+1]} h_1[n+1] h_2^*[n+1] \\
&\quad + \; e^{j\vartheta_2[n]} h_3[n] h_4^*[n]\} \quad . \qquad (4.12)
\end{aligned}
$$

The maximisation of the received gain is coupled to the maximisation of the on-diagonal elements of $\mathbf{G}_n$, which is achieved by setting

$$
\begin{aligned}
\vartheta_1[n] &= -\angle\{h_1[n] h_2^*[n]\} \qquad (4.13) \\
\vartheta_1[n+1] &= -\angle\{h_1[n+1] h_2^*[n+1]\} \qquad (4.14) \\
\vartheta_2[n] &= -\angle\{h_3[n] h_4^*[n]\} \qquad (4.15) \\
\vartheta_2[n+1] &= -\angle\{h_3[n+1] h_4^*[n+1]\}. \qquad (4.16)
\end{aligned}
$$

However, unlike in the stationary case [46], the off-diagonal elements $g_{12}[n]$ and $g_{21}[n]$ are now finite and create inter-symbol interference in the process of detecting $s[n]$ and $s[n+1]$.

4.2.1 Maximum Likelihood Detector

The impact of a time-varying Rayleigh fading channel on the performance of an Alamouti code has been analysed, and several optimal and suboptimal receivers for mitigating the effects of cross-talk between symbols have been proposed in e.g. [2]. Although the suboptimal receivers such as zero-forcing (ZF), and decision-feedback (DF) have lower complexity than a receiver based on the joint maximum likelihood (JML) detector, the JML detector is only able to attain full diversity order. Therefore, based on the observation of the received symbols, the JML estimation of the transmitted symbols $\mathbf{s}_n$ over the EO-STBC channel matrix $\mathbf{H}_n$ can be obtained by maximising likelihood over $\mathbf{s}_n$ and $\mathbf{H}_n$ jointly. Equivalently, the JML estimation is obtained by minimising

$$\hat{\mathbf{s}}_n = \underset{\mathbf{s}}{\operatorname{argmin}} \left\{ \|\mathbf{r}_n - \mathbf{H}_n \mathbf{s}\|_2^2 \right\}, \tag{4.17}$$

4.2.2 Degradation due to Time Variation

The channel variation with time will destroy the orthogonality of the channel matrix $\mathbf{H}_n$. Therefore, the deviation of $\mathbf{G}_n$ from a diagonal matrix results in ISI. This issue will be investigated by simulation of a JML detector [2] in order to evaluate up to Doppler frequency which the performance remains acceptable.

4.2.2.1 Degraded Performance

Using the JML decoder of [2], BER performance of an EO-STBC system with perfect channel estimation should show the degradation due only to the non-

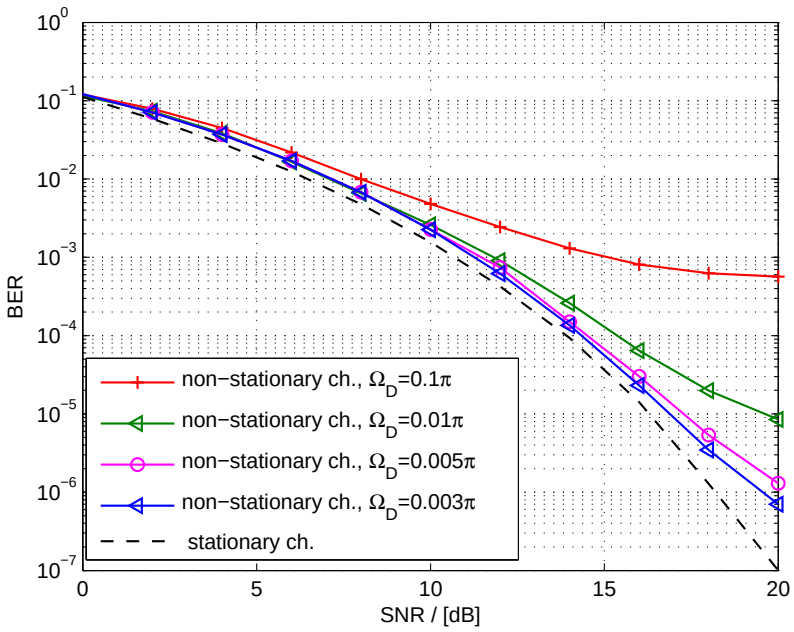

Figure 4.2: BER degraded performance of EO-STBC system with optimum beam-steering angles ϑ_1 and ϑ_2 and known CSI for various maximum angular Doppler spreads Ω_D.

stationary nature of the channel over an EO-STBC transmitted block when $\Omega_D > 0$. Fig. 4.2 shows BER vs SNR curves averaged over an ensemble of frequency-dispersive channels with various normalised Doppler frequencies Ω_D. For $\Omega_D < 0.01\pi$, the performance degradation in terms of BER appears only gradual and somewhat insignificant. Once the normalised angular Doppler frequency $\Omega_D = 0.01\pi$, the BER performance drops more noticeably, because the off-diagonal elements $g_{12}[n]$ and $g_{21}[n]$ are becoming larger and create sufficiently high inter-symbol interference to degrade the JML decoder in the process of detecting $s[n]$ and $s[n+1]$. The obtained BER curves with known channels will be used as benchmark results for channel estimation later.

4.2.3 Differential Feedback

For many wireless applications, the maximum Doppler shift Ω_D can be considered small. This leads to a smooth evolution of channel coefficients, which enables differentially encoding single bit feedback over a realistic range of maximum Doppler shifts Ω_D. Differentially quantised feedback requires optimisation of the quantiser step size μ, which causes a trade-off between slope overload due to too slow tracking for small values of μ, and too coarse quantisation for larger values of μ that causes poor performance irrespective of the rate of change. Below, we will aim to construct channel estimation and tracking techniques that can complement the differential feedback which we had previously explored in Chap. 3 [73]. Based on the results given later in Tab. 3.1, differential feedback can be performed with near optimum performance when optimum steps size are used corresponding to an angular Doppler shift set $\Omega_D = \{0.003\pi, 0.005\pi, 0.01\pi\}$.

4.3 Channel Estimation

Several types of estimation techniques can be exploited. For example, either a least squares (LS) approach or if the signal-to-noise ratio (SNR) is known a priori, minimum mean square error (MMSE) approaches represent candidates for channel estimation. The EO-STBC receiver requires the knowledge of the channel coefficients both for detecting symbols as well as for computing the optimum phase angles $\vartheta_{i,n}$, $i = \{1, 2\}$, to be used for beam-steering. Therefore, below an approach to track the channel coefficients is presented, which is initialised and interleaved with channel estimation steps.

4.3.1 Initial Channel Estimation

An initial channel estimate for the MISO system $\mathbf{h}_n$ can be obtained by transmitting a training sequence over L symbols. If this transmit data is assembled in a data matrix $\tilde{\mathbf{S}} \in \mathbb{C}^{2L\times 4}$ and transmitted without beam-steering, the MMSE solution for $\hat{\mathbf{h}}_n$ for $L \geq 4$ can be calculated as

$$\hat{\mathbf{h}}_{\text{MMSE}} = \left(\tilde{\mathbf{S}}_n^{\text{H}}\tilde{\mathbf{S}}_n + \gamma_n \mathbf{I}\right)^{-1} \tilde{\mathbf{S}}_n^{\text{H}} \begin{bmatrix} \mathbf{r}_{n-2(L+1)} \\ \vdots \\ \mathbf{r}_{2n} \\ \mathbf{r}_n \end{bmatrix}, \tag{4.18}$$

where γ_n is the SNR at the receiver. The formulation in (4.18) includes the ZF estimate with the case $\gamma_n \to \infty$.

For $L = 4$, the data matrix only, $\tilde{\mathbf{S}}_n^{\text{H}} = [\mathbf{s}_{n-2}\ \mathbf{s}_{n-1}\ \mathbf{s}_n\ \mathbf{s}_{n+1}]$ to be inserted into (4.18). The MMSE solution requires the left pseudo-inverse [74], and due to orthogonality of $\mathbf{S}_n$ simplifies to

$$\hat{\mathbf{h}}_{\text{MMSE}} = \left(\tilde{\mathbf{S}}_n^{\text{H}}\tilde{\mathbf{S}}_n + \gamma_n \mathbf{I}\right)^{-1} \tilde{\mathbf{S}}_n^{\text{H}} \begin{bmatrix} \mathbf{r}_{n-2} \\ \mathbf{r}_n \end{bmatrix} \tag{4.19}$$

Either (4.18) or (4.19) can be used to initialise the subsequent Kalman tracking, and can also be employed to re-initialise the tracking system in periodic intervals.

4.3.2 Impact of Estimation Errors

The accuracy of channel estimation will affect the performance of the system. Generally, a trade-off is expected for the length of the temporal window L over which coefficients are estimated. Too short a window will result in estimates that lack confidence and are prone to noise influence. Too long a window will lead to

situations where the channel can no longer be assumed stationary over the period of L symbols, and a reliance on outdated samples will lead to incorrect results from temporal averaging.

4.4 Kalman Tracking with Temporal Smoothness

The Kalman filter approach based on Bayesian estimation by incorporating prior knowledge and observational evidence has been utilised widely for channel tracking. In EO-STBC, detection is performed over two block periods, and the update of coefficients spans two sampling periods rather than one. Therefore, the difference between subsequent values is going to increase (due to a decrease in correlation) and selection of the correlation factor is theoretically optimum but the value has been found to be imprecise. This motivates a simple modified prediction step of the Kalman filter based on a higher order model to approximate the time-varying nature of a channel with temporal smoothness.

4.4.1 Impact of Beamsteering on Channel Tracking

Some channel coefficients are modified through the application of a time-varying phase rotations, and the resulting variation in value can be much greater than expected from the actual Doppler spread. Therefore, to avoid tracking rotated channel coefficients will improve the performance. It can be noted from equation (3.1), that the feedback angles $\vartheta_1[n]$ and $\vartheta_2[n]$ in the beam-steering diagonal matrix $\mathbf{\Lambda}_n$ can be absorbed into either the transmission channel $\mathbf{h}_n$, or into the transmitted vector $\mathbf{s}_n$. Let the channel vector with incorporated angles can be given by $\mathbf{h}_n^r = \mathbf{\Lambda}_n \mathbf{h}_n$, and in similar way the transmitted vector with incorporated angles be given by $\mathbf{s}_n^r = \mathbf{\Lambda}_n \mathbf{s}_n$. To track the unrotated channel, a simple correction

can extract the true channel coefficients from the estimate ones by incorporating the known beamsteering angles as

$$\mathbf{h}_n = \mathbf{\Lambda}_n^{-1}\mathbf{h}_n^r = \mathbf{\Lambda}_n^*\mathbf{h}_n^r. \tag{4.20}$$

4.4.2 Prediction Model Based on AR Process

For Kalman tracking of Alamouti O-STBC in [75], the channel is updated based on a first order auto-regreesive model (AR-1). However, the smooth channel variation motivates the use of a higher order auto-regressive model for a priori prediction. In [64], the system model including temporal correlation of channel coefficients $h[n]$ is based on

$$\rho_\tau = r_h[\tau] = \mathcal{E}\{h[n]h^*[n-\tau]\}, \tag{4.21}$$

and a trajectory of channel coefficients can be approximated by M order AR process (AR-M) with coefficient vector $\mathbf{a}$, which linearly combines the last M values of the channel coefficient trajectory such that

$$h[n] = \mathbf{a}^{\mathrm{H}} \begin{bmatrix} h[n-1] \\ h[n-2] \\ \vdots \\ h[n-M] \end{bmatrix} = \mathbf{a}^{\mathrm{H}}\mathbf{h}_{n-1} + u[n], \tag{4.22}$$

where $u[n]$ is the prediction error. Minimisation of this error can be obtained through the principl of orthogonality $\mathcal{E}\{\mathbf{h}_{n-1}u[n]^*\} = 0$, which in our context can be expressed as

$$\mathcal{E}\{\mathbf{h}_{n-1}h[n]^*\} = \mathcal{E}\{\mathbf{h}_{n-1}\mathbf{h}_{n-1}^{\mathrm{H}}\}\mathbf{a}. \tag{4.23}$$

Including temporal correlation in (4.21) leads to

$$\mathbf{R}_h = \mathcal{E}\{\mathbf{h}_{n-1}\mathbf{h}_{n-1}^{\mathrm{H}}\} = \begin{bmatrix} \rho_0 & \rho_1 & \cdots & \rho_{M-1} \\ \rho_1^* & \rho_1 & & \vdots \\ \vdots & & \ddots & \\ \rho_{M-1}^* & & & \rho_0 \end{bmatrix}, \tag{4.24}$$

with an appropriately defined cross-correlation vector $\mathbf{p}$ given in matrix notation as follows

$$\mathbf{p} = \mathcal{E}\{\mathbf{h}_{n-1}h[n]^*\} = \begin{bmatrix} \rho_1 \\ \rho_2 \\ \vdots \\ \rho_M \end{bmatrix}. \tag{4.25}$$

Therefore, we can rewrite (4.23) in the form

$$\mathbf{a} = \mathbf{R}_h^{-1}\mathbf{p} = \begin{bmatrix} \rho_0 & \rho_1 & \cdots & \rho_{M-1} \\ \rho_1^* & \rho_1 & & \vdots \\ \vdots & & \ddots & \\ \rho_{M-1}^* & & & \rho_0 \end{bmatrix}^{-1} \begin{bmatrix} \rho_1 \\ \rho_2 \\ \vdots \\ \rho_M \end{bmatrix}. \tag{4.26}$$

Similar to [64], a diagonal loading technique with a small positive constant ϵ can be used to avoid that $\mathbf{R}_h$ is singular and therefore invertible, where some noise variance is added into $\mathbf{R}_h$ to make it as

$$\mathbf{a} = \left(\mathbf{R}_h + \epsilon\mathbf{I}\right)^{-1}\mathbf{p}. \tag{4.27}$$

The identical process noise variance σ_u^2 in the Kalman filter is identical to the

mean squared prediction error,

$$\sigma_u^2 = \mathcal{E}\{u[n]u[n]^*\} = \sigma_h^2 - \Re\left\{\mathbf{a}^{\mathrm{H}}\mathbf{P}\right\} + \mathbf{a}^{\mathrm{H}}\mathbf{R}_h\mathbf{a}. \tag{4.28}$$

An auto-regressive (AR) process is commonly implemented as white noise $u[n]$ filtered by an all-pole linear time-invariant (LTI) system. Therefore, the M coefficients of $\mathbf{a}$ can now be inserted directly into the transition matrix $\mathbf{A}$ as

$$\mathbf{A} = \begin{bmatrix} a_1 & a_2 & \cdots & a_{M-1} & a_M \\ 1 & 0 & \cdots & 0 & 0 \\ 0 & 1 & \cdots & 0 & 0 \\ \vdots & \vdots & \ddots & \vdots & \vdots \\ 0 & 0 & \cdots & 1 & 0 \end{bmatrix}. \tag{4.29}$$

4.4.3 Kalman Filter Algorithm

The Kalman filter keeps track of the estimated state of time-varying channels $\mathbf{h}$ and observation $r[n]$. The process noise covariance $\mathcal{E}\left\{\mathbf{u}_n\mathbf{u}_n^H\right\}$ and measurement noise variance σ_n^2 are assumed to be constant and independent. The Kalman filter algorithm works in update and correction steps process. In the update step, an a priori estimate is performed based on the prediction model. Thereafter, in the correction step, the predicted state is subsequently refined using the current observation assuming that $\mathbf{s}_n$ has been suitably detected. The summary of is given in Tab. 4.1.

4.4.4 Decision-Directed Mode

In this section, we formalise a joint scheme using a decision-directed channel estimation approach given in [48] [70] for the purpose of our proposed architecture. The structure of Fig. 4.1 considers tracking a trajectory of a time-varying channel

Table 4.1: Kalman Filter for MISO systm.

$\mathbf{P}_0 = \sigma_h^2 \mathbf{I}_4$

1. Update step
   (a) Predict a priori estimates
   $\mathbf{h}_{n/n-1} = \mathbf{A}\mathbf{h}_{n-1/n-1}$
   (b) Predict a priori error covariance
   $\mathbf{P}_{n/n} = \mathbf{A}\mathbf{P}_{n/n-1}\mathbf{A}^{\mathrm{T}} + \mathcal{E}\left\{\mathbf{u}_n \mathbf{u}_n^H\right\}$
2. Correction step
   (a) Obtain Kalman gain
   $\mathbf{K}_n = \mathbf{P}_{n/n}\mathbf{s}_n[\mathbf{s}_n^{\mathrm{T}}\mathbf{P}_{n/n}\mathbf{s}_n + \sigma_n^2]^{-1}$
   (b) Obtain a posteriori estimate
   $\mathbf{h}_{n/n} = \mathbf{h}_{n/n-1} + \mathbf{K}_n.\left[r[n] - \mathbf{h}_{n/n-1}^{\mathrm{T}}\mathbf{s}_n\right]$
   (c) Obtain a posteriori error covariance
   $\mathbf{P}_{n/n} = (\mathbf{I} - \mathbf{K}_n\mathbf{s}_n)\mathbf{P}_{n/n-1}$

cofficient, given an observation symbols which training sequence prior to EO-STBC transmission. Compared to [48] [70], here the Kalman filter is customised to take the EO-STBC setup into account, as depicted in Fig. 4.1. With Kalman algorithm in Tab. 4.1, thereby, two a-priori estimates are performed to predict the time-varying channel vectors during the current EO-STBC block. Thereafter, both a-priori estimates are updated similar to [76].

When the SNR is low, error propagation occurs and convergence to the optimum is not guaranteed. However, in the conventional Kalman filter algorithm described Tab. 4.1, it is already assumed that $\mathbf{s}_n$ has been suitably detected, so that the periodic insertion of pilot symbols can offer an initial channel estimation for reliable tracking performance in DD mode, as outlined in Tab. 4.2.

Table 4.2: Kalman-based AR-M for tracking unrotated channel with decision-directed updating over two successive symbol periods.

initial values

$\bar{\mathbf{h}} = 0^{4M\times 1}$, $\bar{\mathbf{s}} = 0^{1\times 4M}$, $\mathbf{P}_0 = \sigma_h^2\mathbf{I}_{4M}$,$\mathbf{\Phi} = \text{diag}\{\mathbf{A},\mathbf{A},\mathbf{A},\mathbf{A}\}$

$\mathbf{Q} = \mathbf{diag}\{\mathbf{U},\mathbf{U},\mathbf{U},\mathbf{U}\}$, $\mathbf{U}$ =diag $\left\{\sigma_u^2, 0, \cdots, 0\right\}$.

known

$\begin{bmatrix} r[n] \\ r^*[n+1] \end{bmatrix}$, σ_u^2, and σ_v^2. $\mathbf{h}_0 \in \mathbb{C}^{4\times 1}$,

$\bar{\mathbf{h}}_0[1:M:4M] = \mathbf{h}_0$

for K symbols do

1. Predict a priori estimates
   $\bar{\mathbf{h}}_{n/n-1} = \Phi\bar{\mathbf{h}}_{n-1/n-1}$
   $\bar{\mathbf{h}}_{n+1/n-1} = \mathbf{\Phi\Phi}\bar{\mathbf{h}}_{n-1/n-1}$
   $\mathbf{P}_{n|n-1} = \mathbf{\Phi P}_{n-1|n-1}\mathbf{\Phi}^{\mathrm{T}} + \mathbf{Q}$

2. Compute a priori beamsteering $\mathbf{\Lambda}_{n|n-1}$and $\mathbf{\Lambda}_{n+1|n-1}$
   Obtain a priori rotated channel
   $\mathbf{h}^r_{n|n-1} = \mathbf{\Lambda}_{n|n-1}\bar{\mathbf{h}}_{n/n-1}[1:M:4M]$
   $\mathbf{h}^r_{n+1|n-1} = \mathbf{\Lambda}_{n+1|n-1}\bar{\mathbf{h}}_{n+1/n-1}[1:M:4M]$

3. Form a priori space-time matrix $\mathbf{H}_{n|n-1}$with a priori rotated channel as described in (4.3).

4. Decode feedback symbols $\hat{s}[n]$ and $\hat{s}[n+1]$ as shown in (4.8).

5. Feedback symbols
   $\bar{\mathbf{s}}_{n|n-1}[1:M:4M] = \frac{1}{2}\mathbf{\Lambda}_{n|n-1}[s[n], s[n], [n+1], [n+1]]$.
   $\bar{\mathbf{s}}_{n+1|n-1}[1:M:4M] = \frac{1}{2}\mathbf{\Lambda}_{n+1|n-1}[-s^*[n+1], -s^*[n+1], s^*[n], s^*[n]]$.

6. Use the modified feedback symbols for a posteriori estimates
   $\mathbf{K}_{n/n-1} = \mathbf{P}_{n/n-1}\bar{\mathbf{s}}^{\mathrm{T}}_{n|n-1}[\bar{\mathbf{s}}_{n|n-1}\mathbf{P}_{n/n-1}\bar{\mathbf{s}}^{\mathrm{T}}_{n|n-1} + \boldsymbol{\sigma^2}_v]^{-1}$
   $\bar{\mathbf{h}}_{n/n} = \bar{\mathbf{h}}_{n/n-1} + \mathbf{K}_{n/n-1}\left[r[n] - \bar{\mathbf{h}}^{\mathrm{T}}_{n/n-1}\bar{\mathbf{s}}_{n|n-1}\right]$
   $\mathbf{P}_{n/n} = (\mathbf{I} - \mathbf{K}_{n|n-1}\mathbf{s}_{n|n-1})\mathbf{P}_{n/n-1}$
   $\mathbf{P}_{n+1|n} = \mathbf{\Phi P}_{n|n}\mathbf{\Phi}^{\mathrm{T}} + \mathbf{Q}$
   $\mathbf{K}_{n+1/n} = \mathbf{P}_{n+1/n}\bar{\mathbf{s}}^{\mathrm{T}}_{n+1|n-1}[\bar{\mathbf{s}}_{n+1|n-1}\mathbf{P}_{n+1/n}\bar{\mathbf{s}}^{\mathrm{T}}_{n+1|n-1} + \boldsymbol{\sigma^2_{\mathbf{v}}}]^{-1}$
   $\bar{\mathbf{h}}_{n+1/n} = \bar{\mathbf{h}}_{n+1/n} + \mathbf{K}_{n+1/n}\left[r[n+1] - \bar{\mathbf{h}}^{\mathrm{T}}_{n+1/n-1}\bar{\mathbf{s}}_n\right]$
   $\mathbf{P}_{n+1/n+1} = (\mathbf{I} - \mathbf{K}_{n+1|n}\mathbf{s}_{n+1|n-1})\mathbf{P}_{n+1/n}$

7. Compute a posteriori beamsteering $\mathbf{\Lambda}_{n|n}$and $\mathbf{\Lambda}_{n+1|n}$

8. Differential feedback of most recent beamsteering angles

9. Obtain a posteriori rotated channel
   $\mathbf{h}^r_{n|n} = \mathbf{\Lambda}_{n|n}\bar{\mathbf{h}}_{n/n}[1:M:4M]$ and $\mathbf{h}^r_{n+1|n} = \mathbf{\Lambda}_{n+1|n}\bar{\mathbf{h}}_{n+1/n}[1:M:4M]$

10. Form a posteriori space-time matrix $\mathbf{H}_{n|n}$ as described in (4.3).

11. Decode the transmitted symbol $\hat{\mathbf{s}}_{n|n}$ as shown in (4.8).

12. If necessary, iterate from 6 and 9 to improve tracking performance.

$K \leftarrow K + 2$

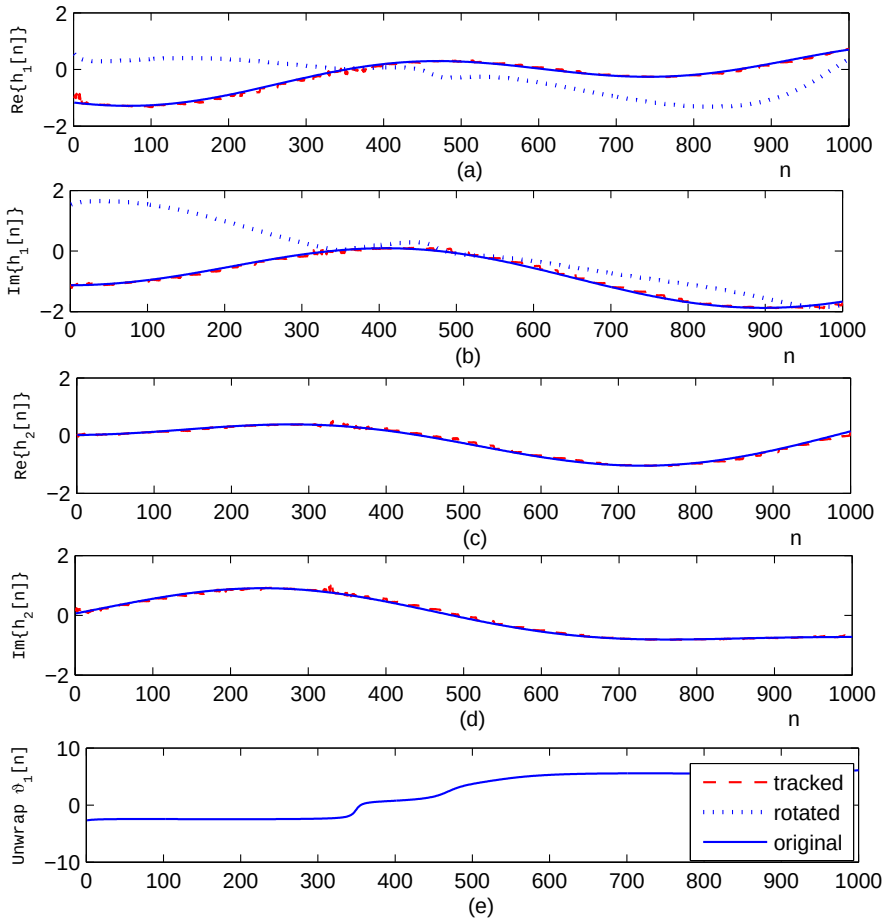

Figure 4.3: Coefficient evolution of channel coefficients; channel one with (a) real and (b) imaginary part, channel two with (c) real and (d) imaginary part, and (e) evolution of the angle returned to the transmitter via feedback.

4.5 Simulations and Results

Fiestly, tracking unrotated channel coefficients is given in Sec. (4.5.1). In simulations, we have compared mean square error of Channel testimation (MSE) for Kalman filter tracking with AR-$\{1, 2, 3\}$, and compared performances in term of BER using a BPSK signal constellation.

$M = 1$	$a = 1$	$\sigma_u^2 = 4.45 \times 10^{-5}$
$M = 2$	$\mathbf{A} = \begin{bmatrix} 1.9993 & -0.9993 \\ 1 & 0 \end{bmatrix}$	$\sigma_u^2 = 6.10 \times 10^{-8}$
$M = 3$	$\mathbf{A} = \begin{bmatrix} 1.3601 & 0.2794 & -0.6396 \\ 1 & 0 & 0 \\ 0 & 1 & 0 \end{bmatrix}$	$\sigma_u^2 = 4.20 \times 10^{-8}$

Table 4.3: Transition matrix $\mathbf{A}$ and process noise variance σ_u^2 for $\Omega_D = 0.003\pi$.

4.5.1 Tracking Unrotated Channel Coefficients

An illustrative simulation of Kalman tracking is presented below, which involves tracking the unrotated channel coefficients based on the correction by true feedback angles. According to Fig. 4.1, the feedback angles $\vartheta_1[n]$ and $\vartheta_2[n]$ are absorbed into the original channels of antennas one and three. Fig. 4.3 shows the channel variations when $\Omega_D = 0.003\pi$. Fig. 4.3 (a)–(d) shows real and imaginary parts of the trajectories of the true channel coefficients $h_i[n]$, $i = \{1, 2\}$ and, in case of $h_1[n]$, real and imaginary part of the trajectory of the modified coefficient (dashed curves) in Figs. 4.3 (a) and (b). The trajectory of the feedback angle $\vartheta_1[n]$ is shown in Fig. 4.3 (e). In order to avoid divergence of the Kalman filter, a re-initialisation with an MMSE estimate driven by pilot symbols is performed every K symbols, with the default value set to $K = 48$. This is necessary, since e.g. a coefficient trajectory passing close to the origin leads to rapidly changing angles, and therefore a higher degree of non-stationarity. Particularly Fig. 4.3 (a) and (b) clearly show how beamsteering angles affect the rate of change in terms of the coefficients. Although the problem occurs in channel $h_1[n]$ due to the beam-steering, the impact is felt across all channel coefficients.

4.5.2 AR-$\{1, 2, 3\}$ Model

For this set of simulations, the channel tracking error is evaluated. It is assumed that (i) the initial state $\mathbf{h}_0$, is previously estimated and known, and (ii) we could

$M = 1$	$a = 0.9999$	$\sigma_u^2 = 1.23 \times 10^{-4}$
$M = 2$	$\mathbf{A} = \begin{bmatrix} 1.9996 & -0.9997 \\ 1 & 0 \end{bmatrix}$	$\sigma_u^2 = 6.76 \times 10^{-8}$
$M = 3$	$\mathbf{A} = \begin{bmatrix} 1.5207 & -0.0419 & -0.4790 \\ 1 & 0 & 0 \\ 0 & 1 & 0 \end{bmatrix}$	$\sigma_u^2 = 5.13 \times 10^{-8}$

Table 4.4: Transition matrix $\mathbf{A}$ and process noise variance σ_u^2 for $\Omega_D = 0.005\pi$.

$M = 1$	$a = 0.9998$	$\sigma_u^2 = 4.90 \times 10^{-4}$
$M = 2$	$\mathbf{A} = \begin{bmatrix} 1.9993 & -0.9998 \\ 1 & 0 \end{bmatrix}$	$\sigma_u^2 = 1.82 \times 10^{-7}$
$M = 3$	$\mathbf{A} = \begin{bmatrix} 2.4491 & -1.8992 & 0.4498 \\ 1 & 0 & 0 \\ 0 & 1 & 0 \end{bmatrix}$	$\sigma_u^2 = 1.48 \times 10^{-7}$

Table 4.5: Transition matrix $\mathbf{A}$ and process noise variance σ_u^2 for $\Omega_D = 0.01\pi$.

isolate the error corresponding to the phase angles from the estimation due to time variation and channel estimation and by in which the compensation for phase modification is based on true phase angles. Simulations are performed over an ensemble of 10^4 randomised channel realisations. We consider that the four links are in fading with the normalised Doppler spread $\Omega_D = \{0.003\pi, 0.005\pi, 0.01\pi\}$ lead to the state-space models, Transition matrix $\mathbf{A}$ and process noise variance σ_u^2, which are incorporated in the Kalman filter given in Tabs. 4.3, 4.4, and 4.5 respectively. The listed matrices are obtained experimentally using (4.27) with added noise variance $\epsilon = 1 \times 10^{-8}$.

4.5.3 MSE of Channel Estimation

A frequently used design criterion is the mean square error (MSE). Tabs. 4.6, 4.7, and 4.8 show the linear values of average MSE per channel of EO-STBC with Kalman tracking based on different AR orders M, with $M = 1, 2, 3$ form $\Omega_D = \{0.003\pi, 0.005\pi, 0.01\pi\}$ respectively. It can be seen that $M = 2, 3$ have a significant advantage over the standard first order model with $M = 1$. In

SNR/[dB]	5	10	15	20	25
$M = 1$	0.1192	0.0981	0.0794	0.0739	0.0718
$M = 2$	0.01718	0.01152	0.0081	0.0051	0.0042
$M = 3$	0.0150	0.0101	0.0072	0.0046	0.0036

Table 4.6: Average MSE/channel with $\Omega_D = \{0.003\pi\}$ for use of different AR-$\{1, 2, 3\}$ models in the Kalman tracker with 48.

SNR/[dB]	5	10	15	20	25
$M = 1$	0.2245	0.1869	0.1622	0.1477	0.1404
$M = 2$	0.0250	0.0201	0.0151	0.0115	0.0095
$M = 3$	0.0236	0.0181	0.0135	0.0101	0.0085

Table 4.7: Average MSE/channel with $\Omega_D = \{0.005\pi\}$ for use of different AR-$\{1, 2, 3\}$ models in the Kalman tracker with $K = 48$.

addition, it can be noted that $M = 3$, although it incurs a higher computational complexity than the case of $M = 2$, does not offer a significant improvement over the latter. It is important to notice that increasing Ω_D will increase the MSE will be increased, but $M = 2, 3$ still offers a significant advantage over the standard first order model with $M = 1$, with $M = 3$ still having a small advantage over the $M = 2$ Kalman approach. The performances of both $M = 2$ and $M = 3$ are close, with a negligible advantage for $M = 3$, such that $M = 2$ provides a good trade-off between system performance and complexity. Therefore, below simulations are performed for BER performance with $M = \{1, 2\}$.

SNR/[dB]	5	10	15	20	25
$M = 1$	0.7224	0.5254	0.3882	0.3261	0.2974
$M = 2$	0.3532	0.2250	0.1472	0.1064	0.0856
$M = 3$	0.3200	0.2110	0.1380	0.0990	0.0782

Table 4.8: Average MSE/channel with $\Omega_D = \{0.01\pi\}$ for use of different AR-$\{1, 2, 3\}$ models in the Kalman tracker $K = \{48\}$.

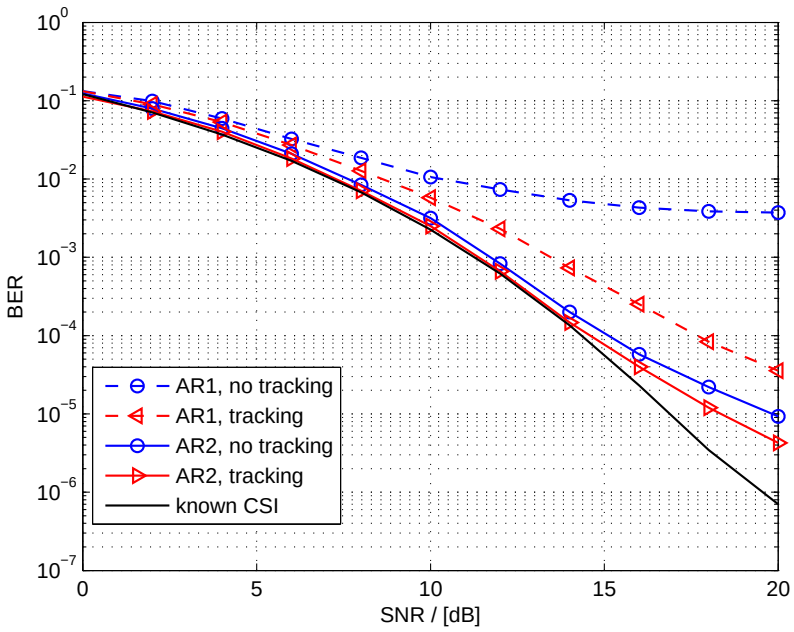

Figure 4.4: BER performance of EO-STBC system with Kalman-based channel tracking based on an AR-M with $M = 1, 2$ for $\Omega_D = 0.003\pi$, compared to perfect CSI.

4.5.4 Performance of AR-$\{1, 2\}$

4.5.4.1 BER Performance

In the following, the BER performance of EO-STBC with differential feedback and Kalman-based channel tracking is explored. We show the BER performances, whereby AR-M systems of first and second order are compared for $\Omega_D = \{0.003\pi.0.005\pi, 0.01\pi\}$. The channel tracking is initialised, and interleaved every $K = 48^{th}$ block by a channel identification. The Kalman filter is either operated in a prediction mode only (labelled as "no tracking") or with a correction step based on DD updating ("tracking").

It can be seen that the AR-2 performance for $\Omega_D = \{0.003\pi.0.005\pi\}$ in Figs. 4.4,and 4.5 are very close to the one where the receiver has perfect knowledge of the channel state information (CSI).

In Fig. 4.6 with $\Omega_D = \{0.01\pi\}$, the BER for AR-1 levels out early, but AR-2 is

still performing well. Simulations show that BERs performance with AR-2 significantly outperform BERs performance with AR-1. Moreover, BER performances with AR-2 for $\Omega_D = \{0.003\pi, 0.005\pi\}$ are near to the optimum while the BER performance for $\Omega_D = \{0.01\pi\}$ show a significant degradation from the case of known CSI . Therefore, significant improvements can be realised via the inclusion of AR-2 model compared to the standard first order system.

4.5.4.2 Impact of Tracking Period Length

We now study the impact of the pilot insertion period K on the performance of the AR-2 system. Figs. 4.7, and 4.8 show the MSE and BER performances , respectively, for pilots interleaved after every $K = \{48, 72, 96, 120\}$ symbol periods. It can be seen that K significantly affects the performance, but that for the case of angular Doppler spread $\Omega_D = \{0.01\pi\}$, $K > 72$ lead to an acceptable uncoded BER result.

4.6 Conclusions

EO-STBC requires feedback of the steering angles, which can be calculated from channel estimates at the receiver. Since the channel requires to be estimated in order to estimate transmitted symbols and beamsteering angles as well, we have discussed a channel estimation and a Kalman estimator for channel tracking. Smooth variation of the channel coefficients' trajectories has previously motivated a differentially encoded feedback of feedback angles in Chapter 3, and here additionally motivates to replace the AR-1 model of the basic Kalman channel estimator with an AR-$\{2, 3\}$ model that is capable of imposing additional smoothness. The improvements of using AR-$\{2, 3\}$ have been shown by MSE simulation, with a negligible advantage for the $M = 3$ system over $M = 2$. The

performance comparison of $M = \{1, 2\}$ clearly shows that the overall EO-STBC system achieves suitable BER values even for longer tracking periods, and that the performance of the proposed system offers a distinct advantage over realistic Doppler spreads.

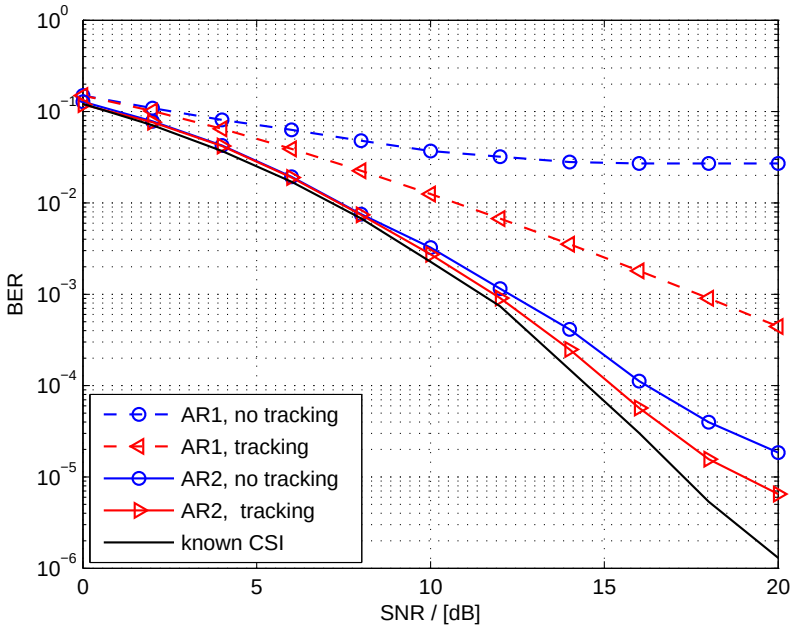

Figure 4.5: BER performance of EO-STBC system with Kalman-based channel tracking based on an AR-M with $M = 1, 2$ $\Omega_D = 0.005\pi$, compared to perfect CSI.

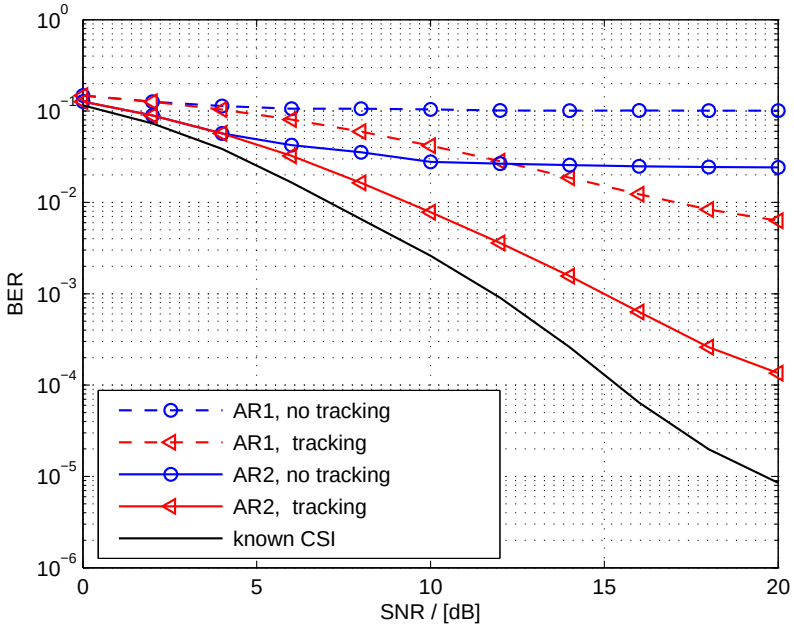

Figure 4.6: BER performance of EO-STBC system with Kalman-based channel tracking based on an AR-M with $M = 1, 2$ $\Omega_D = 0.01\pi$, compared to perfect CSI.

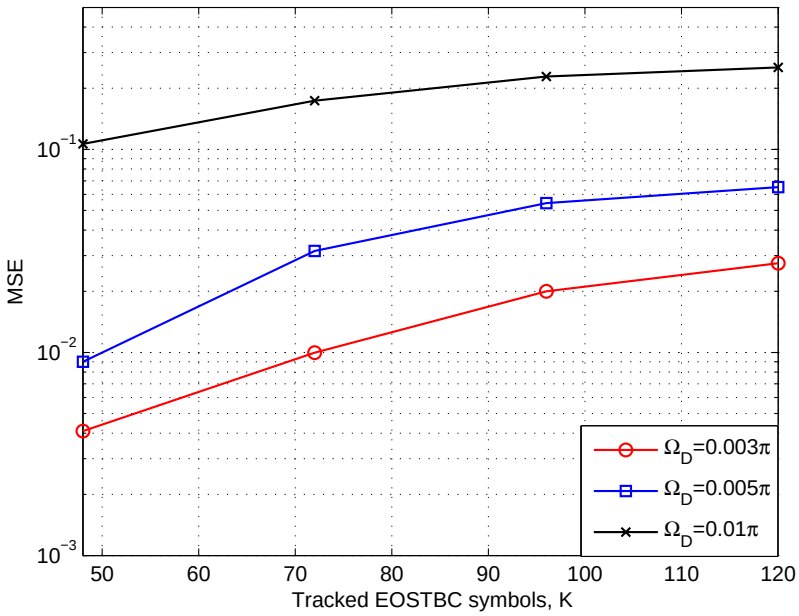

Figure 4.7: Average MSE performance at 20 dB SNR for EO-STBC system with Kalman-based tracking based on different tracking periods K.

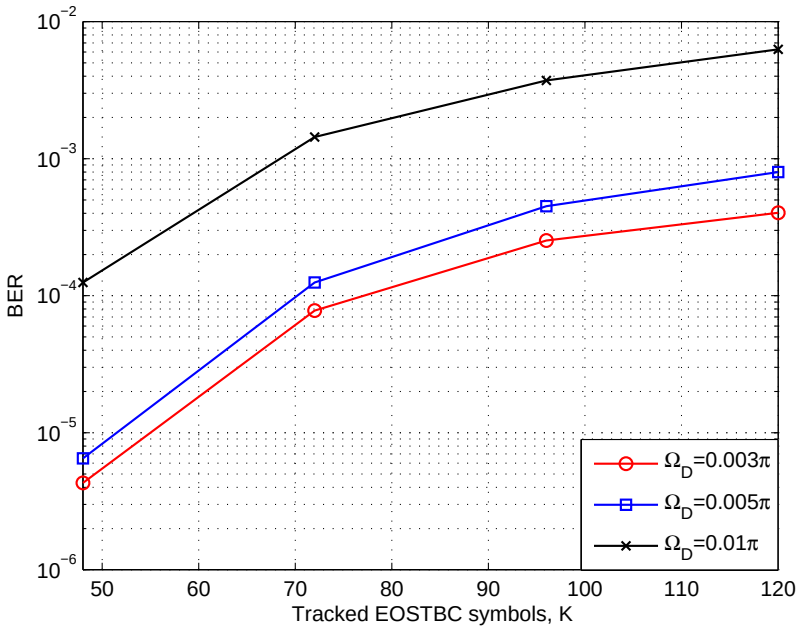

Figure 4.8: Average BER performance at 20 dB SNR for EO-STBC system with Kalman-based tracking based on different tracking periods K.

Chapter 5

FrFT-Based Multi-Carrier Approach for EO-STBC over Doubly-Dispersive Channels

This chapter focuses on the enhancement of extended orthogonal STBC (EO-STBC) when transmitting over a doubly-dispersive channel. The frequency selective nature of the channel favours the combination with a multi-carrier approach such as orthogonal frequency division multiplexing (OFDM). However, as Doppler spread increases, OFDM loses its orthogonality, resulting in severe inter-symbol (ISI) and inter-carrier interference (ICI). This is addressed firstly by the generalisation of OFDM to fractional Fourier transform (FrFT) based multicarrier approaches, which can provide better resilience in the presence of Doppler spread. In higher mobility scenarios, an equalisation scheme is employed, whose low complexity in an FrFT-based multicarrier setting compared to standard OFDM. Simulation results highlight the potential performance improvements.

This chapter is organised as follows. Sec. 5.1 motivates the work within this chapter. In Sec. 5.2, we present a multi-carrier system model based on the FrFT,

into which EO-STBC will be embedded. In Sec. 5.3, the decoding is derived for a low-Doppler situation and a higher-Doppler scenario, whereby additional equalisation is introduced. Finally, simulation results are provided in Sec. 5.5 and conclusions are drawn in Sec 5.6.

5.1 Introduction

In the last ten years, orthogonal frequency division multiplexing (OFDM), has gained considerable attention and has found its way into a large number of wireless and wireline standards. OFDM is a multi-carrier block transmission scheme which decouples the broadband system into independent sub-carriers, which are ISI-free. Therefore, it is particularly popular to apply in time dispersive situations, where otherwise long equalisers would be required; the creation of decoupled narrowband subchannels instead requires only single-tap equalisers in order to adjust the phase and amplitude of individual sub-carriers, which is significantly cheaper and offers performance robustness against noise amplification compared to wideband equalisation.

Space-time block coding (STBC) algorithms such as the Alamouti scheme [32] have been developed in the context of narrowband, stationary channels. In frequency-selective channel conditions, a popular approach is the combination with multicarrier methods such as OFDM [77] in order to operate narrowband STBC schemes in decoupled sub-carriers which are free of inter-symbol (ISI) and inter-carrier interference (ICI). In the case of narrowband time-varying systems, the algorithm degradation is barely felt as long as the channel variation over one STBC symbol can be considered very small. In the context of advanced diversity schemes such as extended orthogonal STBC (EO-STBC), where rate one and maximum diversity order are achieved simultaneously despite an operation with 4 transmit antennas due to the use of additional beam-steering based on feedback

of channel state information (CSI) [42] [78], time variation can be accommodated, and the smoothness of coefficient trajectories due to Doppler spread can be exploited for low-cost high-performance differential feedback of information [73].

However, if a time-varying channel exhibits significant delay spread, then the classical use of multicarrier methods requires considerably longer OFDM symbols. Combined with Doppler spread of the channel, this will compound the lack of quasi-stationarity over an STBC symbol period, requiring the introduction of e.g. equalisation approaches. Equalisation in the DFT-domain has been proposed in the context of OFDM, such as zero-forcing (ZF) and minimum mean-square error (MMSE) schemes [79]. Other receivers are applied to the individual sub-carriers, including the zero-forcing (ZF), decision-feedback (DF), and joint maximum-likelihood (JML) detectors [3], [2]; however, the neglected ICI introduces an error floor into the BER performance as the degree of non-stationarity increases.

In OFDM systems based on the FFT operating in doubly-dispersive channels, ICI and ISI increase and significantly degrade the performance of the system. Expressions for the ICI variance bounds corresponding to Doppler spread have been obtained by [80] [81]. Recently, multi-carrier schemes based on the fractional Fourier transformer (FrFT) have been developed [82], [83], [84]. The FrFT uses chirp signals as carriers, and even though its performance does not entirely decouple the channel in the stationary case, thus leaving an ICI/ISI term, in the time-varying case, the FrFT has demonstrated advantages in terms of admitting lower ICI/ISI errors. The FrFT multi-carrier approach is inferior to FFT-based OFDM in the stationary case because of the FrFT's inability to diagonalise a circulant channel matrix in the way the DFT/FFT does. However, in Doppler scenarios, the FrFT multi-carrier system retains more energy near the main diagonal of the channel matrix, compared to a much degraded OFDM system.

Therefore, we aim to utilise an FrFT multi-carrier system in combination with EO-STBC, which for moderate Doppler spread can be sufficiently resilient on its own. In addition, for higher Doppler spreads, we will explore the combination with equalisation methods [85], [86] based on block minimum mean squared error equalisation. Due to the FrFT's ability to retain the channel energy near the main diagonal of the equivalent channel matrix even for time-varying systems, equalisation approaches for FrFT-based multi-carrier systems can operate a reduced minimum mean square error (MMSE) equaliser when compared to FFT-based OFDM approaches.

MMSE equalisation in the context of FrFT multicarrier transmission assumes that the channel matrix is banded, which will be demonstrated to be sufficient in order to attain good performance with a very low complexity. Such a band structure has previously been exploited for similar OFDM equalisation schemes using an $\mathrm{LDL}^{\mathrm{H}}$ decomposition [87] or an algorithm for sparse linear equations as sparse least squares residual (LSQR) [88]. Additionally, to further reduce the system complexity, we compute a regularised solution of a linear system involving the channel matrix by means of a recently proposed least squares minimum residual (LSMR) algorithm [89].

5.2 System Model

In order to address the time-dispersive nature of the transmission channel, in this section we will discuss multi-carrier techniques in combination with EO-STBC. The proposed system uses a multi-carrier approach for EO-STBC, which is well-established using OFDM in the stationary case. The idea is that OFDM decouples the broadband system into independent sub-carriers, which are ISI-free. Therefore, narrowband space-time coding approaches such as EO-STBC can be applied to individual sub-carriers. However, in the case of a non-stationary chan-

nel, OFDM loses its orthogonality, resulting in ISI and a subsequently degraded performance. Therefore, Sec. 5.2.2 will analyse a generalised multicarrier OFDM-style system based on the FrFT for the single-input single-output case, which can provide a higher resilience in non-stationary situations compared to OFDM. Thereafter, Sec. 5.2.3 will integrate this multicarrier approach with EO-STBC in a MISO system setting.

5.2.1 Discrete Fractional Fourier Transform

The fraction Fourier transform (FrFT) is a generalisation of the Fourier transform, and performs an analysis with respect to chirp signals rather than complex exponentials. Without further commenting on the continuous form of the FrFT, we below focus on the discrete-time FrFT as defined in [90, 91], and for brevity refer to this discrete version as FrFT.

One way to calculate the FrFT is from an eigenvalue decomposition (EVD) of the DFT matrix $\mathbf{T}$. We assume that the DFT matrix is normalised,

$$[\mathbf{T}]_{(n,k)} = \frac{1}{\sqrt{N}} e^{-j\frac{2\pi}{N}nk} \quad , \tag{5.1}$$

such that $\mathbf{T}$ is unitary. For such a normalised N-point DFT matrix $\mathbf{T} = \mathbf{E}\mathbf{\Lambda}\mathbf{E}^{-1}$, the eigenvalues are contained in the diagonal matrix $\mathbf{\Lambda}$, with the corresponding eigenvectors forming the columns of the matrix $\mathbf{E}$. Based on this decomposition, the N-point FrFT matrix $\mathbf{F}_a$ of order a is

$$\mathbf{F}_a = \mathbf{E}\mathbf{\Lambda}^a\mathbf{E}^{-1} \quad . \tag{5.2}$$

Even though this definition in [91] does not reveal the chirp basis of this transform, a few characteristics of the FrFT are immediately obvious. Firstly, for $a = 1$, the FrFT is identical to the DFT matrix, $\mathbf{T} = \mathbf{F}_a|_{a=1}$. Secondly, the inverse FrFT

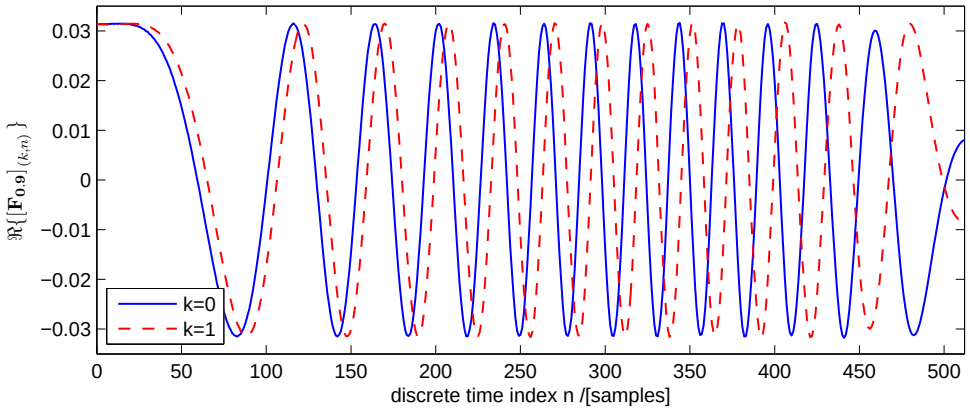

Figure 5.1: FrFT basis functions for an $N = 2^{10}$ point FrFT of order $a = 0.9$, forming the first two rows of $\mathbf{F}_{0.9}$.

(IFrFT) matrix of order a is given by $\mathbf{F}_{-a}$, since it is easily verified from (5.2) that

$$\mathbf{F}_a\mathbf{F}_{-a} = \mathbf{F}_{-a}\mathbf{F}_a = \mathbf{I} \quad . \tag{5.3}$$

Lastly, with $\mathbf{F}_1 = \mathbf{T}$ and (5.3), we can deduce that an FrFT matrix of order $a = -1$ is identical to an inverse DFT (IDFT) matrix, $\mathbf{F}_{-1} = \mathbf{T}^{-1} = \mathbf{T}^*$.

To demonstrate that the FrFT analyses w.r.t. chirp bases, Fig. 5.1 shows the first two rows of the 2^{10}-point FrFT matrix $\mathrm{F}_{0.9}$.

Only the real part is shown, but it is evident that-different from the DFT-the FrFT aim to express an input vector $\mathbf{x}$ in terms of a superposition of orthogonal chirps, whose amplitude and phase will define the FrFT domain coefficients in the transform domain vector $\mathbf{y} = \mathbf{F}_a\mathbf{x}$.

Efficient implementations of the FrFT have been considered in [90], and are linked to the way the FFT exploits redundant calculations of the DFT matrix, such that the computational complexity is of order $\mathcal{O}(N \log_2 N)$, with a slight increase of calculations over an N-point FFT calculation. Therefore, there is no significant computational penalty in replacing the DFT by an FrFT in applications where the generalisation offers potential performance advantages.

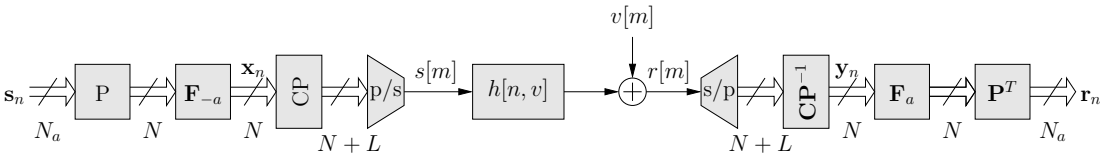

Figure 5.2: FrFT-OFDM system using N sub-carriers and a cyclic prefix of length L to transmit over a doubly-dispersive channel $h[m, v]$, whereby $\mathbf{P}$ maps symbols onto $N_a \leqslant N$ active subcarriers and $\mathbf{F}_a$ is the FrFT matrix.

5.2.2 FrFT-Based Multi-Carrier System

A multi-carrier approach based on the FrFT has been proposed in [82], whereby the discrete FrFT replaces the FFT block in OFDM, and can be used for EO-STBC in high Doppler spread with the advantages of increasing the output SNR. This multicarrier transceiver based on the FrFT is shown in Fig. 5.2.

5.2.2.1 FrFT-OFDM Modulation and Demodulation

Letting N denote the number of subcarriers, in order to reduce adjacent channel interference (ACI) without additional processing, OFDM typically allows $N_a < N$ active sub-carriers.

Following an IFrFT block a cyclic prefix (CP) is included for each OFDM symbol. To eliminate ICI and ISI caused by the time dispersion of the channel, the CP length N_g must be chosen longer than or equal to the channel order L, i.e., $N_g \geq L$. The block $\mathbf{x}_n \in \mathbb{C}^{N+L}$ is transmitted in series over the doubly-dispersive channel. At the receiver side, the signal is serial-to-parallel converted, and, after discarding of the CP, and FrFT matrix is applied.

5.2.2.2 Transmission Channel Matrix

We assume that the above transmit and receive architecture operates at both ends of a frequency selective channel with a finite impulse response (FIR) of length L. Assuming a wide sense stationary uncorrelated scattering (WSSUS)

channel, it is modelled as a complex Gaussian stochastic process is given by $[\ h\,[n,0] \quad h\,[n,1] \quad \cdots \quad h\,[n,L-1]\ ]$, where $h\,[n,l]$ holds the l^{th} channel coefficient at time n. We assume that $h\,[n,l]$ is a zero mean complex Gaussian random variable with variance σ_l^2. The classical Doppler spectrum based on Jake's as applied in [3] has been adopted.

The effect of the channel can be represented by a channel matrix $\mathbf{H}[n]$, which is is derived by trans-multiplexing across the channel $h[n,l]$ in Fig. 5.2, and can be formulated as

$$[\mathbf{H}[n]]_{i,j} = \begin{cases} h[n-L+i, i-j] & i \geq j, \\ h[n-L+i, L+i-j-1] & i < j. \end{cases} . \tag{5.4}$$

Due to its circulant property, the matrix in (5.4) can be decoupled by the DFT if the channel impulse response (CIR) remains constant over one OFDM symbol period. If the CIR varies within one OFDM symbol period, $\mathbf{H}[n]$ cannot be decoupled by the DFT. Here, the application of the FrFT matrix $\mathbf{F}_a$ as a generalisation of the DFT can provide benefits in time-varying scenarios, where a suitable selection of the order a can provide a better concentration of energy near the main diagonal than for the DFT with a fixed $a = 1$ [92].

The multi-carrier transceiver system in Fig. 5.2 further includes a reduction of the total number N of sub-carriers by a masking matrix $\mathbf{P}$,

$$\mathbf{P} = \left[\mathbf{0}_{N_\mathrm{a}\times(N-N_\mathrm{a})/2}\ \ \mathbf{I}_{N_\mathrm{a}}\ \ \mathbf{0}_{N_\mathrm{a}\times(N-N_\mathrm{a})/2}\right]^\mathrm{T}, \tag{5.5}$$

where the 0's indicate the guard bands to only utilise $N_a \leq N$ active users. The purpose of $\mathbf{P}$ is to ease the burden on the spectral mask requirements typically implemented via transmit and receive filters, as well as to ensure that the equivalent system matrix

$$\mathbf{C}[n] = \mathbf{P}^{\mathrm{H}}\mathbf{F}_a\mathbf{H}[n]\mathbf{F}_{-a}\mathbf{P}, \tag{5.6}$$

contains only diagonal and near-diagonal terms, but no longer components in its lower left and upper right corners. The received signal after multiplication by the FrFT matrix $\mathbf{F}_a$ is

$$\mathbf{r}_n = \mathbf{F}_a\mathbf{y}_n = \mathbf{C}[n]\mathbf{s}_n + \tilde{\mathbf{v}}_n, \tag{5.7}$$

while the channel noise $\tilde{\mathbf{v}}_n = \mathbf{F}_a\mathbf{v}_n$ retains its power after processing by the DFrFT since $\mathbf{F}_a$ is a unitary matrix. With the above defined FrFT-OFDM defined this multi-carrier scheme, we can now exploit this system to enable EO-STBC transmission over frequency-selective channel and potentially time-varying channels in the next section.

5.2.3 Closed-Loop EO-STBC

EO-STBC is a diversity scheme based on four transmit and one receive antennas. Since normally no space-time coder can achieve both full rate and full diversity gain for such a system dimension, additional phase rotations applied in the transmitter ensure not only full diversity but also an array gain [42], which has been shown to be $\gamma = 4 + \pi$ in Chapter 3.2.3. The rotations are optimised based on channel state information in the receiver, and need to be fed back to the transmitter, which is here assumed to be delay-less and error-free for simplicity. In broadband scenarios, EO-STBC can be easily embedded in a multi-carrier transmission scheme [77] such as outlined in Sec. 5.2.2, and as shown in the block diagram in Fig. 5.3. The dimension of the input vector $\mathbf{a}[n]$ and of all remaining vectors is equivalent to the number of active sub-carriers, N_a. The OFDM transmit symbols $\mathbf{s}_i[n]$, $i = 1...2$, emitted from the four antennas are defined over two

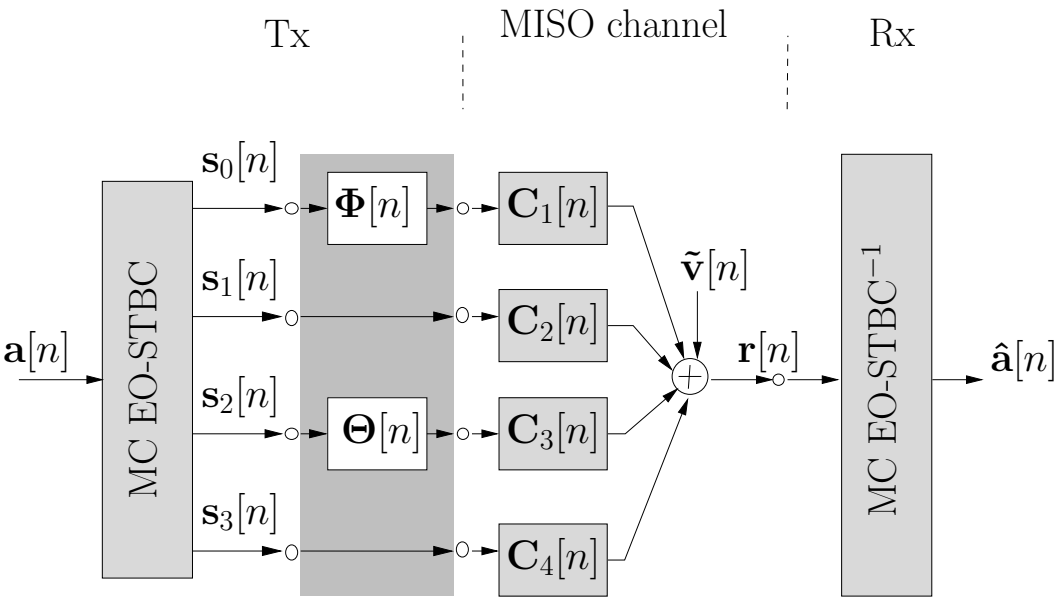

Figure 5.3: EO-STBC in a multi-carrier configuration with equivalent multi-carrier channel matrices $\mathbf{C}_i[n]$, $i = 1 \ldots 4$, and beam-steering by rotations $\mathbf{\Phi}[n]$ and $\mathbf{\Theta}[n]$ which are based on feedback from the receiver to the transmitter, and can maximise the diversity and array gain of this system.

consecutive symbol periods as

$$\mathbf{s}_j[n] = \begin{cases} \mathbf{a}[n], & n \text{ even}, \\ \mathbf{a}^*[n], , & n \text{ odd}, \end{cases} \tag{5.8}$$

$$\mathbf{s}_{j+2}[n] = \begin{cases} \mathbf{a}[n+1], & n \text{ even}, \\ \mathbf{a}^*[n-1], , & n \text{ odd}, \end{cases} \tag{5.9}$$

for $j \in \{1, 2\}$. The first and third antenna signal include a modification according to Fig. 5.3, whereby the matrices

$$\mathbf{\Phi}[n] = \text{diag}\left\{e^{j\varphi_1[n]} \ldots e^{j\varphi_{Na}[n]}\right\} \tag{5.10}$$

$$\mathbf{\Theta}[n] = \text{diag}\left\{e^{j\vartheta_1[n]} \ldots e^{j\vartheta_{Na}[n]}\right\}, \tag{5.11}$$

apply a rotation to every sub-carrier. Using the equivalent multi-carrier channel model defined in (5.6) to describe every of the four transmit paths connecting the transmitter with the receiver, according to Fig. 5.3, the received signal vector $\mathbf{r}[n]$ is given by

$$\mathbf{r}_n = \tilde{\mathbf{C}}_1[n]\mathbf{s}_1[n] + \mathbf{C}_2\mathbf{s}_2[n] + \tilde{\mathbf{C}}_3[n]\mathbf{s}_3[n] + \mathbf{C}_3\mathbf{s}_3[n] + \tilde{\mathbf{v}}_n, \tag{5.12}$$

with $\tilde{\mathbf{C}}_1[n] = \mathbf{C}_1[n]\mathbf{\Phi}[n]$ and $\tilde{\mathbf{C}}_3[n] = \mathbf{C}_3[n]\mathbf{\Theta}[n]$, and $\tilde{\mathbf{v}}_n = \mathbf{P}\mathbf{F}_a\mathbf{v}_n$, where $\mathbf{v}_n$ is a circularly symmetric zero mean white complex Gaussian random noise vector with covariance $\mathcal{E}\left\{\mathbf{v}_n\mathbf{v}_n^H\right\} = \sigma_v^2\mathbf{I}_{N_a}$, as shown in Fig. 5.3. Gathering data over two successive OFDM symbol periods, the received signal vector can be written as

$$\begin{bmatrix} \mathbf{r}[n] \\ \mathbf{r}^*[n+1] \end{bmatrix} = \mathbf{G}[n] \begin{bmatrix} \mathbf{a}[n] \\ \mathbf{a}[n+1] \end{bmatrix} + \begin{bmatrix} \mathbf{v}[n] \\ \mathbf{v}^*[n+1] \end{bmatrix}, \tag{5.13}$$

with

$$\mathbf{G}[n] = \begin{bmatrix} \tilde{\mathbf{C}}_1[n] + \mathbf{C}_2[n] & \tilde{\mathbf{C}}_3[n] + \mathbf{C}_4[n] \\ \tilde{\mathbf{C}}_3^*[n+1] + \mathbf{C}_4^*[n+1] & -\tilde{\mathbf{C}}_1^*[n+1] - \mathbf{C}_2^*[n+1] \end{bmatrix}. \tag{5.14}$$

As long as the MISO channel is stationary and the FrFT chirp rate $a = \pm 1$, i.e. the FrFT particularises to the Fourier transform, the equivalent system channel matrices $\mathbf{C}_i[n]$ will be diagonal, ensuring that sub-carriers can be EO-STBC decoded individually and ICI can be neglected.

5.3 Proposed Low Doppler Spread Space-Time Decoding

Below, we discuss proposed solutions for decoding the FrFT-based multi-carrier EO-STBC transmission scheme introduced in Sec. 5.2. For low Doppler spread, we will simply ignore the effect of coupling between carriers as well as ISI, while the impact for higher Doppler spread motivates the introduction of an additional low complexity equaliser to mitigate the impact of increased ICI and ISI terms.

For low Doppler scenarios with a near-stationary channel, symbols are detected by ignoring ICI, using only the elements on the main diagonal of the equivalent channel matrices. Here we discuss individual per-carrier decoding using classical OFDM with $\mathbf{F}_a$ for $a = 1$ [3]. This implies that any off-diagonal components in the equivalent channel matrices $\mathbf{C}_i[n]$ are ignored, and that EO-STBC decoding is based on the reduced system matrix

$$\mathbf{\Gamma}_n = \begin{bmatrix} \mathbf{I} & \mathbf{I} \\ \mathbf{I} & \mathbf{I} \end{bmatrix} \odot \mathbf{G}[n], \tag{5.15}$$

where $\odot$ represents element-wise multiplication. Thus decoding is performed as

$$\begin{bmatrix} \hat{\mathbf{a}}[n] \\ \hat{\mathbf{a}}[n+1] \end{bmatrix} = \mathbf{\Gamma}_n^{\mathrm{H}} \mathbf{G}[n] \begin{bmatrix} \mathbf{a}[n] \\ \mathbf{a}[n+1] \end{bmatrix} + \mathbf{\Gamma}^{\mathrm{H}}[n] \tilde{\mathbf{v}}_n. \tag{5.16}$$

This is equivalent to the isolation of individual sub-carriers. If cross-talk is considered, [2], [3] show that the JML detector can achieve full diversity gain at low Doppler spread. The error in approximating the true system matrix $\mathbf{G}[n]$ by the diagonalised version $\mathbf{\Gamma}_n$ introduces an error $\mathbf{E}[n] = \mathbf{G}[n] - \mathbf{\Gamma}_n$. For low Doppler spread, this error can be considered small with an upper bound on ICI provided in [81], which, together with the noise term $\mathbf{\Gamma}_n^{\mathrm{H}} \tilde{\mathbf{v}}_n$ in (5.16), can be treated as additive channel noise collected in the vector $\mathbf{u}[n]$ in

$$\begin{bmatrix} \hat{\mathbf{a}}[n] \\ \hat{\mathbf{a}}[n+1] \end{bmatrix} = \mathbf{\Gamma}_n^{\mathrm{H}} \mathbf{\Gamma}_n \begin{bmatrix} \mathbf{a}[n] \\ \mathbf{a}[n+1] \end{bmatrix} + \mathbf{u}[n], \tag{5.17}$$

for the decoding process. Moreover, the cascade of $\mathbf{\Gamma}_n$ with its matched filter $\mathbf{\Gamma}_n^{\mathrm{H}}$ yields a matrix whose on-diagonal terms represent the gain while off-diagonal terms represent crosstalk. The diversity gain obtained from (5.17) can be maximised by ensuring that the angles in $\mathbf{\Phi}[n]$ and $\mathbf{\Theta}[n]$ maximise the on-diagonal terms of $\mathbf{\Gamma}_n^{\mathrm{H}} \mathbf{\Gamma}_n$ in (5.17). The explicit calculation of the angles is omitted here, but leads to the selection

$$\mathbf{\Phi}[n] = -\angle\{\mathbf{I} \odot \mathbf{C}_1[n]\mathbf{C}_2^*[n]\} \tag{5.18}$$

$$\mathbf{\Theta}[n] = -\angle\{\mathbf{I} \odot \mathbf{C}_3[n]\mathbf{C}_4^*[n]\} \tag{5.19}$$

$$\mathbf{\Phi}[n+1] = -\angle\{\mathbf{I} \odot \mathbf{C}_3[n+1]\mathbf{C}_4^*[n+1]\} \tag{5.20}$$

$$\mathbf{\Theta}[n+1] = -\angle\{\mathbf{I} \odot \mathbf{C}_1[n+1]\mathbf{C}_2^*[n+1]\}. \tag{5.21}$$

These values need to be calculated in the receiver based on the estimate of $\mathbf{\Gamma}_n$, and appropriately fed back to the transmitter, e.g. via a quantised feedback channel [42], [38], where with N_a, sub-carriers, the total number of feedback bits will then be $N_a B$. Unfortunately, even with low rate quantisation, the feedback requirements generally grow in proportion to the number of active sub-carriers.

In an OFDM system, coherence across sub-carriers can be exploited, leading to a reduced feedback scheme [42], whereby the sub-carriers are divided into groups that span no further than the channel coherence bandwidth. Thus only the feedback bits B corresponding to one sub-carrier from each group are fed back, while the remaining sub-carriers are obtained by interpolation. In slow fading scenarios, coefficients evolve slowly with time, and a significant further reduction

on feedback overheads can be achieved by differential feedback of rotation angles [73].

5.3.1 EO-STBC Detectors for Near-Stationary Channel

In this section, we discuss EO-STBC receivers to combat crosstalk resulting from low Doppler spread for every subblock of carriers in order to achieve full diversity gain. In STBC systems, the channels are normally assumed to remain constant over one STBC block. In this case, the equivalent system channel matrices are orthogonal and symbols can be decoded by a simple maximum likelihood (SML) algorithm, which decodes symbols separately with low complexity [3]. However, in time selective fading channels, the channels are non-stationary over one STBC block; therefore, the equivalent system channel matrices are no longer orthogonal, so decoding to decrease the effect of cross-talk can be performed by the joint maximum likelihood (JML) algorithm, which performs joint detection of several symbols with a higher complexity than decoders that have been proposed by [2]. The derivation of EO-STBC cross-talk receivers is outlined below; for further details we refer the reader to [3].

For instance decoding are performed for individual per-carrier using classical OFDM with $\mathbf{F}_a$ for $a = 1$ discussed in Sec. 5.3, in which the $\mathbf{\Gamma}[n]$ in (5.15) can be rearranged into permuted banded channel system $\bar{\mathbf{\Gamma}}_n$ by multiplication with a permutation matrix similar to [93]. The permutation matrix $\mathbf{P}_{M,N_a}$ is $(MN_a \times MN_a)$ given as

$$[\mathbf{P}_{M,N_a}]_{i,j} = \begin{cases} 1 & ,\{i+1,\ \lfloor i/M \rfloor + 1 + N_a \mathrm{mod}\,(i,M)\}_{i=0}^{MN_a-1} \\ 0 & \text{elsewhere.} \end{cases} . \tag{5.22}$$

Therefore, the permutation of rows of $\underline{\mathbf{r}}_n = \mathbf{P}_{2,N_a}\mathbf{r}_n$ as well as rows and columns

of $\underline{\Gamma}_n = \mathbf{P}_{2,N_a}\mathbf{\Gamma}_n\mathbf{P}_{2,N_a}^{\mathrm{T}}$, yields

$$\underline{\mathbf{r}}_n = \left[\begin{array}{cccc} \bar{\mathbf{r}}_n, & \bar{\mathbf{r}}_{n+2}, & \cdots & \bar{\mathbf{r}}_{n-2N_a+2} \end{array} \right]^{\mathrm{T}} \tag{5.23}$$

$$\underline{\Gamma}_n = \text{blockdiag}\left\{ \begin{array}{cccc} \bar{\mathbf{\Gamma}}_n, & \bar{\mathbf{\Gamma}}_{n+2}, & \cdots & \bar{\mathbf{\Gamma}}_{n-2N_a+2} \end{array} \right\}, \tag{5.24}$$

we view $\underline{\Gamma}_n$ as a $2N_a \times 2N_a$ of 2×2 subblock $\bar{\mathbf{\Gamma}}_n$, which is equivalent to per-carrier EO-STBC channel matrix. Therefore, we can collect transmitted signals on sub-carrier basis as

$$\left[\begin{array}{c} \bar{r}[n] \\ \bar{r}^*[n+1] \end{array} \right] = \bar{\mathbf{\Gamma}}_n \left[\begin{array}{c} \bar{a}[n] \\ \bar{a}[n+1] \end{array} \right] + \left[\begin{array}{c} \bar{u}[n] \\ \bar{u}^*[n+1] \end{array} \right], \tag{5.25}$$

where $\bar{\mathbf{\Gamma}}_n$ collects the coefficients of system channel in (5.14) over two successive time slots of four identical subcarriers given as

$$\bar{\mathbf{\Gamma}}_n = \left[\begin{array}{cc} \tilde{C}_1[n] + C_2[n] & \tilde{C}_3[n] + C_4[n] \\ \tilde{C}_3^*[n+1] + C_4^*[n+1] & -\tilde{C}_1^*[n+1] - C_2^*[n+1] \end{array} \right]. \tag{5.26}$$

5.3.1.1 JML Detector

The ML detector chooses the message $\bar{\mathbf{a}}$, which yields the smallest distance between the received vector $\bar{\mathbf{r}}_n$, and hypothesised message $\bar{\mathbf{\Gamma}}_n\bar{\mathbf{a}}$, i.e. $\hat{\bar{\mathbf{a}}}_n$ is given by

$$\hat{\bar{\mathbf{a}}}_n = \arg\min_{\bar{\mathbf{a}}} \left\| \bar{\mathbf{r}}_n - \bar{\mathbf{\Gamma}}_n\bar{\mathbf{a}} \right\|^2. \tag{5.27}$$

Alternatively, for EO-STBC matched filtering decoding can be performed by multiplying by $\mathbf{D}_M$ on both sides of (5.25),

$$\bar{\mathbf{r}}_M = \bar{\mathbf{\Gamma}}_M.\bar{\mathbf{a}}_n + \bar{\mathbf{u}}_M, \tag{5.28}$$

where $\mathbf{D}_M = \mathbf{A}_M\bar{\mathbf{\Gamma}}_n^{\mathrm{H}}$, $\bar{\mathbf{\Gamma}}_M = \mathbf{D}_M\bar{\mathbf{\Gamma}}_n$, and $\bar{\mathbf{u}}_M = \mathbf{D}_M\bar{\mathbf{u}}_n$ with covariance $\mathcal{E}\left\{\bar{\mathbf{u}}_M\bar{\mathbf{u}}_M^{\mathrm{H}}\right\} = \sigma_v^2\bar{\mathbf{\Gamma}}_M\mathbf{A}_M^{\mathrm{H}}$. The real valued diagonal matrix $\mathbf{A}_M$ is chosen such that the diagonal elements of $\mathcal{E}\left\{\bar{\mathbf{u}}_M\bar{\mathbf{u}}_M^{\mathrm{H}}\right\}$ are $\sigma_{\bar{u}}^2$, therefore requiring

$$\mathbf{A}_M = \begin{bmatrix} (\alpha_1+\beta_1)^{-\frac{1}{2}} & 0 \\ 0 & (\alpha_2+\beta_2)^{-\frac{1}{2}} \end{bmatrix}, \tag{5.29}$$

where

$$\begin{aligned}
\alpha_1 &= \sum_{m=1}^{2}|C_m[n]|^2 + \sum_{m=3}^{4}|C_m[n+1]|^2 && (5.30)\\
\beta_1 &= 2\Re\{e^{j\varphi[n]}C_1[n]C_2^*[n] + e^{j\vartheta[n+1]}C_3[n+1]C_4^*[n+1]\} && (5.31)\\
\alpha_2 &= \sum_{m=1}^{2}|C_m[n+1]|^2 + \sum_{m=3}^{4}|C_m[n]|^2 && (5.32)\\
\beta_2 &= 2\Re\{e^{j\varphi[n+1]}C_1[n+1]C_2^*[n+1] + e^{j\vartheta[n]}C_3[n]C_4^*[n]\}. && (5.33)
\end{aligned}$$

Furthermore, let the cascade of $\bar{\mathbf{\Gamma}}_n$ with its matched filter $\bar{\mathbf{\Gamma}}_n^{\mathrm{H}}$ be

$$\bar{\mathbf{G}}_n = \bar{\mathbf{\Gamma}}_n^{\mathrm{H}}\bar{\mathbf{\Gamma}}_n = \begin{bmatrix} (\alpha_1+\beta_1) & \xi \\ \xi^* & (\alpha_2+\beta_2) \end{bmatrix}, \tag{5.34}$$

which is a positive semi-definite matrix with

$$\begin{aligned}
\xi &= e^{j(\vartheta[n]-\varphi[n])}C_1^*[n]C_3[n] - e^{j(\vartheta[n+1]-\varphi[n+1])}C_1^*[n+1]C_3[n+1] + e^{-j\varphi[n]}C_1^*[n]C_4[n]\\
&\quad -e^{-j\varphi[n+1]}C_1^*[n+1]C_4[n+1] + e^{j\vartheta[n]}C_2^*[n]C_3[n] - e^{j\vartheta[n+1]}C_2^*[n+1]C_3[n+1]\\
&\quad +C_2^*[n]C_4[n] - C_2^*[n+1]C_4[n+1]. \qquad (5.35)
\end{aligned}$$

Therefore for matrix $\bar{\mathbf{\Gamma}}_M$ of (5.28), we obtain

$$\bar{\mathbf{\Gamma}}_M = \mathbf{A}_M \bar{\mathbf{G}}_n = \begin{bmatrix} (\alpha_1 + \beta_1)^{\frac{1}{2}} & \xi\,(\alpha_1 + \beta_1)^{-\frac{1}{2}} \\ \xi^*\,(\alpha_2 + \beta_2)^{-\frac{1}{2}} & (\alpha_2 + \beta_2)^{\frac{1}{2}} \end{bmatrix}. \tag{5.36}$$

The JML detection rule in (5.27) is now equivalent to

$$\hat{\bar{\mathbf{a}}}_n = \arg\min_{\bar{\mathbf{a}}} \left\{ \left(\bar{\mathbf{r}}_M - \bar{\mathbf{\Gamma}}_M \cdot \bar{\mathbf{a}}\right)^{\mathrm{H}} \left(\bar{\mathbf{\Gamma}}_M \mathbf{A}_M^{\mathrm{H}}\right)^{-1} \left(\bar{\mathbf{r}}_M - \bar{\mathbf{\Gamma}}_M \cdot \bar{\mathbf{a}}\right) \right\}. \tag{5.37}$$

Hence we conclude that matched filter is equivalent to JML detection, which is optimal and can achieve full diversity gain but with higher complexity compared to suboptimal detection with low expected complexity and lower diversity gain.

5.3.1.2 SML Detector

From (5.28), without considering the correlation of the noise $\mathbf{v}_M$ and the cross-talk i.e., the off-diagonal terms of $\bar{\mathbf{\Gamma}}_M$, the SML detector simply obtains the decision about $\hat{\bar{a}}[n]$ and $\hat{\bar{a}}[n+1]$ separately

$$\hat{\bar{a}}[n+i] = \arg\min_{\bar{a}} \left\{ \left| \bar{r}_M[n+i] - (\alpha_i + \beta_i)^{\frac{1}{2}} \cdot \bar{a} \right|^2 \right\},\ i = \{1, 2\}, \tag{5.38}$$

which has a lower complexity compared to the JML detector defined in (5.37).

5.3.1.3 DF Detector

Because $\bar{\mathbf{G}}$ in (5.34) is Hermitian, it possesses a unique Cholesky factorization of the form $\bar{\mathbf{G}} = \mathbf{L}^{\mathrm{H}}\mathbf{L}$, where $\mathbf{L}$ is lower triangular with real diagonal elements and

can be expressed as

$$\mathbf{L} = \begin{bmatrix} \zeta\left(\alpha_2+\beta_2\right)^{-\frac{1}{2}} & 0 \\ \xi^*\left(\alpha_2+\beta_2\right)^{-\frac{1}{2}} & \left(\alpha_2+\beta_2\right)^{\frac{1}{2}} \end{bmatrix}, \tag{5.39}$$

where

$$\zeta^2 = \left(\alpha_1+\beta_1\right)\left(\alpha_2+\beta_2\right) - \left(\xi^*\right)^2. \tag{5.40}$$

Once the above processing is performed, we employ the whitening matched filter on the received ST codeword, that is, multiplying on both sides of (5.28) yields

$$\bar{\mathbf{r}}_W = \mathbf{C}_W\bar{\mathbf{r}}_n = \mathbf{L}\cdot\bar{\mathbf{a}}_n + \bar{\mathbf{u}}_W, \tag{5.41}$$

where $\mathbf{C}_W = \left(\mathbf{L}^{-1}\right)^{\mathrm{H}}\bar{\mathbf{\Gamma}}_n^{\mathrm{H}}$, and $\mathbf{C}_W\bar{\mathbf{r}}_n$ is whitened-matched filter (WMF) for the matrix channel $\bar{\mathbf{\Gamma}}_n$, with its name derived from the fact that $\bar{\mathbf{u}}_W$ is still white with the same statistics as $\bar{\mathbf{u}}_n$. Based on the WMF output, the DF detector makes a decision on n without crosstalk from $\bar{s}[n+1]$. Assuming this decision is correct, the estimates $\hat{\mathrm{s}}[n]$ is then incorporated into the estimation of $\hat{\mathrm{s}}[n+1]$, namely

$$\begin{cases} \hat{\bar{a}}[n] = \arg\min\limits_{\bar{a}}\left\{\left|\bar{r}_Z[n] - \zeta\left(\alpha_1+\beta_1\right)^{-\frac{1}{2}}\cdot\bar{a}\right|^2\right\} \\ \hat{\bar{a}}[n+1] = \arg\min\limits_{\bar{a}}\left\{\left|\bar{r}_Z[n+1] - \xi^*\zeta\left(\alpha_2+\beta_2\right)^{-\frac{1}{2}}\cdot\bar{a}[n] - \zeta\left(\alpha_2+\beta_2\right)^{\frac{1}{2}}\bar{a}\right|^2\right\} \end{cases}. \tag{5.42}$$

5.3.1.4 ZF Detector for Subblock of Sub-carriers

Starting from (5.28), the ZF detector forces the crosstalk to zero. Multiplying by $\mathbf{D}_Z$ on both sides of (5.25) gives

$$\bar{\mathbf{r}}_Z = \mathbf{A}_Z\cdot\bar{\mathbf{a}}_n + \bar{\mathbf{u}}_Z, \tag{5.43}$$

where $\mathbf{A}_Z = \mathbf{D}_Z \bar{\mathbf{\Gamma}}_n^{-1}$, and $\mathbf{v}_Z = \mathbf{D}_Z \bar{\mathbf{u}}_M$. The real diagonal matrix $\mathbf{A}_Z$ is chosen such that the diagonal elements of $\mathcal{E}\left\{\bar{\mathbf{u}}_Z \bar{\mathbf{u}}_Z^{\mathrm{H}}\right\}$ are $\sigma_{\bar{u}}^2$, and is given by

$$\mathbf{A}_Z = \begin{bmatrix} \zeta\left(\alpha_2 + \beta_2\right)^{-\frac{1}{2}} & 0 \\ 0 & \zeta\left(\alpha_1 + \beta_1\right)^{-\frac{1}{2}} \end{bmatrix}. \tag{5.44}$$

Consequently, according to (33), the ZF detector can make decisions about $\hat{a}[n]$ and $\hat{a}[n+1]$ independently. That is

$$\begin{cases} \hat{\bar{a}}[n] = \arg\min\limits_{\bar{a}} \left\{ \left| \bar{r}_Z[n] - \zeta\left(\alpha_2 + \beta_2\right)^{-\frac{1}{2}} \cdot \bar{a} \right|^2 \right\} \\ \hat{\bar{a}}[n+1] = \arg\min\limits_{\bar{a}} \left\{ \left| \bar{r}_Z[n+1] - \zeta\left(\alpha_1 + \beta_1\right)^{-\frac{1}{2}} \cdot \bar{a} \right|^2 \right\} \end{cases}. \tag{5.45}$$

5.4 Proposed Open Loop Decoding with Equalisation

Doppler spread or an FrFT parameter selection $a \neq \pm 1$ causes the equivalent channel matrix (5.6) to loose its diagonal structure such that the system matrix (5.14) introduces coupling between at least adjacent sub-carriers. Since OFDM systems are likely to operate at different mobility situations, the coupling due to non-stationary system characteristics arising from high Doppler spreads can become very significant. In order to mitigate the impact of high Doppler spread on the EO-STBC decoding performance, in the following an equaliser is introduced, which is an extension of the work in [92] to EO-STBC. This equaliser increases the receiver complexity, but removes the need for feedback of angles to the transmitter, where therefore the beamsteering matrices are simply set as $\mathbf{\Phi}[n] = \mathbf{\Theta}[n] = \mathbf{I}$.

5.4.1 Banded Linear Block MMSE Decoding

Assuming perfect channel state information, a linear block MMSE equaliser is defined based on the system matrix $\mathbf{G}[n]$ in (5.14) as

$$\mathbf{W}_{n,\mathrm{MMSE}} = \mathbf{G}[n]^{\mathrm{H}} \left(\mathbf{G}[n]\mathbf{G}[n]_n^{\mathrm{H}} + \gamma^{-1}\mathbf{I}\right)^{-1}, \tag{5.46}$$

where γ is the signal to noise ratio (SNR) at the input to the equaliser, assuming corruption by white Gaussian noise. The matrix inversion in (5.46) requires requires $\mathcal{O}\left((2N_a)^3\right)$ flops which is impractical for high values of $(2N_a)$. The zero-forcing ZF equaliser $\mathbf{W}_{n,\mathrm{ZF}}$, which applies the inverse of the $\mathbf{G}[n]$ in (5.14), can be calculated from (5.51) for the special case

$$\mathbf{W}_{n,\mathrm{ZF}} = \mathbf{W}_{n,\mathrm{MMSE}}|_{\gamma\to\infty}. \tag{5.47}$$

Similar to (5.46), the matrix inversion in (5.47) is of order $\mathcal{O}\left((2N_a)^3\right)$. Therefore, OFDM equalisation generally schemes use banded equalisers which can offer lower complexity.

To reduce the computational cost, we assume that ICI induced by widely separated sub-carriers can be neglected. This is based on the observation in [92] that most energy of the equivalent channel matrix is concentrated in the vicinity of the main diagonal such that the channel matrix $\mathbf{G}[n]$ can be approximated by banded sub-matrices incorporating Q off-diagonals neither side. The parameter Q can be selected to balance between performance and complexity. The restriction of the equivalent channel matrix to a banded form can be enforced by means of a binary masking matrix $\mathbf{M}$ with elements

$$[\mathbf{M}]_{ij} = \begin{cases} 1 & 0 \le |i-j| \le Q, \\ 0 & Q < |i-j| < N_{\mathrm{a}}. \end{cases} \tag{5.48}$$

Obviously, a larger Q leads to a smaller approximation error and hence a performance improvement. On the other hand, for higher bandwidth of $\mathbf{M}$ the complexity will be increasing. The value of Q can be chosen according to some rules of thumb in [79]. Usually we take $1 \leq Q \leq 5$, which is an appropriate choice for Rayleigh fading channels and which is smaller than the number of sub-carriers N_a.

Assuming perfect knowledge of the channel matrix $\mathbf{G}[n]$, based on the masked matrix $\mathbf{M}$ in (5.48), $\mathbf{G}[n]$ can be transformed into banded sub-matrices $\mathbf{B}_n$,

$$\mathbf{B}_n = \begin{bmatrix} \mathbf{M} & \mathbf{M} \\ \mathbf{M} & \mathbf{M} \end{bmatrix} \odot \mathbf{G}[n]. \tag{5.49}$$

Additionally, the banded sub-matrices $\mathbf{B}_n$ can be rearranged by multiplication with a permutation matrix in (5.22) to take the shape of the matrix shown in Fig. 5.4. The above matrix can permute $\mathbf{B}_n$ such that the permuted received and transmitted signal from the same sub-carriers of different transmit antennas are grouped together,

$$\mathbf{P}_{2,N_a} \begin{bmatrix} \mathbf{r}[n] \\ \mathbf{r}^*[n+1] \end{bmatrix} = \mathbf{P}_{2,N_a} \mathbf{B}_n \mathbf{P}_{2,N_a}^{\mathrm{T}} . \mathbf{P}_{2,N_a} \begin{bmatrix} \mathbf{a}[n] \\ \mathbf{a}[n+1] \end{bmatrix} + \mathbf{P}_{2,N_a} \begin{bmatrix} \mathbf{v}[n] \\ \mathbf{v}^*[n+1] \end{bmatrix}. \tag{5.50}$$

Therefore, the permutation of rows of $\bar{\mathbf{r}}_n = \mathbf{P}_{2,N_a} \mathbf{r}_n$ as well as rows and columns of $\bar{\mathbf{B}}_n = \mathbf{P}_{2,N_a} \mathbf{B}_n \mathbf{P}_{2,N_a}^{\mathrm{T}}$ can be obtained by re-indexing, yielding the sparse structure as shown in Fig. 5.4 (right).

Next, we present the MMSE equaliser based on the banded structure of $\bar{\mathbf{B}}_n$. Analogously to [94] the MMSE equaliser can be defined as

$$\bar{\mathbf{W}}_{n,\mathrm{MMSE}} = \bar{\mathbf{B}}_n^{\mathrm{H}} \left(\bar{\mathbf{B}}_n \bar{\mathbf{B}}_n^{\mathrm{H}} + \gamma^{-1} \mathbf{I} \right)^{-1}, \tag{5.51}$$

where $\bar{\mathbf{W}}_{n,\mathrm{MMSE}}$ is a new banded matrix, but with width $4\,(Q+1)$.

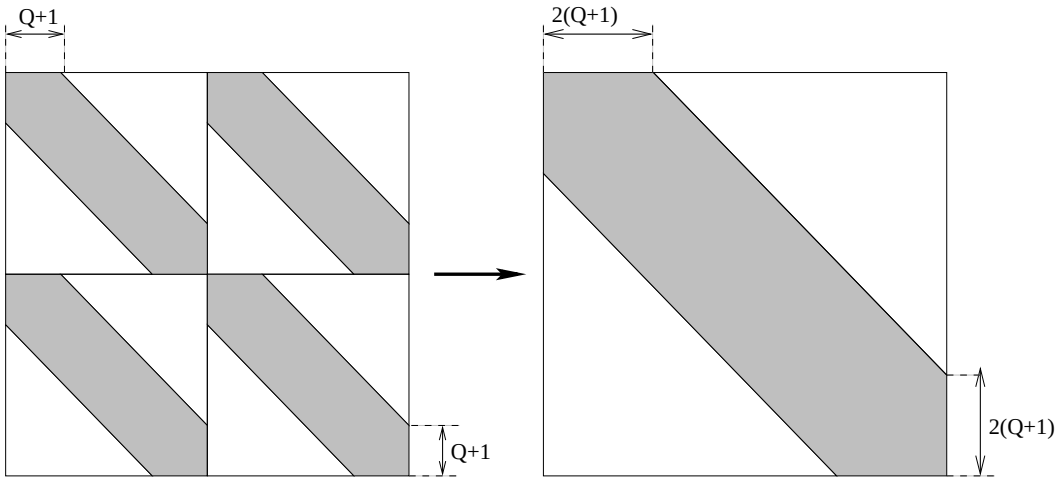

Figure 5.4: Structure of (left) the banded submatrices in $\mathbf{B}_n$ and (right) the permuted banded channel system $\bar{\mathbf{B}}_n$

5.4.2 Low-Complexity LSMR Algorithm

The least squares minimum residual (LSMR) algorithm is a recently proposed iterative approach, reported in [89], which solves the matrix inversion iteratively to reduce the MMSE equaliser complexity. Hence, it is solving linear systems $\mathbf{Ax} = \mathbf{b}$, least-squares problems $\min \|\mathbf{Ax} - \mathbf{b}\|_2$, and regularized least squares given as

$$\min \left\| \begin{pmatrix} \mathbf{A} \\ \lambda \mathbf{I} \end{pmatrix} \mathbf{x} - \begin{pmatrix} \mathbf{b} \\ 0 \end{pmatrix} \right\|_2 . \tag{5.52}$$

It's reduced complexity system from known sparsity of the system matrix $\mathbf{A}$. Given the sparsity of the equivalent channel matrix in Fig. 5.4 (right), the LSMR appears suited to equalising the above multi-carrier approach.

The equalisation scheme using the sparse least squares (LSQR) algorithm is equivalent to the conjugate gradient (CG) method applied to

$$\left(\mathbf{A}^{\mathrm{T}}\mathbf{A} + \lambda^2 \mathbf{I}\right) \mathbf{x} = \mathbf{A}^{\mathrm{T}}\mathbf{b}. \tag{5.53}$$

LSQR has the property of reducing the residual $\|\mathbf{b} - \mathbf{Ax}\|$ monotonically. However, the LSMR algorithm is based on the Golub–Kahan process [95], which is analytically equivalent to the minimum residuals applied to (5.53), which has the property of reducing both $\|\mathbf{b} - \mathbf{Ax}\|$ and $\left\|\mathbf{A}^{\mathrm{T}}(\mathbf{b} - \mathbf{Ax})\right\|$ monotonically. Although LSQR and LSMR ultimately converge to similar points, LSMR converges faster, which comes at the price of a slightly increased computational complexity per iteration step, we follow the route of the LSMR algorithm to exploit its benefit of providing a faster converging solution to the MMSE equaliser in (5.51).

5.4.3 MMSE Equaliser based on LSMR Algorithm

In the case of MMSE decoding with equalisation for EO-STBC, regularised least squares LSMR offers lower complexity and high numerical stability for solving a system of sparse linear equations. MMSE equalisation is formulated as

$$\left(\bar{\mathbf{B}}_{\mathbf{n}}\bar{\mathbf{B}}_{\mathbf{n}}^{\mathrm{H}} + \gamma^{-1}\mathbf{I}\right)\begin{bmatrix} \hat{\mathbf{a}}[n] \\ \hat{\mathbf{a}}^{*}[n+1] \end{bmatrix} = \bar{\mathbf{B}}_{n}^{\mathrm{H}}\begin{bmatrix} \bar{\mathbf{r}}[n] \\ \bar{\mathbf{r}}^{*}[n+1] \end{bmatrix}, \tag{5.54}$$

which is equivalent to the regularised least squares equation in (5.53), with the parameter λ related to the noise power γ^{-1}. Note that the optimal number of LSMR iterations depends on the noise level, and on the maximum Doppler spread and the maximum delay spread that affect the distribution of the singular values of the channel matrix.

5.4.4 Complexity Analysis

LSMR is particularly attractive due to its numerical stability, inherent potential for regularisation, and low computational complexity. We turn our attention to computational complexity calculations. For simplicity reasons, we consider $\bar{\mathbf{B}}_n$ as a $2N_a \times 2N_a$ approximately banded matrix with bandwidth parameter

$2Q+1$. Typically, matrix inversion is extremely process intensive. The inversion of matrix (5.46) requires a substantial number of $\mathcal{O}\left((2N_a)^3\right)$ flops , which is impractical for real systems with a large number of sub-carriers. By applying an $\mathbf{LDL}^H$ factorisation in calculating either MMSE or ZF solutions in (5.51) and (5.47), the number of complex operations compared to standard matrix inversion methods such as Gaussian elimination [74] can be reduced to $(32Q^2+76Q+34)2N_a$ complex operations [94]. Being an iterative algorithm for solving least squares problem, the most computationally expensive part of each iteration of LSMR are two matrix-vector products. The LSMR implementation of either MMSE or ZF solution requires $\mathcal{O}(4N_a(Q+1))$ flops at each iteration. LSMR can achieve the same accuracy of inversion with a considerably lower number of iterations, hence leading to an overall saving in complexity [89].

5.5 Simulations and Results

This section details simulations, which use an FrFT-based multicarrier system, whereby the discrete FrFT matrix $\mathbf{F}_a$ with $a = 1$ implements the standard OFDM based FFT with $N = 128$ sub-carriers, of which $N_a = 96$ are active sub-carriers, and number of guard samples in the cyclic prefix is 32. Simulation parameters consider a typical cellular system with a carrier frequency $f_c = 1.8$ GHz and a channel bandwidth BW = 800 kHz, which is equal to the sampling rate $f_s =$ BW.128/(128+32) at which the received signal is acquired prior to serial/parallel conversion and CP removing.

In the simulation below, the channel impulse response has a length of $L = 12$, with Rayleigh fading coefficients, which can be modelled as a tapped delay line [96] with fixed tap spacing $T_s = 1/f_s$. Assuming time and frequency synchronisation at the receiver side and considering the channel has an exponential power-delay profile with a root mean square (RMS) delay spread of 3 sampling periods. The

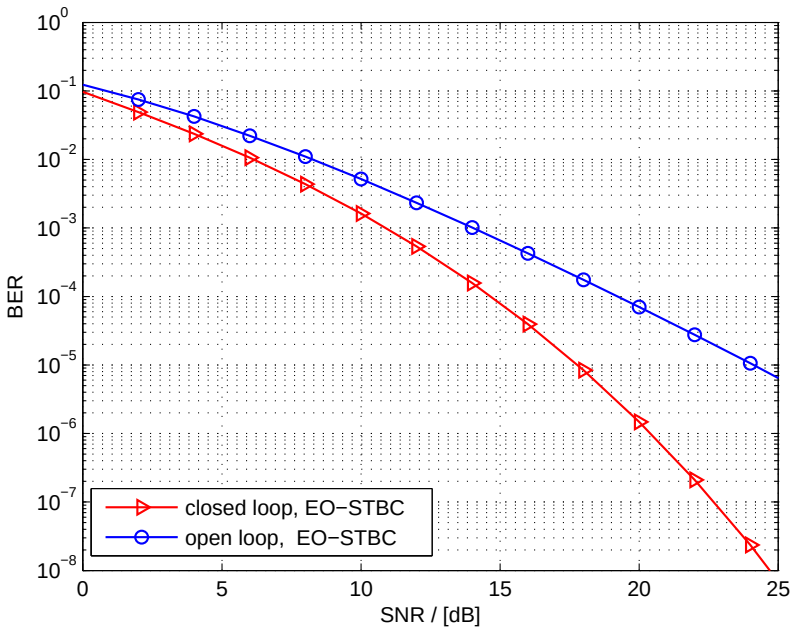

Figure 5.5: BER comparison of open and closed loop multi-carrier EO-STBC system for stationary channel conditions with $\Omega_D = 0$.

temporal variation of the channel with Jakes' Doppler spectrum is governed by a maximum Doppler spread $f_D = \Omega_D/2\pi$, corresponding to a mobile speed $v = cf_D\left(f_s/128\right)/f_c$ m/s, where $c = 3 \times 10^8$ m/s is the speed of light. All simulations below assume that the channel is perfectly known. Results below are averaged across an ensemble of 10^4 channel realisation.

5.5.1 Stationary Channel Conditions

In stationary channel conditions, the BER performance against SNR is simulated by transmitting binary phase shift keying (BPSK) encoded symbols over a multi-carrier based EO-STBC transmission system. Due to the channel being stationary, we employ FrFT-OFDM as a multi-carrier approach, whereby the discrete FrFT matrix $\mathbf{F}_a$ is selected with $a = 1$, such that the system particularises to an FFT-OFDM transmission. In this case, the length 32 of the cyclic prefix

ensures that the equivalent matrix is diagonalised, thus suppressing ISI and ICI.

In Fig. 5.5, simulation results comparing the performance of open-loop and closed-loop schemes are provided. The closed loop scheme uses optimum phase rotation feedback and open loop simply implies that no rotation angles are selected, i.e. $\mathbf{\Phi}[n] = \mathbf{\Theta}[n] = \mathbf{I}$, as shown in Fig. 5.3. It can be seen that the closed-loop scheme attains better performance than the open loop scheme, which demonstrates that closed-loop EO-STBC benefits from additional array gain in addition to the diversity gain that the open-loop scheme offers.

5.5.2 Near-Stationary Channel Conditions

This section presents simulations for the proposed particular FFT-OFDM multi-carrier transmission using $\mathbf{F}_a$ with $a = 1$ based EO-STBC transceiver , distinguishing between results for the near-stationary approach using EO-STBC decoding with 4 crosstalk receivers have been proposed in [2], [3]. The maximum normalised angular Doppler spread $\Omega_D = 2\pi f_D / f_s$, and is here selected as $\Omega_D = [0.001, 0.003] \triangle\Omega$ corresponds to mobile speeds $v = [3, 9]\,\mathrm{km/h}$.

5.5.2.1 Performance of Cross-Talk Detectors

The uncoded BER performance of the EO-STBC multi-carrier system with all 4 cross-talk receivers that have been proposed in [2], [3] are investigated for open-loop and closed-loop systems.

Fig. 5.6 compares the performance of the detectors in [3] for open loop scheme and closed loop scheme with a mobile speed $v = 3\,\mathrm{km/h}$. In this case, the closed loop scheme outperforms the open loop scheme for all 4 cross-talk receivers. As far as low complexity is concerned, the ZF and DF detectors, which have lower complexity than the JML detector, can offer near JML detector performance and further can significantly outperform the SML detector. There is a trade-off

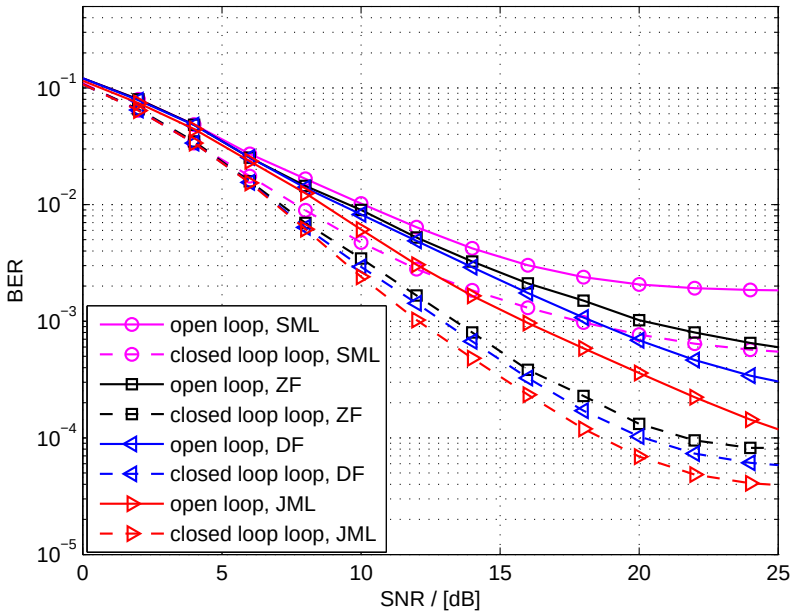

Figure 5.6: BER comparison of the open (solid lines) and closed loop (dashed lines) multicarrier EO-STBC system for a mobile speed $v = 3\,\mathrm{km/h}$, with the crosstalk receivers have been proposed in [2], [3].

between BER performance and decoding complexity, the complexity of ZF, and DF detectors in this design is higher than SML and lower than JML. Thus, for near-stationary channel conditions, the JML detector offers the best performance, but bearing in mind the computation complexity of the receiver, ZF and DF detectors represent attractive alternatives.

Fig. 5.7 compares the performance of the ZF and DF detectors to the performance of the JML detectors when the mobile speed increases to $v = 9\,\mathrm{km/h}$ for open loop and closed loop schemes. It can be seen that the closed loop scheme outperforms the open loop scheme, but only the JML detector can reduce the cross-talk and noise simultaneously, while the ZF and DF detectors fail to reach satisfactory performance. To judge the JML detector more objectively, below we detail its performance for open-loop and closed-loop schemes in dependency of different Doppler spreads.

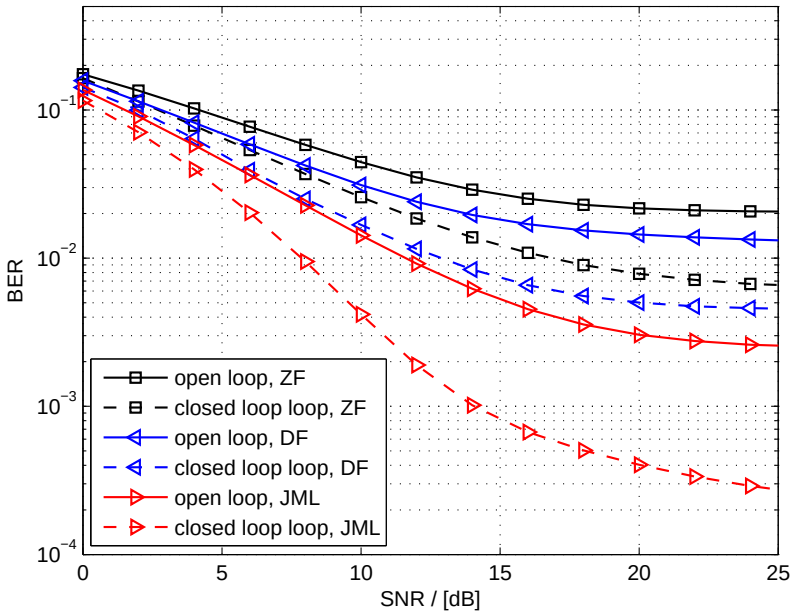

Figure 5.7: BER Comparison of the open and closed loop multicarrier EO-STBC system for a mobile speed $v = 9\,\text{km/h}$ with the crosstalk receivers have been proposed in [2], [3].

5.5.2.2 Performance of JML Detector

In Fig. 5.8, for various $\Omega_D = [0.001, 0.002, 0.003, 0.004, 0.005, 0.01]\,\triangle\Omega$ or, equivalently, for mobile speeds v of 3, 6, 9, 12, 15, and 30 km/h, we examine the effects on the performance of JML at SNR = 20dB. The simulation shows that the JML detector can provide a BER $\leq 10^{-3}$ when the speed v is less than 9 km/h and less than 12 km/h for open loop and closed loop schemes respectively. However, the differences between open loop and closed loop performance curves reduce as Ω_D increases. Therefore, for a maximum Doppler spread $\Omega_D \geq 0.004\,\triangle\Omega$ corresponding to speed which is greater than or equal to 12 km/h, the JML detector is unreliable. These trends in Fig. 5.8 suggest that the design of the closed-loop scheme with cross-talk receivers proposed in [2], [3] is not beneficial in non-stationary channel conditions. Therefore, we propose an equalisation scheme based on a low complexity MMSE Equaliser for the FrFT-OFDM system in the next section.

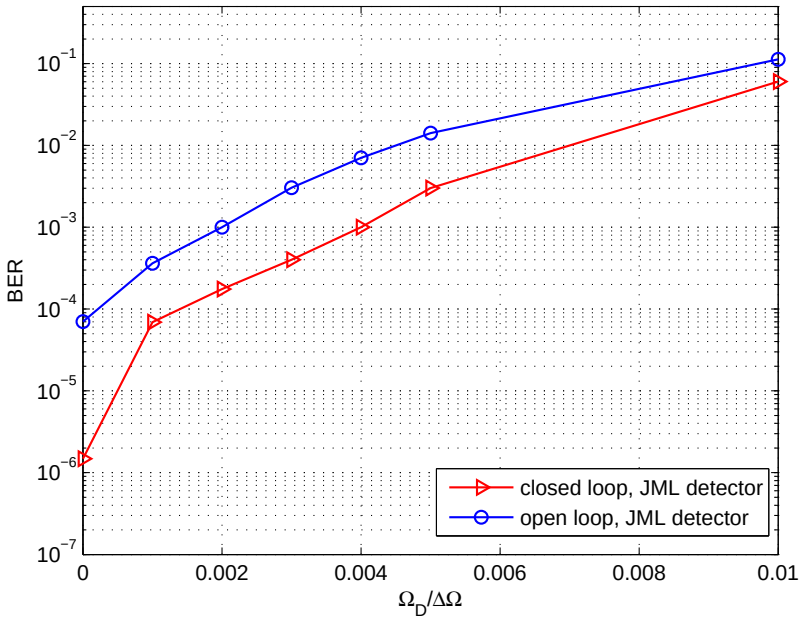

Figure 5.8: BER comparison of open and closed loop multicarrier EO-STBC system performance at SNR = 20dB with the JML detector in dependency of various Doppler spreads .

5.5.3 Fading Scenario with Equaliser

To mitigate the ICI problem at a maximum Doppler spread $\Omega_D = \{0.01, 0.05\}\ \triangle\Omega$ equivalent to the mobile speeds 30 and 150 km/h, we test the proposed MMSE equaliser for a multicarrier FrFT-OFDM system based on open loop EO-STBC transmission. The MMSE equaliser is employed to overcome degradation due to non-stationary channel conditions, and can offer an appropriate solution to reduce ICI and achieve diversity gain.

5.5.3.1 Selection of Optimum FrFT Parameter a

For non-stationary channel conditions, the transmitted signals can rather match the time-varying channel characteristics by selecting the optimal order a such that the discrete FrFT matrix $\mathbf{F}_a$ is selected with optimal order a. Hence, frac-

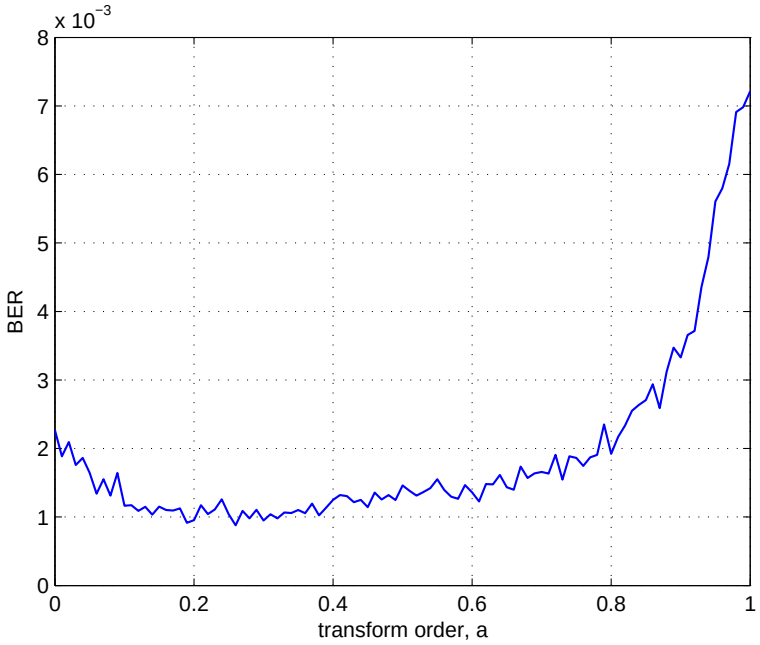

Figure 5.9: Optimum FrFT parameter a selection for a mobile speed $v = 30\,\text{km/h}$.

tional domain requires optimisation to obtain the best time-frequency resolution, therefore, we need to find the optimal order a to obtain the optimum BER performance. The optimal orders are $a = [0.25, 0.33]$ obtained by simulations, as shown in Figs. 5.9 and 5.10. Which are optimised at SNR of 20dB, and further below their BER performances will be compared to performances of other orders a that includes $a = 1$ corresponding to the FFT-OFDM transmission.

5.5.3.2 Performance of MMSE Equaliser in FrFT Domain

Based on results obtained in Sec. 5.5.3.1, we present simulations that show the BER performances of the multicarrier FrFT-OFDM system based on EO-STBC, where the BERs of the MMSE equaliser in (5.46) for mobile speeds $v = 30\,\text{km/h}$ and $v = 150\,\text{km/h}$ are plotted in Figs. 5.11 and 5.12. We consider the comparison of the BER results with optimum and non-optimum values of a, as it can be seen that the transformer order selection impacts on the performance. Interestingly,

the selection of the DFT/FFT with $a = 1$ presents the worst case.

Concentrating on the BER results at SNR = 20 dB in Fig. 5.11 shows that the BER at optimum order is around 1×10^{-3}, which significantly outperforms the BER corresponding to the ordinary FFT for $a = 1$, which is around 5×10^{-3}. Moreover in Fig. 5.12, a slight decreasing in BERs at SNR = 20 dB due to increasing time variations can be observed where the BER at optimum order is around 2×10^{-3}, while the BER corresponding to the ordinary FFT for $a = 1$ is around 5.2×10^{-3}.

FrFT-OFDM has distinct advantages when operating in doubly-dispersive channels over FFT-OFDM with a similar complexity. Simulations indicate that MMSE Equaliser in FrFT domain outperforms equalisation based on conventional FFT domain.

5.5.3.3 Performance of Low Complexity MMSE Equaliser in FrFT Domain

In this section we show the BER performances of the low complexity banded MMSE equaliser in (5.51) for FrFT-OFDM system with optimum order a with compared to the ordinary FFT for $a = 1$. Further, we show the comparison of the LSMR approach in (5.54).

From Figs. 5.13, 5.14, we observe that when the equivalent matrices are banded to $Q+1 = 6$ and $Q+1 = 12$ for mobile speeds 30 and 150 km/h respectively, firstly the FrFT-OFDM systems with optimum orders a are still outperform the systems for $a = 1$, and secondly the banded equalisers have an error floor due to the band approximation error of the channel. Note that LSMR approach can offer a low complexity with enhanced performance due to numerical robustness, but there is a slight increase in the error floor compared to the banded MMSE equaliser in (5.51). Thus, FrFT-OFDM with banded equaliser based on LSMR

algorithm can offer a good trade-off between system performance and computational complexity.

5.6 Conclusions

In this chapter, we have considered a multicarrier FrFT-OFDM system based on EO-STBC transmission over doubly-dispersive channels. For enhancing the diversity gain, we have studied near-stationary and non-stationary channel conditions. For near-stationary case, performance of closed-loop scheme can outperform the open loop scheme with the sub-optimal crosstalk receivers used ZF and DF detectors. These detectors can approach the performance of the optimum JML detector. Moreover, simulation results have shown that JML detector can maintain satisfactory performance even at relative high mobile speeds.

For non-stationary systems, neither closed loop nor open loop schemes can perform sufficiently well with the JML detector. However, to mitigate performance degradation we propose a low complexity MMSE equalisation based on banded system matrix. Moreover, its computational complexity has been further reduced by using LSMR iterative algorithm.

Simulation results have highlighted that a multi-carrier scheme operating on the basis of an FrFT can outperform standard OFDM based on DFT/FFT. OFDM based on FrFT tends to retain more channel energy in and along the main diagonal than classical OFDM based on FFT, which allows to achieve better system performance, making FrFT-OFDM an attractive alternative to FFT-OFDM in wireless broadband communications. For the banded MMSE equaliser, the values of Q used in the various band approximations depends on the maximum Doppler spread; thus, adjusting Q together with the transformer order a provides parameters to optimise the FrFT multi-carrier system.

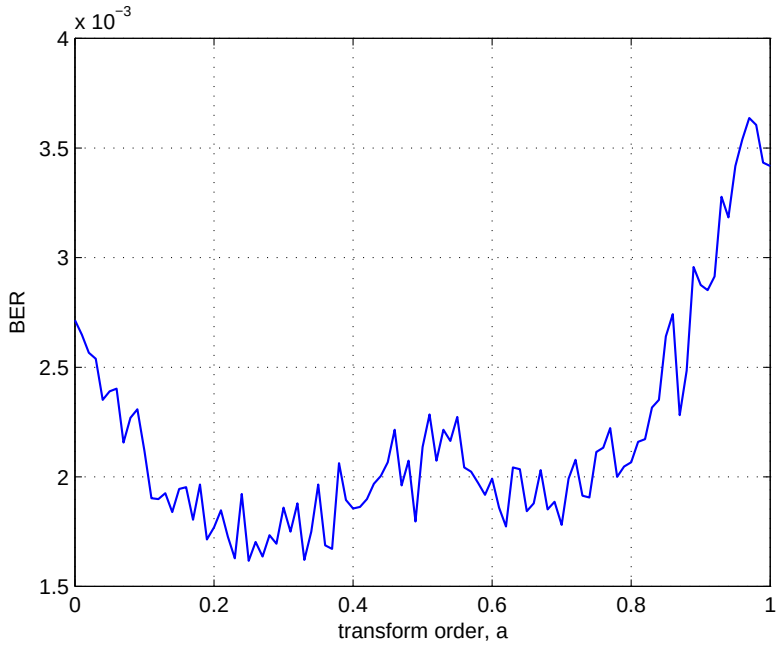

Figure 5.10: Optimum FrFT parameter a selection for a mobile speed $v = 150\,\mathrm{km/h}$

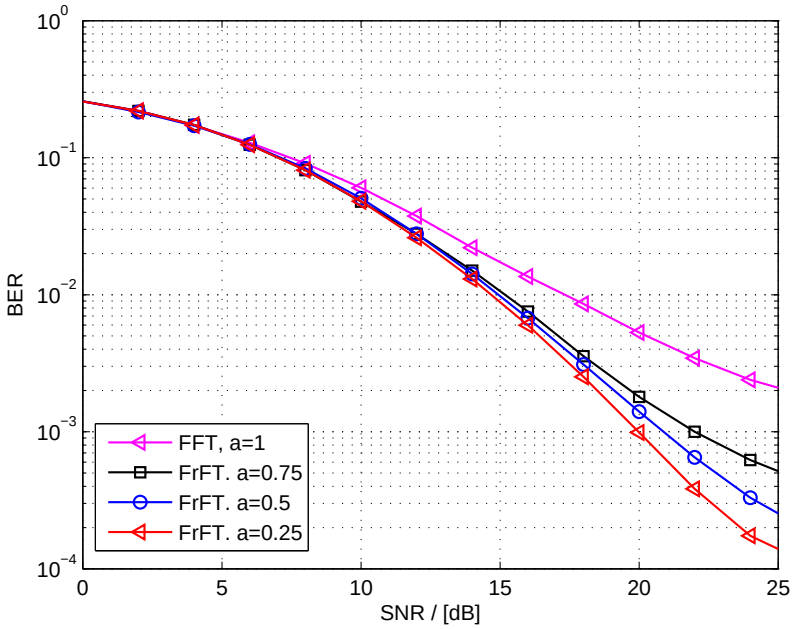

Figure 5.11: BER comparison of a multicarrier FrFT-OFDM system based on EO-STBC transmission with MMSE equaliser for a mobile speed $v = 30\,\mathrm{km/h}$.

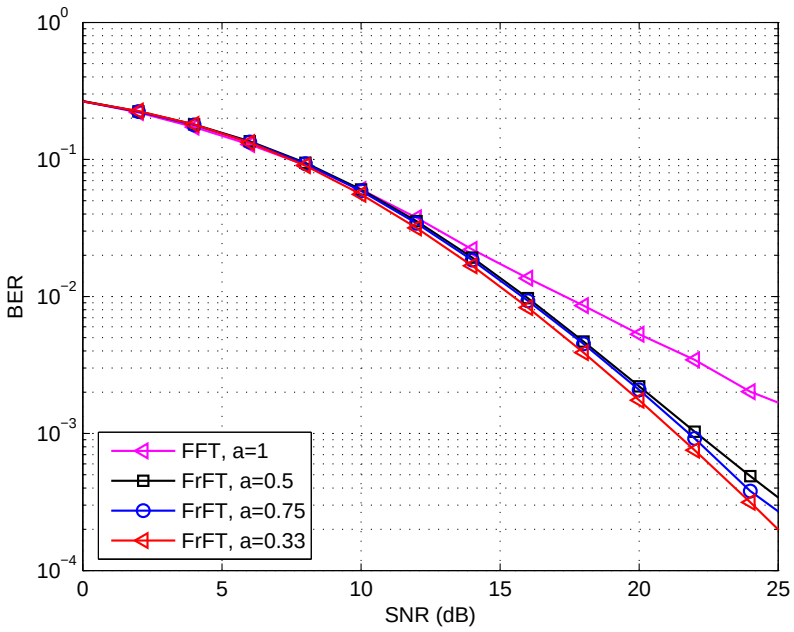

Figure 5.12: BER comparison of a multicarrier FrFT-OFDM system based on EO-STBC transmission with MMSE equaliser for a mobile speed $v = 150\,\mathrm{km/h}$.

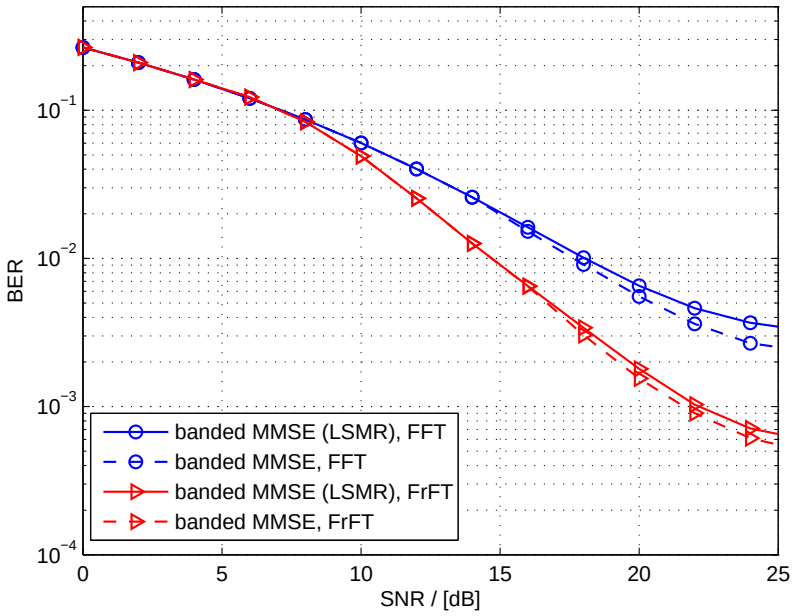

Figure 5.13: BER comparison of a multicarrier FrFT-OFDM system based on EO-STBC transmission based on low complexity MMSE equaliser with a banded equivalent system matrices to $Q + 1 = 6$, for a mobile speed $v = 30\,\mathrm{km/h}$.

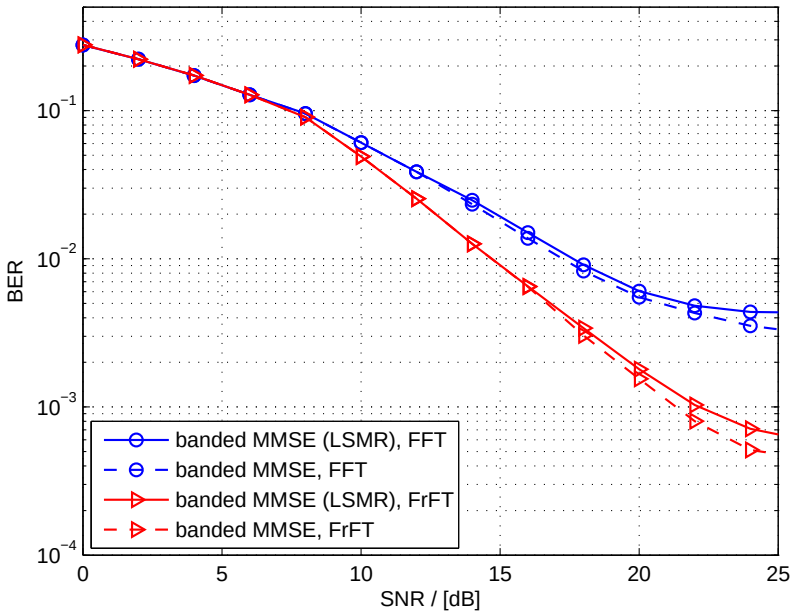

Figure 5.14: comparison of a multicarrier FrFT-OFDM system based on EO-STBC transmission based on low complexity MMSE equaliser with a banded equivalent system matrices to $Q + 1 = 12$, for a mobile speed $v = 150\,\mathrm{km/h}$, .

Chapter 6

Conclusions and Future Work

In this chapter, a summary and some concluding remarks are given, and several directions for future work are discussed.

6.1 Summary

Phase rotated EO-STBC for a system with four transmit and one receive antennas was adopted in this thesis because it can achieve full diversity plus additional array gain at code rate one, and low decoding low complexity. The array gain, admitted through the inclusion to phase rotation at two transmit antennas, can be maximised in the presence of quantised feedback as presented in Chapter 2. The performance of EO-STBC was compared with precoded Alamouti as well as QO-STBC and its advantages were discussed.

The maximum achievable diversity and array gain with EO-STBC was theoretically derived in Chapter 3. To attain maximum this gain with low bandwidth in the feedback channel, a differential encoding approach for the rotation angles was proposed. We have demonstrated that with a single bit encoding per angle can lead to near-optimum performance in terms of diversity and array gain.

In order to calculate the optimum feedback angles in the receiver, the channel must be known. Hence, channel estimation with Kalman filter tracking was considered, whereby the Kalman filter was adapted to form a decision-directed scheme based on the detection of EO-STBC symbols, and accommodate the rotation of some of the channel's cofficients within EO-STBC. Chapter 4 results have shown the feasibility of longer tracking periods with a reduced MSE by higher order models for the channel evolution inside the Kalman filter. Although the complexity of the higher-order model is slightly higher than the conventional Kalman filter, it has been shown that such a deployment yields significant improvements in terms of tracking ability and BER performance.

In Chapter 5 a rotated EO-STBC over near-stationary doubly dispersive channel was presented. To address the frequency-selectivity of the channel, a multicarrier approach was adopted. We have utilised a new fractional Fourier transform based system which uses chirps as mutli-carriers and generalises the standard DFT/FFT-OFDM, offering advantages in non-stationary environments. In a stationary case, we can operate DFT/FFT-OFDM by realising EO-STBC in every subband. For near-stationary channels, we have adopted a cross-talk detector, which can address the inter-symbol-interference and inter-carrier interferences that occurs as a result of the channel's non-stationarity. For faster time-varying channels, the benefit of feeding back rotation angles from the receiver disappeared, and we have proposed an open-loop system, which however incorporates an equaliser to address ISI and ICI. The FrFT approach here enables a lower-cost equaliser than standard OFDM, which was further improved through a fast-converging approach for the solution of sparse linear equations, as found in the FrFT case.

EO-STBC with beam steering angles is an efficient transmission scheme to increase the diversity gain of MIMO systems over near-stationary channel conditions. Due to increasing demands for wireless communication systems providing

higher data rate and high quality of service, the design of EO-STBC schemes with equalisation presented over stationary channels are beneficial and desirable in the practical future wireless applications.

6.2 Future Work

There are several possibilities for future work based on the research presented throughout this thesis. In the following, some further directions are outlined.

The phase rotation beam-steering with proposed differential feedback scheme in Chapter 3 can be generalised to more than 4 transmit antennas, e.g., five or six antennas. We can go further in this direction and consider mutual correlation between the antenna elements that possibly have an effect on the diversity gain.

In Chapter 4, we have proposed an AR-2 model to exploit the smooth evolution of the channel coefficients' trajectories in slow fading scenarios. In order to reduce AR-2 complexity, the inclusion of a drift vector in the Kalman model may also be considered [72]. This scheme can be also considered for distributed relaying systems [97].

Moreover, in Chapter 4, the coefficients of estimated channel are used to compute the feedback angles. It will be interesting to investigate the estimation error resulting of estimated feedback angles. When the channel estimation error increases, the estimated feedback angles for the beamsteering processing will need to be adjusted to maintain efficient performance. The required form of the tracking feedback angles should be investigated in future research.

Throughout Chapter 5, it has been assumed that the channel matrix with ICI terms is perfectly known at the OFDM receiver. In the context of channel estimation and symbol detection, the consideration of Kalman filtering for tracking of coefficients to exploit smoothness in the channel evolution in both time and frequency could be investigated, possibly extending the use of the proposed AR-2

model. The influence of the estimation error, in connection with other synchronisation errors, on the system performance would also form a worthwhile task for future research in this area.

Bibliography

[1] N. Eltayeb, S. Lambotharan, and J. Chambers, "A Phase Feedback Based Extended Space-Time Block Code for Enhancement of Diversity," in *IEEE 65th Vehicular Technology Conference*, pp. 2296–2299, April 2007.

[2] A. Vielmon, Y. Li, and J. Barry, "Performance of Alamouti Transmit Diversity over Time-Varying Rayleigh-Fading Channels," *IEEE Transactions on Wireless Communications*, vol. 3, no. 5, pp. 1369 – 1373, Sept. 2004.

[3] D. Lin, P. Chiang, and H. Li, "Performance Analysis of Two-Branch Transmit Diversity Block-Coded OFDM systems in time-varying multipath Rayleigh-fading channels," *IEEE Transactions on Vehicular Technology*, vol. 54, no. 1, pp. 136–148, Jan. 2005.

[4] A. Alexiou and M. Haardt, "Smart Antenna Technologies for Future Wireless Systems: Trends and Challenges," *IEEE Communications Magazine*, vol. 42, no. 9, pp. 90–97, Sep. 2004.

[5] J. B. Andersen, "Array Gain and Capacity for Known Random Channels with Multiple Element Arrays at Both Ends," *IEEE Journal on Selected Areas in Communications*, vol. 18, no. 11, pp. 2172–2178, Nov. 2000.

[6] A. Constantinides and A. Shacham, "MIMO Wireless Systems," tech. rep., Columbia. edu, May 2004.

[7] M. A. Jensen and J. W. Wallace, "A Review of Antennas and Propagation for MIMO Wireless Communications," *IEEE Transactions on Antennas and Propagation*, vol. 52, no. 11, pp. 2810–2824, Nov. 2004.

[8] M. T. Ivrlac, W. Utschick, and J. A. Nossek, "Fading Correlations in Wireless MIMO Communication Systems," *IEEE Journal on Selected Areas in Communications*, vol. 21, no. 5, pp. 819–828, Jun. 2003.

[9] Y. Li and Z.-Q. Luo, "Parallel Detection for V-BLAST System," in *IEEE International Conference on Communications*, vol. 1, New York, NY, USA, pp. 340–344, 2002.

[10] A. A. Abouda, *Characterization of MIMO Channel Capacity in Urban Microcellular Environment*. PhD thesis, Helsinki University of Technology, 2007.

[11] W. R. H. Jr. and A. Paulraj, "Switching Between Multiplexing and Diversity Based on Constellation Distance," *IEEE Transactions on Communications*, vol. 53, no. 6, pp. 962 – 968, Jun. 2005.

[12] A. Swindlehurst, "Simultaneous Channel Estimation and Decoding for Diagonal Space-Time Codes," in *Proceedings of the IEEE Sensor Array and Multichannel Signal Processing Workshop*, pp. 173 –177, 2000.

[13] M. Vu and A. Paulraj, "MIMO Wireless Linear Precoding," *IEEE Signal Processing Magazine*, vol. 24, no. 5, pp. 86–105, Sep. 2007.

[14] J. Heath, R.W. and A. Paulraj, "A simple Scheme for Transmit Diversity Using Partial Channel Feedback," in *32th Asilomar Conference on Signals, Systems, and Computers*, vol. 2, pp. 1073 –1078 vol.2, Nov. 1998.

[15] A. Narula, M. Lopez, M. Trott, and G. Wornell, "Efficient Use of Side Information in Multiple-Antenna Data Transmission over Fading Channels,"

IEEE Journal on Selected Areas in Communications, vol. 16, no. 8, pp. 1423 –1436, Oct. 1998.

[16] U. W. Joham, M. and J. Nossek, "Linear Transmit Processing in MIMO Communications Systems," *IEEE Transactions on Signal Processing*, vol. 53, no. 8, no. 8, pp. 2700–2712, 2005.

[17] M. Hasna and M. Alouini, "End-to-End Performance of Transmission Systems with Relays over Rayleigh-Fading Channels," *IEEE Transactions on Wireless Communications*, vol. 2, no. 6, pp. 1126 – 1131, Nov. 2003.

[18] L. Sun, T. Zhang, L. Lu, and H. Niu, "Cooperative Communications with Relay Selection in Wireless Sensor Networks," *IEEE Transactions on Consumer Electronics*, vol. 55, no. 2, pp. 513 –517, May 2009.

[19] J. Laneman and G. Tse, D. N. C.and Wornell, "Cooperative Diversity in Wireless Networks: Efficient Protocols and Outage Behavior," *IEEE Transactions on Information Theory*, vol. 50, no. 12, pp. 3062–3080, Dec. 2004.

[20] C. Patel, G. Stuber, and T. Pratt, "Statistical Properties of Amplify and Forward Relay Fading Channels," *IEEE Transactions on Vehicular Technology*, vol. 55, no. 1, pp. 1 – 9, Jan. 2006.

[21] K. Romer, F. Mattern, and E. Surich, "The Design Space of Wireless Sensor Networks," *IEEE Transactions on Wireless Communication*, vol. 11, no. 6, pp. 54–61, Dec. 2004.

[22] Y. Jing and H. Jafarkhani, "Single and multiple relay selection schemes and their achievable diversity orders," *IEEE Transactions on Wireless Communications*, vol. 8, no. 3, pp. 1414 –1423, Mar. 2009.

[23] A. Sendonaris, E. Erkip, and B. Aazhang, "User Cooperation Diversity. Part I. System Description," *IEEE Transactions on Communications*, vol. 51, no. 11, pp. 1927 – 1938, Nov. 2003.

[24] A. Panah and R. Heath, "MIMO Two-Way Amplify-and-Forward Relaying With Imperfect Receiver CSI," *IEEE Transactions on Vehicular Technology*, vol. 59, no. 9, pp. 4377–4387, Nov. 2010.

[25] Y. Han, S. H. Ting, C. K. Ho, and W. H. Chin, "Performance Bounds for Two-Way Amplify-and-Forward Relaying," *IEEE Transactions on Wireless Communications*, vol. 8, no. 1, pp. 432 –439, Jan. 2009.

[26] Y. Han, S. H. Ting, C. K. Ho, and W. H. Chin, "High Rate Two-Way Amplify-and-Forward Half-Duplex Relaying with OSTBC," in *IEEE 67th Vehicular Technology Conference*, pp. 2426 –2430, May 2008.

[27] H. Sampath, S. Talwar, J. Tellado, V. Erceg, and A. Paulraj, "A Fourth-Generation MIMO-OFDM Broadband Wireless System: Design, Performance, and Field Trial Results," *IEEE Communications Magazine*, vol. 40, no. 9, pp. 143–149, 2002.

[28] G. Stuber, J. Barry, S. McLaughlin, Y. Li, M. Ingram, and T. Pratt, "Broadband MIMO-OFDM wireless Communications," *Proceedings of the IEEE*, vol. 92, no. 2, pp. 271–294, Feb. 2004.

[29] A. van Zelst and T. Schenk, "Implementation of a MIMO OFDM-Based Wireless LAN System," *IEEE Transactions on Signal Processing*, vol. 52, no. 2, pp. 483–494, Feb. 2004.

[30] X. Li and Z.-P. Nie, "Mutual Coupling Effects on the Performance of MIMO Wireless Channels," *IEEE Antennas and Wireless Propagation Letters*, vol. 3, no. 1, pp. 344–347, 2004.

[31] P. Dighe, R. Mallik, and S. Jamuar, "Analysis of Transmit-Receive Diversity in Rayleigh Fading," *IEEE Transactions on Communications*, vol. 51, no. 4, pp. 694 – 703, April 2003.

[32] S. Alamouti, "Asimple Transmit Diversity Technique for Wireless Communications," *IEEE Journal on Selected Areas in Communications*, vol. 16, no. 8, pp. 1451 – 1458, Oct. 1998.

[33] H. Jafarkani, "A Quasi-Orthogonal Space-Time Block Code," *IEEE Transactions on Communications*, vol. 49, no. 1, pp. 1 – 4, Jan. 2001.

[34] P. Ding, D. Love, J. Wang, and M. Zoltowski, "Low Complexity Adaptive Design for Full-Diversity Full-Rate Space-Time Codes," *IEEE Transactions on Signal Processing*, vol. 54, no. 8, pp. 3180 –3189, Aug. 2006.

[35] C. C. Chiau, *Study of the Diversity Antenna Array for the MIMO Wireless Communication Systems*. PhD thesis, Queen Mary, University of London, United Kingdom, April 2006.

[36] D. Gesbert, M. Shafi, D. Shiu, and A. Naguib, "From Theory to Practice: An Overview of MIMO Space-Time Coded Wireless Systems," *IEEE Journal on selected areas in Communications*, vol. 21, no. 3, pp. 281–302, April 2003.

[37] H. Tarokh, V. Jafarkhanni and A. Calderbank, "Space Time Block Codes from Orthogonal Designs," *IEEE Transactions on Information Theory*, vol. 45, no. 5, pp. 1456 –1467, Jun. 1999.

[38] J. Akhtar and D. Gesbert, "Extended Orthogonal Block Codes with Partial Feedback," *IEEE Transactions on Wireless Communications*, vol. 3, no. 6, pp. 1959 – 1962, Nov. 2004.

[39] A. Goldsmith, *Wireless Communications*. Cambridge University Press, 2005.

[40] B. Sklar, *Digital Communications: Fundamentals and Applications*. Prentice Hall, Englewood Cliffs, 1988.

[41] *Guidelines for Evaluation of Radio Transmission Technologies for IMT 2000*, Recommendation (1997) ITU R M.1225.

[42] C. Toker, S. Lambotharan, and J. Chambers, "Closed-Loop Quasi-Orthogonal STBCs and their Performance in Multipath Fading Environments and when Combined with Turbo Codes," *IEEE Transactions on Wireless Communications*, vol. 3, no. 6, pp. 1890 – 1896, Nov. 2004.

[43] M. Celebi, S. Sahin, and U. Aygolu, "Full Rate Full Diversity Space-Time Block Code Selection for More Than Two Transmit Antennas," *IEEE Transactions on Wireless Communications*, vol. 6, no. 1, pp. 16–19, Jan. 2007.

[44] J. Laneman and G. Wornell, "Distributed Space-Time-Coded Protocols for Exploiting Cooperative Diversity in Wireless Networks," *IEEE Transactions on Information Theory*, vol. 49, no. 10, pp. 2415 – 2425, Oct. 2003.

[45] F. T. Alotaibi and J. Chambers, "Extended Orthogonal Space Time Block Codes in Wireless Relay Networks," in *IEEE Workshop on Statistical Signal Processing, Cardiff, UK*, 2009.

[46] N. Eltayeb, *Space-Time Coding for Broadband Point-to-Point and Collabrative Wireless Communications*. PhD thesis, Lougborough University, 2009.

[47] M. Enescu and V. Koivunen, "Time-Varying Channel Tracking for Space-Time Block Coding," in *IEEE 55th Vehicular Technology Conference*, vol. 1, pp. 294 – 297, 2002.

[48] C. Cozzo and B. Hughes, "Joint Channel Estimation and Data Detection in Space-Time Communications," *IEEE Transactions on Communications*, vol. 51, no. 8, pp. 1266 – 1270, Aug. 2003.

[49] S. Haykin, K. Huber, and Z. Chen, "Bayesian Sequential State Estimation for MIMO Wireless Communications," *Proceedings of the IEEE*, vol. 92, no. 3, pp. 439 – 454, Mar. 2004.

[50] A. Barg and D. Nogin, "Bounds on Packings of Spheres in the Grassmann Manifold," *IEEE Transactions on Information Theory*, vol. 48, no. 9, no. 9, pp. 2450–2454, 2002.

[51] E. Larsson, G. Ganesan, P. Stoica, and W. Wong, "On the Performance of Orthogonal Space Time Block Coding with Quantized Feedback," *IEEE Communications Letters*, vol. 12, no. 6, pp. 487–489, 2002.

[52] D. Love and R. Heath, "Diversity Performance of Precoded Orthogonal Space-Time Block Codes using Limited Feedback," *IEEE Communications Letters*, vol. 8, no. 5, pp. 305–307, 2004.

[53] A. Ashikhmin and A. Calderbank, "Grassmannian Packings From Operator Reed Muller Codes," *IEEE Transactions on Information Theory*, vol. 56, no. 11, pp. 5689–5714, Oct. 2010.

[54] Y. Cho, J. Kim, W. Yang, and C. Kang, *MIMO-OFDM Wireless Communications with MATLAB*. John Wiley & Sons Pte Ltd, 2010.

[55] B. Hochwald, T. Marzetta, T. Richardson, W. Sweldens, and R. Urbanke, "Systematic Design of Unitary Space-Time Constellations," *IEEE Transactions on Information Theory*, vol. 46, no. 6, pp. 1962 –1973, Sep. 2000.

[56] G. T. 36.211, "Evolved Universal Terrestrial Radio Access (E-UTRA), Physical Channels and Modulation," Jan. 2011.

[57] C. Yuen, Y. L. Guan, and T. T. Tjhung, "Full-Rate Full-Diversity STBC with Constellation Rotation," in *57th IEEE Semiannual Vehicular Technology Conference*, vol. 1, pp. 296 – 300, April 2003.

[58] C. Yuen, Y. L. Guan, and T. T. Tjhung, "Quasi-Orthogonal STBC with Minimum Decoding Complexity," *IEEE Transactions on Wireless Communications*, vol. 4, no. 5, pp. 2089 – 2094, Sept. 2005.

[59] J. Milleth, K. Giridhar, and D. Jalihal, "Closed-Loop Transmit Diversity Schemes for Five and Six Transmit Antennas," *IEEE Signal Processing Letters*, vol. 12, no. 2, pp. 130 – 133, Feb. 2005.

[60] J. Wu, H. Horng, J. Zhang, and C. Xiao, "Adaptive Transmit Diversity with Quadrant Phase Constraining Feedback," in *15th IEEE International Symposium on Personal, Indoor and Mobile Radio Communications*, vol. 3, pp. 2262 – 2266, Sept. 2004.

[61] G. Jongren and M. Skoglund, "Quantized Feedback Information in Orthogonal Space-Time Block Coding," *IEEE Transactions on Information Theory*, vol. 50, no. 10, pp. 2473 – 2486, Oct. 2004.

[62] W. H. Chin and C. Yuen, "Design of differential quantization for low bitrate channel state information feedback in mimo-ofdm systems," in *In IEEE Vehicular Technology Conference*, pp. 827–831, May 2008.

[63] H. Koorapaty, L. Krasny, and R. Ramesh, "Delta Modulation for Channel Feedback in Transmit Diversity Systems," in *Vehicular Technology Conference, 2005. VTC 2005-Spring. 2005 IEEE 61st*, vol. 1, pp. 644–648 Vol. 1, May-1 June 2005.

[64] B. N. Baddour, K.E., "Autoregressive Modeling for Fading Channel Simulation," *IEEE Transactions on Wireless Communications*, vol. 4, no. 4, pp. 1650 – 1662, July 2005.

[65] A. A. Hutter, S. Mekrazi, B. N. Getu, and F. Platbrood, "Alamouti-based Space-Frequency Coding for OFDM," *Wireless Personal Communications*, vol. 35. no. 1-2, Oct. 2005.

[66] J. Salo, H. M. El-Sallabi, and P. Vainikainen, "The Dsitribution of the Product of Rayleigh Distributed Random Variables," *IEEE Transactions on Antennas and Propagation*, vol. 54, no. 2, pp. 639–643, Feb. 2006.

[67] Z. Liu, G. Giannakis, and B. Hughes, "Double Differential Space-Time Block Coding for Time-Selective Fading Channels," in *IEEE Wireless Communications and Networking Conference*, vol. 1, pp. 13 –17, 2000.

[68] B. Hughes, "Differential Space-Time Modulation," *IEEE Transactions on Information Theory*, vol. 46, no. 7, pp. 2567 –2578, Nov. 2000.

[69] M. Dong, L. Tong, and B. Sadler, "Optimal Insertion of Pilot Symbols for Transmissions over Time-Varying Flat Fading Channels," *IEEE Transactions on Signal Processing*, vol. 52, no. 5, pp. 1403 – 1418, May 2004.

[70] Z. Liu, X. Ma, and G. Giannakis, "Space-Time Coding and Kalman Filtering for Time-Selective Fading Channels," *IEEE Transactions on Communications*, vol. 50, pp. 183 –186, Feb. 2002.

[71] B. D. O. Anderson and J. B. Moore, "The Kalman-Bucy Filter as a True Time-Varying Wiener Filter," *IEEE Transactions on Systems*, vol. 1, pp. 119–128, 1971.

[72] M. N. Hussin and S. Weiss, "Channel Estimation and Tracking for Closed Loop EO-STBC with Differentially Encoding Feedback," in *IEEE International Symposium on Signal Processing and Information Technology*, pp. 478 –483, Dec. 2011.

[73] M. Hussin and S. Weiss, "Extended Orthogonal Space-Time Block Coded Transmission with Quantised Differential Feedback," in *7th IEEE International Symposium on Wireless Communication Systems*, pp. 179 –183, Sep. 2010.

[74] G. H. Gloub and C. F. V. Loan, *Matrix Computations*. The Johns Hopkins University Press, 1996.

[75] L. M. Giannakis, G.B. and Zhou.S, *Space-Time Coding for Broadband Wireless Communications*. John Wiley & Sons, Inc., Hoboken, New Jersey, 2007.

[76] R. Lyman and W. Edmonson, "Decision-Directed Tracking of Fading Channels using Linear Prediction of the Fading Envelope," in *Record of the Thirty-Third Asilomar Conference on Signals, Systems, and Computers*, vol. 2, pp. 1154 –1158, Oct. 1999.

[77] D. Agrawal, V. Tarokh, A. Naguib, and N. Seshadri, "Space-time Coded OFDM for High Data-Rate Wireless Communication over Wideband Channels," vol. 3, pp. 2232 –2236, May 1998.

[78] J. Kim and S. Ariyavistakul, "Optimum 4-Transmit-Antenna STBC/SFBC with Angle Feedback and a Near-Optimum 1-bit feedback scheme," *IEEE Communications Letters*, vol. 11, no. 11, pp. 868 –870, Nov. 2007.

[79] P. Schniter, "Low-Complexity Equalization of OFDM in Doubly Selective Channels," *IEEE Transactions on Signal Processing*, vol. 52, no. 4, pp. 1002 – 1011, April 2004.

[80] M. Russell and G. Stuber, "Interchannel Interference Analysis of OFDM in a Mobile Environment," in *IEEE 45th Vehicular Technology Conference*, vol. 2, pp. 820–824 vol.2, 1995.

[81] Y. Li and L. Cimini, "Bounds on the Interchannel Interference of OFDM in Time-Varying Impairments," *IEEE Transactions on Communications*, vol. 49, no. 3, pp. 401 –404, Mar. 2001.

[82] M. Martone, "A multicarrier System based on the Fractional Fourier Transform for Time-Frequency-Selective Channels," *IEEE Transactions on Communications*, vol. 49, no. 6, pp. 1011 –1020, Jun. 2001.

[83] D. Stojanovic, I. Djurovic, and B. Vojcic, "Interference Analysis of Multicarrier Systems Based on Affine Fourier Transform," *IEEE Transactions on Wireless Communications*, vol. 8, no. 6, pp. 2877 –2880, Jun. 2009.

[84] J. Zheng and Z. Wang, "ICI Analysis for FrFT-OFDM Systems to Frequency Offset in Time-Frequency selective fading channels," *IEEE Communications Letters*, vol. 14, no. 10, pp. 888 –890, Oct. 2010.

[85] I. Barhumi, G. Leus, and M. Moonen, "Equalization for OFDM over Doubly Selective Channels," *IEEE Transactions on Signal Processing*, vol. 54, no. 4, pp. 1445 – 1458, April 2006.

[86] T. Wang, J. Proakis, E. Masry, and J. Zeidler, "Performance Degradation of OFDM Systems due to Doppler Spreading," *IEEE Transactions on Wireless Communications*, vol. 5, no. 6, pp. 1422 –1432, June 2006.

[87] S. Chen and Y. Yang, "Low-Complexity MMSE-SIC Equalizer Employing LDLH Factorization for OFDM Systems Over Time-Varying Channels," *IEEE Transactions on Vehicular Technology*, vol. 59, no. 8, no. 8, pp. 4128–4131, 2010.

[88] C. C. Paige and M. A. Saunders, "LSQR An Algorithm for Sparse Linear Equations and Sparse Least Squares," *ACM Transactions on Mathematical Software*, vol. 8, no. 1, pp. 43–71, 1982.

[89] D. Fong and M. A. Saunders, "LSMR an iterative Algorithm for Sparse Least-Squares Problems," *SIAM Journal on Scientific Computing*, vol. 33, no. 5, pp. 2950–2971, Sep. 2011.

[90] H. Ozaktas, O. Arıkan, M. Kutay, and G. Bozdağı, "Digital computation of the fractional Fourier transform," *IEEE Transactions on Signal Processing*, vol. 44, pp. 2141–2150, September 1996.

[91] C. Candan, M. Kutay, and H. Ozaktas, "The discrete fractional Fourier transform," vol. 48, pp. 1329–1337, May 2000.

[92] A. A. A. Solyman, S. Weiss, and J. J. Soraghan, "Low-Complexity LSMR Equalisation of FrFT-Based Multicarrier Systems in Doubly Dispersive Channels," in *IEEE International Symposium on Signal Processing and Information Technology*, pp. 461 –465, Dec. 2011.

[93] K. Fang, G. Leus, and L. Rugini, "Alamouti Space-Time Coded OFDM Systems in Time- and Frequency-Selective Channels," in *IEEE 6th Global Telecommunications Conference*, vol. 1, pp. 1 –5, Dec. 2006.

[94] L. Rugini, P. Banelli, and G. Leus, "Low-Complexity Banded Equalizers for OFDM Systems in Doppler Spread Channels," *EURASIP J. Appl. Signal Processing*, pp. 1–13, 2006.

[95] G. Golub and W. Kahan, "Calculating the Singular Values and Pseudo-Inverse of a Matrix," *Journal of the Society for Industrial and Applied Mathematics*, vol. 2, no. 2, pp. 205–224, 1965.

[96] G. L. Stüber, *Principles of Mobile Communication*. London, U.K.: Kluwer, 2001.

[97] M. N. Hussin, M. Alrmah, and S. Weiss, "Distributed Closed-Loop EO-STBC for a time-varying Relay Channel Based on Kalman Tracking," in *in 9th IMA International Conference on Mathematics in Signal Processing*, 2012.

Appendix A

Signal Detection with Error due to both Estimation and Time Variation

In this Appendix, derivation of on-diagonal and off-diagonal elements of the term $\hat{\mathbf{H}}_n^{\mathrm{H}}\mathbf{H}_n$ in terms of channel coefficients, which is given in Chap. 4. Note that errors are due to time-variations plus estimation errors.

A.1 Signal Detection

In Chap. 4, we propose the use of Kalman filter for tracking the channel responses in EO-STBC coded systems. To generalise the signal detection to both estimation and time variation errors, it is required to use estimated channel matrix with absorbed beamsteering angles to detect EO-STBC transmitted symbols. The received vector can be decoded in the matched filter sense as

$$\begin{bmatrix} \hat{s}[n] \\ \hat{s}[n+1] \end{bmatrix} = \hat{\mathbf{H}}_n^{\mathrm{H}} \begin{bmatrix} r[n] \\ r^*[n+1] \end{bmatrix}, \tag{A.1}$$

where in cases with estimation and time variation errors, the system matrix is no longer orthogonal. During the EO-STBC time intervals, the system matrix can be written as

$$\hat{\mathbf{H}}_n = \begin{bmatrix} e^{j\vartheta_1[n]}\hat{h}_1[n] + \hat{h}_2[n] & e^{j\vartheta_2[n]}\hat{h}_3[n] + \hat{h}_4[n] \\ e^{-j\vartheta_2[n+1]}\hat{h}_3^*[n+1] + \hat{h}_4^*[n+1] & -e^{-j\vartheta_1[n+1]}\hat{h}_1^*[n+1] - \hat{h}_2^*[n+1] \end{bmatrix} \tag{A.2}$$

A.2 Deviation from a Diagonal Matrix

In the sense that $\mathbf{H}_n^{\mathrm{H}}\mathbf{H}_n$ is diagonal, which indicates that the diagonal matrix $\mathbf{G}_n = \mathbf{H}_n^{\mathrm{H}}\mathbf{H}_n$ can be obtained as

$$\mathbf{H}_n^{\mathrm{H}}\mathbf{H}_n = \begin{bmatrix} \alpha+\beta & 0 \\ 0 & \alpha+\beta \end{bmatrix} \quad . \tag{A.3}$$

where $\alpha + \beta = \sum_{m=1}^{4} |h_m[n]|^2 + \sum_{m=3}^{4} |h_m[n]|^2 + 2\Re\{h_1[n]h_2^*[n] + h_3[n]h_4^*[n]\}$.

In the presence of errors, the matrix $\hat{\mathbf{H}}_n^{\mathrm{H}}\mathbf{H}_n$ is given by

$$\hat{\mathbf{H}}_n^{\mathrm{H}}\mathbf{H}_n = \begin{bmatrix} g_{11}[n] & g_{12}[n] \\ g_{21}[n] & g_{22}[n] \end{bmatrix}$$

with

$$
\begin{aligned}
g_{11}[n] &= (e^{j\vartheta_1[n]}\hat{h}_1[n] + \hat{h}_2[n])^* \cdot (e^{j\vartheta_1[n]}h_1[n] + h_2[n]) + \\
&\quad +(e^{-j\vartheta_2[n+1]}\hat{h}_3^*[n+1] + \hat{h}_4^*[n+1])^* \cdot (e^{-j\vartheta_2[n+1]}h_3^*[n+1] + h_4^*[n+1]) \\
&= \hat{h}_1^*[n]h_1[n] + \hat{h}_2^*[n]h_2[n] + \hat{h}_3[n+1]h_3^*[n+1] + \hat{h}_4[n+1]h_4^*[n+1] \\
&\quad +e^{-j\vartheta_1[n]}\hat{h}_1^*[n]h_2[n] + e^{j\vartheta_1[n]}h_1[n]\hat{h}_2^*[n] \\
&\quad +e^{j\vartheta_2[n+1]}\hat{h}_3[n+1]h_4^*[n+1] + e^{-j\vartheta_2[n+1]}h_3^*[n+1]\hat{h}_4[n+1] \qquad \text{(A.4)} \\
g_{12}[n] &= (e^{j\vartheta_1[n]}\hat{h}_1[n] + \hat{h}_2[n])^* \cdot (e^{j\vartheta_2[n]}h_3[n] + h_4[n]) + \\
&\quad +(e^{j\vartheta_2[n+1]}\hat{h}_3[n+1] + \hat{h}_4[n+1]) \cdot (-e^{-j\vartheta_1[n+1]}h_1^*[n+1] - h_2^*[n+1]) \\
&= e^{j(\vartheta_2[n]-\vartheta_1[n])}\hat{h}_1^*[n]h_3[n] - e^{j(\vartheta_2[n+1]-\vartheta_1[n+1])}h_1^*[n+1]\hat{h}_3[n+1] \\
&\quad +e^{-j\vartheta_1[n]}\hat{h}_1^*[n]h_4[n] - e^{-j\vartheta_1[n+1]}h_1^*[n+1]\hat{h}_4[n+1] \\
&\quad +e^{j\vartheta_2[n]}\hat{h}_2^*[n]h_3[n] - e^{j\vartheta_2[n+1]}h_2^*[n+1]\hat{h}_3[n+1] \\
&\quad +\hat{h}_2^*[n]h_4[n] - h_2^*[n+1]\hat{h}_4[n+1] \qquad \text{(A.5)} \\
g_{21}[n] &= (e^{j\vartheta_2[n]}\hat{h}_3[n] + \hat{h}_4[n])^* \cdot (e^{j\vartheta_1[n]}h_1[n] + h_2[n]) \\
&\quad -(e^{-j\vartheta_1[n+1]}\hat{h}_1^*[n+1] + \hat{h}_2^*[n+1])^* \cdot (e^{-j\vartheta_2[n+1]}h_3^*[n+1] + h_4^*[n+1]) \\
&= e^{j(\vartheta_1[n]-\vartheta_2[n])}h_1[n]\hat{h}_3^*[n] - e^{j(\vartheta_1[n+1]-\vartheta_2[n])}\hat{h}_1[n+1]h_3^*[n+1] \\
&\quad +e^{j\vartheta_1[n]}h_1[n]\hat{h}_4^*[n] - e^{j\vartheta_1[n+1]}\hat{h}_1[n+1]h_4^*[n+1] \\
&\quad +e^{-j\vartheta_2[n]}h_2[n]\hat{h}_3^*[n] - e^{-j\vartheta_2[n+1]}\hat{h}_2[n+1]h_3^*[n+1] \\
&\quad +h_2[n]\hat{h}_4^*[n] - \hat{h}_2[n+1]h_4^*[n+1] \qquad \text{(A.6)} \\
g_{22}[n] &= (e^{j\vartheta_2[n]}\hat{h}_3[n] + \hat{h}_4[n])^* \cdot (e^{j\vartheta_2[n]}h_3[n] + h_4[n]) \\
&\quad +(e^{-j\vartheta_1[n+1]}\hat{h}_1^*[n+1] + \hat{h}_2^*[n+1])^* \cdot (e^{-j\vartheta_1[n+1]}h_1^*[n+1] + h_2^*[n+1]) \\
&= \hat{h}_1[n+1]h_1^*[n+1] + \hat{h}_2[n+1]h_2^*[n+1] + \hat{h}_3^*[n]h_3[n] + \hat{h}_4^*[n]h_4[n] \\
&\quad +e^{j\vartheta_1[n+1]}\hat{h}_1[n+1]h_2^*[n+1] + e^{-j\vartheta_1[n+1]}h_1^*[n+1]\hat{h}_2[n+1] \\
&\quad +e^{j\vartheta_2[n]}h_3[n]\hat{h}_4^*[n] + e^{-j\vartheta_2[n]}\hat{h}_3^*[n]h_4[n] \qquad \text{(A.7)}
\end{aligned}
$$

However, unlike in the stationary case, There are no simplified form to represent the deviation $\mathbf{G}_n - \hat{\mathbf{G}}_n$. It can be noted that off-diagonal elements $g_{12}[n]$ and $g_{21}[n]$ are now finite and create inter-symbol interference in the process of decoding while on-diagonal elements $g_{11}[n]$ and $g_{22}[n]$ are degraded.